Aus der

Berufsgenossenschaftlichen Unfallklinik

Klinik für Unfall- und Wiederherstellungschirurgie an der

Universität Tübingen

Alcohol-Induced Liver Fibrosis Alters Bone *via* BMP Signaling: Modeling Hepatic Osteodystrophy *in vitro*

Inaugural -Dissertation
zur Erlangung des Doktorgrades
der Medizin

der Medizinischen Fakultät
der Eberhard Karls Universität
zu Tübingen

vorgelegt von

Xin, Yuxuan

2025

Dekan: Professor Dr. B. Pichler

1. Berichterstatter: Professor Dr. A. Nüssler
2. Berichterstatter: Professor Dr. M. Krimmel

Tag der Disputation: 28.11.2025

Table of contents

List of Figures

List of Tables

List of abbreviations

2D	Two dimensional
3D	Three dimensional
ALD	Alcoholic liver disease
AP	Alkaline phosphatase
BMP	Bone morphogenetic protein
C/EBPα	CCAAT enhancer binding protein α
CA II	Carbonic anhydrase II
$CaCl_2$	Calcium chloride
CT	Computer tomographic
CYP450	Cytochrome P450
DMSO	Dimethyl sulfoxide
DEPC	Diethyl Pyrocarbonate
DMEM	Dulbecco's modified Eagle's medium
EPHB4–EFNB2	Eph receptor B4– Ephrin B2
Ex/Em	Excitation/Emission
ECM	Extracellular Matrix
EDTA	Ethylenediaminetetraacetic Acid
EGM	Endothelial Growth Medium
FASL–FAS	Fas ligand–Fas receptor
FCS	Fetal calf serum
GLU	Glutamine
HGF	Hepatocyte growth factor
HOD	Hepatic osteodystrophy
hPRP	Human platelet-rich plasma
IL-6	Interleukin 6
L-B	Liver–bone
LCAT	Lecithin-cholesterol acyltransferase
MAFLD	Metabolic associated fatty liver disease
MASH	Metabolic dysfunction-associated steatohepatitis
M-CSF	Macrophage colony stimulating factor
MEM α	Minimum Essential Medium Eagle alpha

miR-144	MicroRNA 144
NaCl	Sodium chloride
NAFLD	Non-alcoholic fatty liver disease
NaOH	Sodium hydroxide
Nrf2	Nuclear factor erythroid 2-related factor 2
NSAIDs	Non-steroidal anti-inflammatory drugs
NTX	N-terminal cross-linking telopeptide of type I collagen
OPG	Osteoprotegerin
PBS	Phosphate buffered saline
PDMS	Polydimethylsiloxane
PGE2	Prostaglandin E2
PMA	Phorbole-12-myristate-13-acetate
PINP	Procollagen Type I N-terminal Propeptide
PPARγ	Peroxisome proliferator-activated receptor γ
P/S	Penicillin/Streptomycin
PTH	Parathyroid hormone
RANKL	Receptor activator of nuclear factor-kappa B ligand
RAU	Relative absorbance units
RFU	Relative fluorescence units
ROS	Reactive oxygen species
SEM	Standard error of the mean
SRB	Sulforhodamine B staining
TBS-T	TRIS-buffered saline/Tween-20
TEMED	Tetramethylethylenediamine
TGF-β	Transforming growth factor beta
TNF-α	Tumor necrosis factor alpha
TRAP	Tartrate-resistant acid phosphatase
UGT	UDP-glucuronosyltransferase
UV	Ultraviolet Sterilization

Chapter 1

1. Introduction

1.1 Hepatic system

1.1.1 Hepatic structure and function

As the largest solid organ, the liver plays vital roles in the human body. It comprises four lobes, each of which is further subdivided into eight segments. Its functional unit is the hepatic lobule, which is approximately 1 mm in diameter and has a polygonal shape (Kleckner 1957). At the periphery of the hepatic lobule, the portal area is identified, comprising the portal vein, hepatic artery, and bile duct, which together constitute the portal triad. These structures work in concert to ensure the normal flow of blood and bile (Figure 1.1 A, B).

Hepatocytes, hepatic stellate cells (HSCs), endothelial and Kupffer cells, and cholangiocytes collectively form the cellular composition of the liver, all of which play essential roles in metabolic processes, detoxification, bile production, immune regulation, and nutrient storage (Figure 1.1 C) (Bonnardel *et al.* 2019, Schulze *et al.* 2019, Kamm and McCommis 2022, Yi *et al.* 2024). The liver's filtration and detoxification functions are critical for maintaining human health, as it transforms endogenous and exogenous toxins into harmless substances through biochemical reactions. These detoxification processes are primarily divided into three phases. Oxidation, reduction, and hydrolysis are the major Phase I reactions mediated by the cytochrome P450 (CYP450) enzyme system, which convert substances such as alcohol, drugs, and chemical toxins into active or intermediate metabolites (Guengerich 2001, Iacopetta *et al.* 2023). In phase II reactions, enzymes such as glucuronosyltransferase and sulfotransferase facilitate conjugation reactions, transforming toxic substances into water-soluble, non-toxic forms (Rowland *et al.* 2013). Finally, in phase III reactions (transfer process), proteins such as P-glycoprotein, organic anion transporters, and adenosine triphosphate (ATP)-binding cassette transporters serve an important function

in the excretion of these metabolites. The resulting non-toxic products are eliminated either *via* bile into the intestines or through the kidneys into the urine (Blanco and Blanco 2017). Throughout these processes, all reactions work in synergy to ensure that the liver efficiently handles and clears toxins, waste products, and metabolic byproducts, thereby maintaining homeostasis in the body.

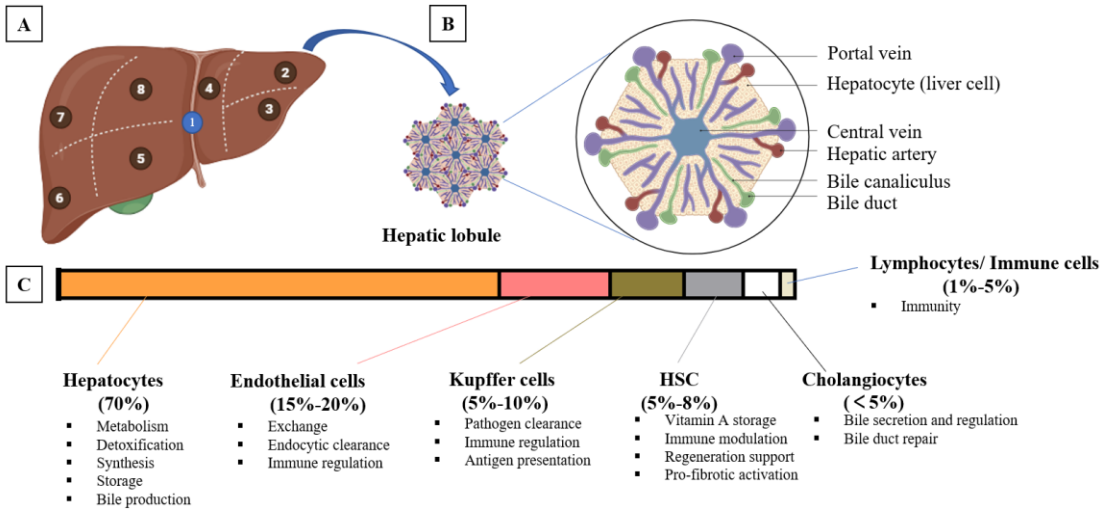

Figure 1.1 Cell types and functional organization of the liver. A. Illustrate the anatomical structure of the liver, highlighting its lobular segmentation. B. Depicts a magnified view of a liver lobule, showing the arrangement of key vascular and biliary structures: portal vein, hepatic artery, central vein, bile canaliculus, bile duct, and hepatocytes. C. The bar graph below quantifies the relative abundance of major liver cell and primary functions. Modified from Kleckner 1957, Bonnardel *et al*. 2019, Schulze *et al*. 2019, Kamm and McCommis 2022, Yi *et al*. 2024. Created with biorender.com.

1.1.2 Liver disease

As a vital organ, the liver performs indispensable roles in metabolism, detoxification, protein production, and nutrient storage (Trefts *et al.* 2017). Damage or dysfunction can result in severe, potentially life-threatening conditions. Liver disease poses a significant global health challenge, leading to roughly 2 million deaths worldwide each year-equivalent to 4% of total worldwide fatalities (Devarbhavi *et al.* 2023, Gan *et al.* 2025).

Liver diseases are categorized as acute liver injury (ALI) or chronic liver injury based on progression. ALI involves a rapid loss of liver function due to extensive hepatocyte

death, caused by factors like drug-induced injury, ischemia-reperfusion damage, autoimmune disorders, and viral hepatitis (Yu *et al.* 2023). In developing countries, viral infections are more common, while drug-related causes are prevalent in developed regions (Devarbhavi *et al.* 2023, Gan *et al.* 2025). Severe ALI can lead to acute liver failure, a critical condition often requiring urgent medical intervention, such as liver transplantation (Lima *et al.* 2019, Ramachandran and Jaeschke 2019).

Chronic liver injury starts from prolonged cycles of hepatic damage and repair, ultimately leading to progressive alterations in liver architecture (Sharma A 2023 Jul 3) (Figure 1.2). A central event in this process is the sustained activation of HSCs (Garbuzenko 2022). Under physiological conditions, HSC activation is a transient and controlled response to acute injury, aiding tissue repair by secreting extracellular matrix (ECM) components and growth factors (Bedossa and Paradis 2003, Kitto and Henderson 2021). However, in chronic liver disease, repeated hepatocyte apoptosis and necrosis trigger persistent inflammatory signaling and continuous activation of Kupffer cells, specialized macrophages localized in the liver. These immune cells release pro-inflammatory cytokines that further stimulate HSCs (Nguyen-Lefebvre and Horuzsko 2015, Wen *et al.* 2021). Over time, HSCs undergo differentiation into myofibroblast-like cells with increased contractility, proliferation, and pathological ECM deposition. This leads to progressive fibrosis, where normal hepatic tissue is replaced by fibrotic septa, disrupting sinusoidal structure, impairing cell–cell communication, and distorting the liver microenvironment (Puche *et al.* 2013, Arriazu *et al.* 2014). In parallel, biliary epithelial cells may undergo reactive proliferation and a ductular reaction (Sato *et al.* 2019), further exacerbating disease progression and promoting cirrhosis.

Based on the etiology, liver diseases can be categorized into infectious, toxic, metabolic and genetic, and autoimmune (Table 1.1) (Gan *et al.* 2025).

Table 1.1 Summary of Major Liver Diseases: Classification, Causes, and Consequences based on etiology.

Type of disease	Specific Type	Cause of diseases	Outcomes
Infectious liver diseases (Talwani *et al.* 2011)	Hepatitis A, B, and C	Viruses (HAV, HBV, HCV), bacteria, or parasites	Liver inflammation and damage; may progress to chronic liver disease or cirrhosis
Toxic liver diseases (David and Hamilton 2010, Osna *et al.* 2017)	Alcoholic Liver Disease Toxic Hepatitis, etc.	Medications, excessive alcohol chemical toxins, and environmental pollutants	Inflammation, fibrosis, or liver failure
Metabolic and genetic liver diseases	MASLD* (Panganiban *et al.* 2025) Wilson's Disease (Stremmel and Weiskirchen 2022) Hemochromatosis (Salomao 2021)	MASLD: obesity, diabetes, metabolic syndrome Inherited metabolic disorders: copper/iron overload, protein accumulation	Fatty liver, inflammation, fibrosis, cirrhosis, potential progression to liver cancer
Autoimmune liver diseases (Sarcognato *et al.* 2021, Filipovic *et al.* 2025)	Autoimmune Hepatitis, Primary Biliary Cholangitis, Primary Sclerosing Cholangitis	Immune system dysfunction	Chronic inflammation, bile duct damage, cholestasis, fibrosis, cirrhosis, liver failure
***MASLD: Metabolic dysfunction-associated steatotic liver disease**			

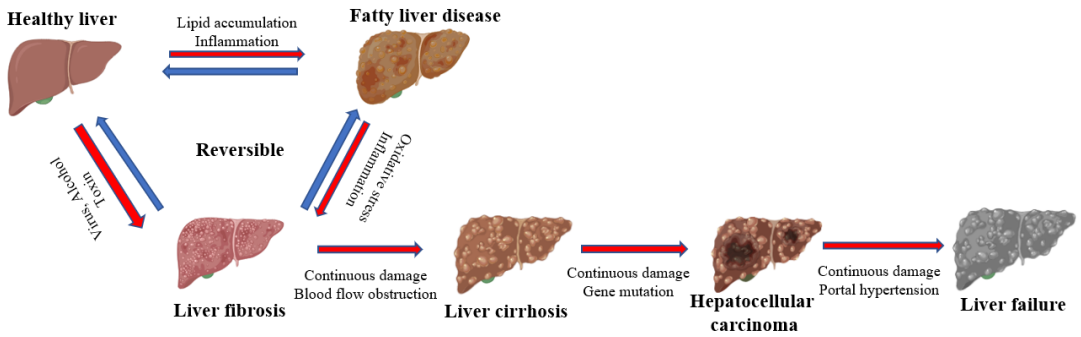

Figure 1.2 Cellular and pathological progression of long-term liver disease. Long-term liver disease progresses from steatosis to liver failure through sustained injury and dysregulated repair. In early stages, hepatocytes accumulate lipids and trigger inflammation, while HSCs

become activated and deposit extracellular matrix, leading to fibrosis—a potentially reversible stage. Persistent damage promotes cirrhosis, genomic instability, and may result in hepatocellular carcinoma and liver failure. Modified from Sharma A 2023 Jul 3, Garbuzenko 2022, Puche *et al*. 2013, Arriazu *et al*. 2014. Created with biorender.com.

1.2 Bone part

1.2.1 Bone formation and function

Within animals, bone is recognized as a mineralized, dynamic connective tissue responsible for structural support, metabolic storage, and physiological homeostasis. Anatomically, bone includes cortical bone, which provides strength, and trabecular bone, which ensures lightweight properties. The bone microenvironment primarily contains osteoblasts, osteocytes, osteoclasts in addition to bone lining cells (Figure 1.3). Bone remodeling relies on a balance between formation and resorption is maintained by osteoblasts and osteoclasts, while bone-lining cells, quiescent flat cells covering the bone surface that help regulate mineral homeostasis, contribute to this balance (Florencio-Silva *et al.* 2015). Embedded in the bone matrix, osteocytes—terminally differentiated from osteoblasts—are essential for controlling bone reconstruction (Wawrzyniak and Balawender 2022, Šromová *et al.* 2023). Effective communication between these cell types *via* autocrine and paracrine pathways is vital for maintaining bone health.

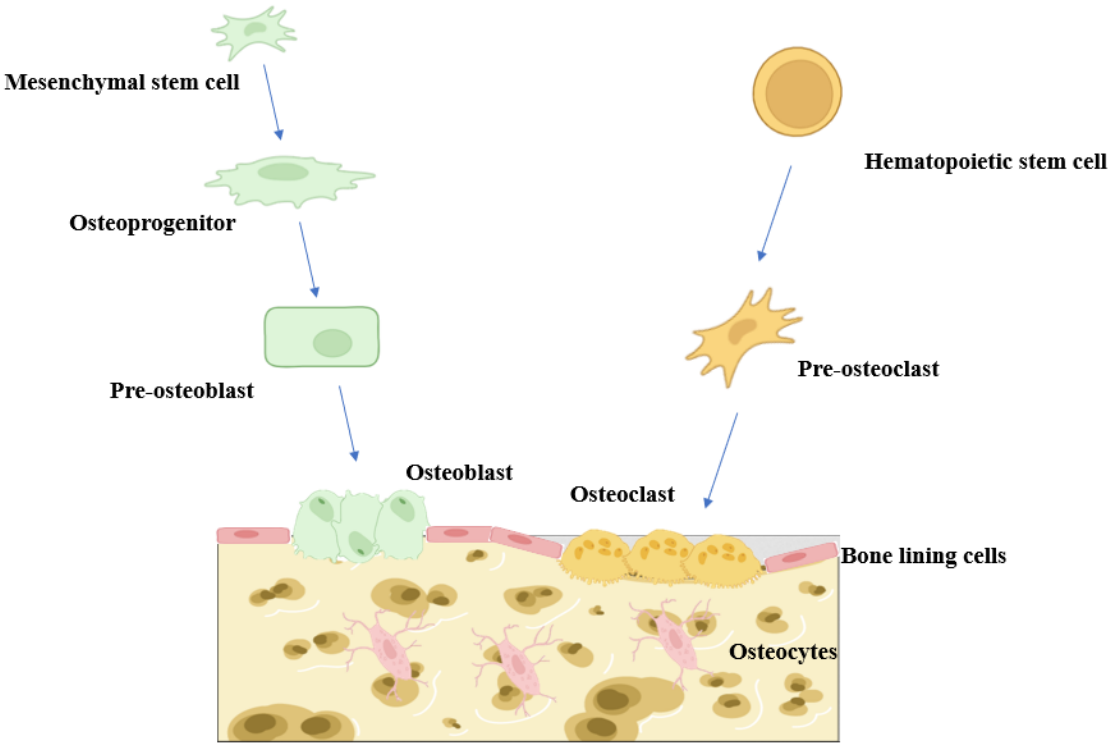

Figure 1.3 Bone cell lineages and development. Derived from mesenchymal stem cells via osteoprogenitors and pre-osteoblast stages, osteoblasts act as essential mediators of bone formation. Osteoclasts, in contrast, develop from hematopoietic stem cells *via* the monocyte/macrophage lineage and differentiate into mature bone-resorbing cells. Osteocytes, embedded within the mineralized bone matrix, are terminally differentiated osteoblasts that make critical contributions to mechanosensation and regulation of bone remodeling. Modified from Šromová *et al.* 2023. Created with biorender.com and Servier Medical Art.

1.2.2 Molecular mechanisms underlying the regulation of bone metabolism

In the process of maintaining bone homeostasis, the receptor activator of nuclear factor kappa-B ligand (RANKL)/ osteoprotegerin (OPG) regulatory system plays a central role: RANKL secreted by osteoblast-derived cells interacts with RANK on osteoclast progenitors, driving their maturation. Osteoblasts also release OPG, a soluble receptor that neutralizes RANKL and suppresses osteoclast differentiation. (Kim *et al.* 2020, Takegahara *et al.* 2022) (Figure 1.4 A). The balance between RANKL and OPG, primarily regulated by osteoblasts, is pivotal in controlling osteoclast activity and bone resorption.

Another critical communication pathway involves the Eph family of tyrosine kinase receptors in osteoblasts and their ephrin ligands on osteoclasts (Edwards and Mundy 2008). The ephrin/Eph signaling pathway is bidirectional: Forward signaling through Eph receptors promotes osteoblast differentiation *via* RhoA, a small GTPase, whose activation mediates this process while reverse signaling through ephrin ligands suppresses osteoclast formation and activity (Zhao *et al.* 2006) (Figure 1.4 B).

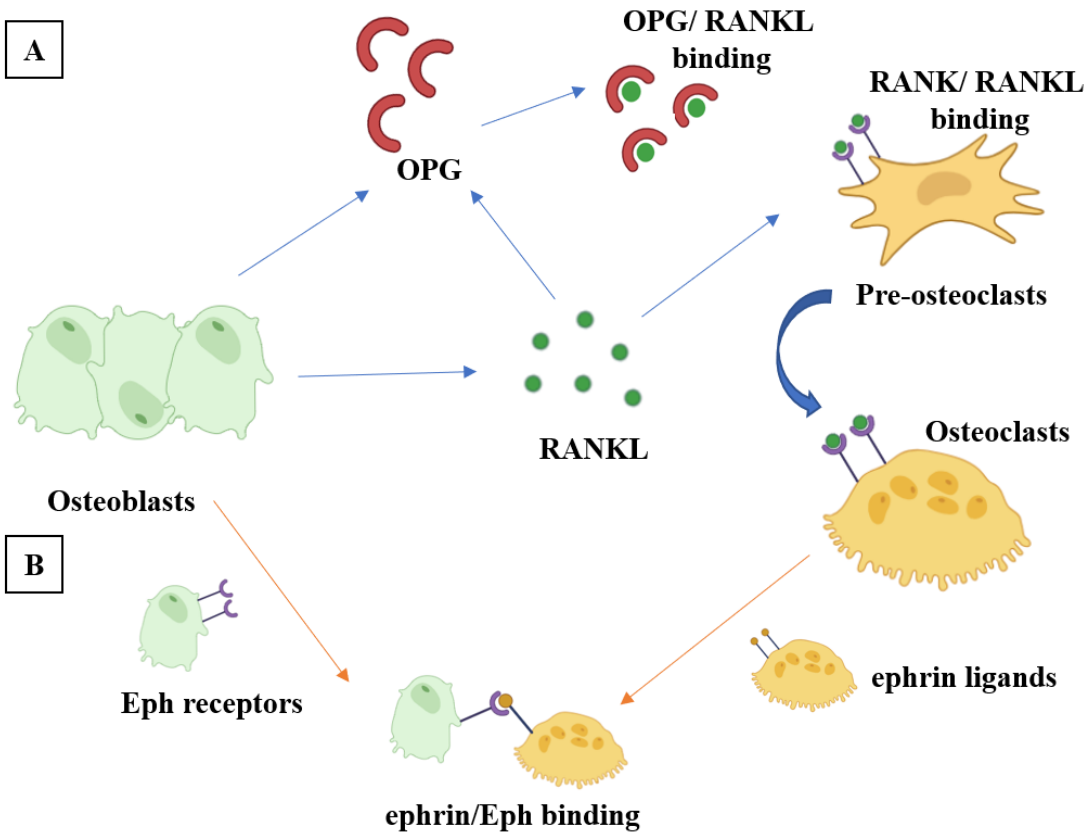

Figure 1.4 Signaling pathways involved in maintaining bone homeostasis. A. illustrates the OPG/RANK/RANKL signaling pathway. Osteoblasts express RANKL that activates RANK signaling in osteoclast precursors, leading to osteoclast differentiation. At the same time, osteoblasts secrete OPG, acts as a competitor to block the interaction between RANK and RANKL. B. shows the ephrin/Eph signaling pathway. Osteoclasts express ephrin ligands, which attach to Eph receptors on osteoblasts, facilitating differentiation. Simultaneously, this interaction suppresses osteoclastic bone resorption. Modified from Kim *et al.* 2020, Takegahara *et al.* 2022, Zhao *et al.* 2006. Created by biorender.com.

Physiologically, bone is a central organ for mineral metabolism, particularly in the storage and dynamic regulation of calcium and phosphorus (Wawrzyniak and Balawender 2022). Through interactions with endocrine factors, including parathyroid hormone and vitamin D, bone contributes to systemic calcium homeostasis and broader metabolic processes (de Paula and Rosen 2013, Khundmiri *et al.* 2016, Bhattarai *et al.* 2020). Within the bone marrow cavity lies a complex microenvironment where hematopoiesis occurs. Mesenchymal stem cells (MSCs) and hematopoietic stem cells coexist and interact with osteoblasts, endothelial cells, and other components to maintain the dynamic equilibrium of bone formation, repair, and hematopoiesis (de Paula and Rosen 2013). MSCs not only regulate the bone marrow microenvironment to support skeletal balance but also retain multipotent capacity to generate osteoblasts, chondrocytes, and adipocytes, thereby making them an attractive target for studies in bone regeneration and tissue engineering (Kode *et al.* 2009, Zhao *et al.* 2014, Xu *et al.* 2024).

1.2.3 Bone disorders

Disorders of the bone are characterized by a variety of abnormalities involving metabolism, structure, or mechanical performance (Seemann *et al.* 2024). Common types include osteoporosis, osteomalacia, Paget's disease, and osteitis. Osteoporosis, the most prevalent and clinically important bone metabolic disorder, is identified by reductions in bone mass, deterioration of bone microarchitecture, and elevated fracture risk, thereby substantially raising the likelihood of fractures. (Sözen *et al.* 2017, LeBoff *et al.* 2022). Because if its common incidence and strong association with aging and chronic conditions, osteoporosis constitutes a critical international public health problem. In our research, we focus specifically on the pathogenesis of osteoporosis, particularly its characteristics during chronic liver injury, to highlight the crucial role of the liver–bone axis in bone metabolism disorders.

The pathogenesis of osteoporosis is primarily explained by an imbalance in bone remodeling, a process precisely regulated by osteoblast-driven bone formation and

osteoclast-driven bone resorption (Föger-Samwald *et al.* 2020). This imbalance may result from one of three major mechanisms.

First, reduced osteoblastic activity leads to insufficient bone formation. This is commonly observed in aging, low vitamin D status, or prolonged inflammation, where the number or differentiation potential of osteoblasts is compromised, impairing matrix synthesis and mineralization (LeBoff *et al.* 2022, Zhang *et al.* 2023). Besides, oxidative stress and dysregulation of critical pathways including Wnt/β-catenin and bone morphogenetic protein (BMP) signaling can further inhibit osteoblastogenesis and promote osteoblast apoptosis. These disruptions lead to a decreased capacity for bone regeneration and contribute significantly to the pathogenesis of osteoporosis (Zhivodernikov *et al.* 2023, Hu *et al.* 2024, Zhao *et al.* 2025) .

Second, enhanced osteoclastic activity is a key contributor to bone loss in osteoporosis. Increased osteoclast formation, activation, or prolonged survival leads to excessive bone resorption that outpaces bone formation. This imbalance is frequently associated with an elevated RANKL/OPG ratio that stimulates osteoclast differentiation, along with higher levels of inflammatory cytokines, notably interleukin 6 (IL-6) and tumor necrosis factor alpha (TNF-α), commonly seen with inicreasing age and chronic inflammation (Weitzmann 2013, Ono *et al.* 2020). Additionally, factors like macrophage colony-stimulating factor and hormonal changes further stimulate osteoclast activity. The resulting excessive bone degradation weakens bone structure and increases fracture risk. Consequently, osteoporosis is defined by a dysregulation of bone remodeling, where reduced osteoblastic formation and excessive osteoclastic resorption synergistically drive net bone loss (Umur *et al.* 2024).

Third, in certain chronic or systemic conditions, both osteoblastic and osteoclastic activities are reduced, resulting in low bone turnover (Jeong and Kim 2019, Aguilar *et al.* 2023). This impaired bone remodeling compromises the renewal of bone microarchitecture and increases bone fragility. Clinical conditions including chronic liver disease, kidney disease, and diabetes mellitus are commonly associated with low-

turnover osteoporosis, where diminished bone remodeling activity leads to poor bone quality despite reduced bone resorption.

1.3 Liver–bone axis

1.3.1 Liver–bone crosstalk

The liver and bones serve as vital secretory organs within the endocrine system (Rhyu and Yu 2021, Zhou *et al.* 2021). The liver impacts the physiological activity of different organs in the body by generating specific factors, while bone-derived factors, produced during bone metabolism, also exert endocrine effects. The functional connection and mutual regulation between the liver and bones, known as the liver–bone axis, highlight the synergistic interplay between these two organs under physiological and pathological conditions. Through the bidirectional regulation of liver and bone-derived factors, the liver–bone axis serves as a key regulator of bone metabolism, maintaining systemic calcium-phosphorus balance, and playing a role in the initiation and advancement of multiple metabolic disorders (Nussler *et al.* 2014, Ehnert *et al.* 2019) (Figure 1.5 A).

1.3.1.1 The impact of hepatic factors on bone

The effect of liver-derived factors on bones is primarily reflected in the regulation of bone cells differentiation and function (Figure 1.5 B). Table 1.2 summarizes liver secreted factors that influence bone cell function.

Table 1. 2. Liver-derived factors affecting bone metabolism

Liver-derived factors	Specific Factor	Liver Source	Mechanism	Effect on Bone
Growth Factors	Insulin-like Growth Factor (IGF) (Khan *et al.* 2025)	Secreted by hepatocytes, growth hormone - regulated	↑ PI3K/AKT, MAPK/ERK; ↑ Runx2; modulates RANKL/OPG (Yuan *et al.* 2019)	↑ Osteoblast proliferation & differentiation; regulates bone remodeling

	Bone Morphogenetic Protein (BMP) (Colucci *et al.* 2021)	From liver sinusoidal endothelial cells	Smad1/5/8, MAPK, WNT; AMPK/β-catenin (Wu *et al.* 2016)	↑ Osteogenesis, promotes osteoblast activity
	Transforming Growth Factor-β (TGF-β)	Produced by hepatocytes, stellate, Kupffer cells (Li *et al.* 2022)	Smad2/3; PI3K/AKT, MAPK; modulates RANKL/OPG (Chen *et al.* 2012)	Osteoblast differentiation; supports bone formation & remodeling
Vitamins and metabolic factors	25-Hydroxyvitamin D	Synthesized in liver, activated in kidneys	Regulates calcium and phosphorus absorption; binds VDR on osteoblasts; PTH (Young *et al.* 2022)	Bone matrix synthesis; maintains mineral balance (Ehnert *et al.* 2019)
	Bile Acids	Synthesized from cholesterol in liver	FXR & TGR5 pathways; regulate cAMP and osteoblast/osteoclast activity (Li *et al.* 2019)	↑ Osteoblast function, ↓ osteoclasts; maintains mineralization (Handzlik-Orlik *et al.* 2016)
Hormone	Sex Hormone-Binding Globulin	Secreted by liver(Qu and Donnelly 2020)	Regulates free estrogen/testosterone; affects RANKL-RANK-OPG (Hsu *et al.* 2024)	↓Bone resorption, ↑ SHBG → ↓ free hormones→ osteoporosis
Inflammatory factors	Tumor necrosis factor-α (TNF-α)	Hepatic inflammation	Activates RANKL → ↑ osteoclasts; inhibits WNT/β-catenin in osteoblasts (Lam *et al.* 2000)	↑ Bone resorption, ↓ osteoblast differentiation
	Interleukin-6 (IL-6) Family	Elevated in liver inflammation and disease	↑ RANKL-RANK ↓ WNT/β-catenin; ↓ osteoblast genes	↑ Bone resorption, ↓ bone formation, ↓ mineralization → osteoporosis (Sellin *et al.* 2023)

1.3.1.2 Consequences of bone-secreted factors for liver function

Bone is not merely a structural organ; it also actively participates in systemic regulation by secreting a variety of signaling molecules—known as osteokines—that influence distant tissues, including the liver (Figure 1.5 B). These bone-derived factors contribute to a bidirectional communication axis between the bone system and the liver, playing critical roles in modulating hepatic metabolism, immune responses, and tissue regeneration (Table 1.3).

Table 1.3. Bone-derived factors affecting liver function

Bone-derived factors	Specific Factor	Bone Source	Mechanism	Effect on liver
Hormones	Osteocalcin	Osteoblasts	Activates PI3K-AKT pathway; activates AMPK and inhibits SREBP-1c; inhibits NF-κB (Ferron *et al.* 2010, Wu *et al.* 2022)	Enhances glucose metabolism and insulin sensitivity; promotes lipid oxidation; suppresses inflammation
Glycoprotein	Sclerostin (Martín González *et al.* 2022)	Osteocytes, Chondrocytes	Inhibits WNT/β-catenin signaling; downregulates VEGF expression	Reduces liver regeneration and angiogenesis; reduce lipid accumulation in NAFLD context (Dreyer *et al.* 2023)
Cytokines	RANKL	Osteoclast precursors, T cells	Binds to RANK on hepatic cells; activates NF-κB and MAPK signaling (Ono *et al.* 2020)	Induces hepatic inflammation; activates hepatic stellate cells; promotes fibrosis and disrupts lipid metabolism (Monti

				et al. 2024)
Growth Factors	BMPs (e.g., BMP7, BMP9)	Osteoblasts, Osteocytes	Activate Smad, MAPK, and PI3K/AKT pathways (Thayer *et al.* 2020, Monti *et al.* 2024)	BMP7: anti-fibrotic, hepatoprotective; BMP9: pro-fibrotic, affects liver microcirculation

1.3.2 Hepatic osteodystrophy (HOD)

HOD, a metabolic bone disease, is identified by changes in bone mineral density occurring in individuals with chronic liver injury (Ehnert *et al.* 2019). Among the prevalent causes are viral hepatitis, pharmacologically induced liver injury, cirrhosis, and nonalcoholic fatty liver disease. As of 2017, More than 1.5 billion individuals globally suffer from chronic liver damage (Moon *et al.* 2020), and nearly 75% of these patients also have bone disorder (Chen *et al.* 2025). This underscores the crosstalk between the liver and bones, which is particularly relevant to the advancement of these diseases.

Alcoholic liver disease (ALD), representing a significant category of chronic liver injury, has been consistently correlated with dysregulated bone metabolism. (Mackowiak *et al.* 2024). Long time alcohol exposure damages hepatocyte, induces oxidative stress, and disrupts immune function, t thereby initiating and maintaining chronic inflammatory response (Dunn and Shah 2016, Tan *et al.* 2020). These pathological changes aggravate liver injury and significantly disrupt bone remodeling by modulating various cytokines and signaling pathways. Research has revealed that liver damage alters the levels of key factors— including transforming growth factor beta 1 (TGF-β1), IL-6, insulin-like growth factor- 1 (IGF-1), and sclerostin—thereby impairing the balance of osteogenesis and osteoclastogenesis, which contributes to progressive bone loss (Gao *et al.* 2024, Wu *et al.* 2024). Notably, liver dysfunction can impair bone cell differentiation and activity by interfering with BMP signaling (Beederman *et al.* 2013, Chen *et al.* 2024). BMPs—such as BMP-2, BMP-9, and BMP-

13—are essential regulators of bone formation, playing critical roles in bone maturation and matrix deposition. During liver injury, the synthesis and secretion of BMPs are affected, leading to impaired bone formation. This liver-driven dysregulation of bone metabolism emphasizes the central role of the liver–bone axis in the development of HOD.

Chronic inflammation is also considered to be a key factor in bone metabolism disorders. Long-term liver damage alters the expression of multiple regulatory factors, including TGF-β, BMP, IGF-1, and IL-6, lecithin–cholesterol acyltransferase (LCAT) and sclerostin, which disrupt the coupling of bone formation and resorption. This disruption in bone metabolism acts as a key regulator of the pathogenesis of HOD, further emphasizing the complex role of the liver–bone axis in the disease's development (Gao *et al.* 2024).

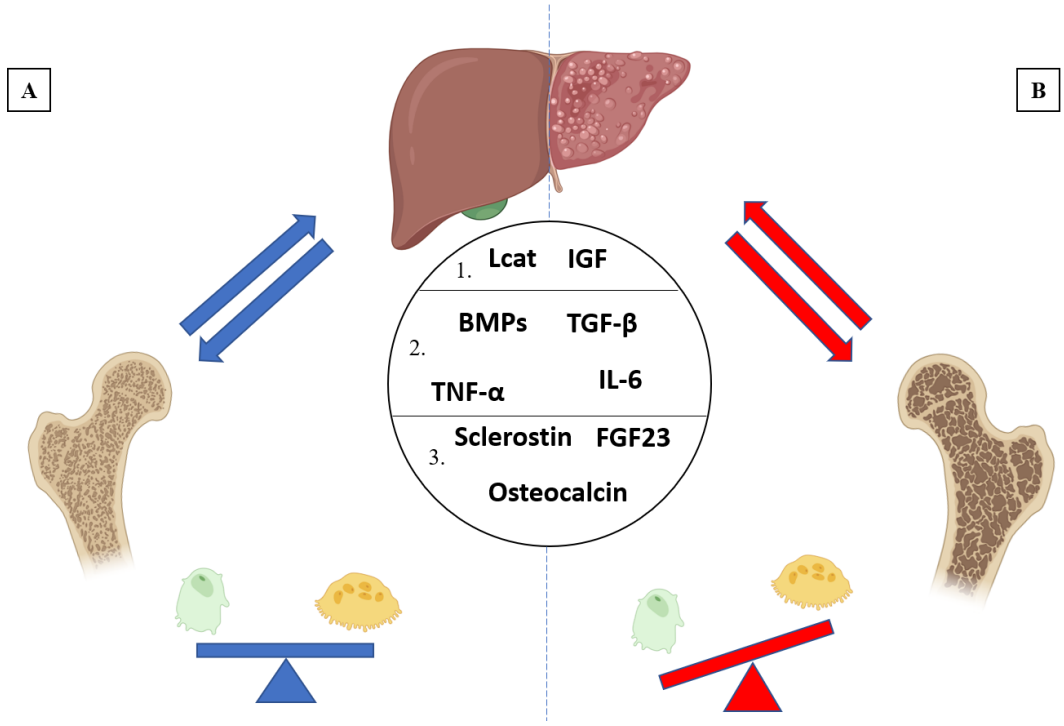

Figure 1.5 Interaction between liver and bone through the liver–bone axis. Within this axis, various secretory factors—including TGF-β, BMPs, TNF-α, IL-6, IGF, osteocalcin, and FGF23—participate in bone remodeling by regulating the dynamic balance between osteoblasts and osteoclasts. A. In a physiological state, bone metabolism remains in balance. B. Under pathological conditions, osteoclast activity is enhanced while osteoblast function is suppressed,

leading to bone loss, a condition known as hepatic osteodystrophy. The bidirectional arrows represent the mutual regulatory relationship between the liver and the skeletal system. 1: Liver-derived molecules, 2: Factors secreted by both liver and bone, 3: Bone-derived regulators Modified from Nussler *et al.* 2014, Ehnert *et al.* 2019, Gao *et al.* 2024, Wu *et al.* 2024. Created by biorender.com.

1.3.3 Signaling pathways of BMPs in HOD

BMPs constitute a major subgroup of the TGF-β superfamily and function as pivotal regulators in skeletal biology, particularly in bone formation, remodeling, and repair (Ehnert *et al.* 2019). In HOD, BMPs act as pivotal mediators in the liver–bone axis, transmitting pathological signals from dysfunctional liver tissue to disrupt bone homeostasis.

BMP-2, BMP-9, and BMP-13 are expressed in bone as well as in the liver, and their synthesis and secretion are altered under conditions of liver injury, particularly alcohol-induced fibrosis (Herrera *et al.* 2018, Peschl *et al.* 2022). This dysregulation of liver-derived BMPs negatively impacts bone metabolism by impairing osteoblast differentiation and enhancing osteoclastogenesis, thereby promoting skeletal deterioration characteristic of HOD.

BMP signaling functions at the molecular level *via* heteromeric complexes formed by type I and type II serine/threonine kinase receptors (Gilboa *et al.* 2000). When a ligand binds, the type II receptor phosphorylates the type I receptor, initiating downstream signaling through receptor-regulated Smads—mainly Smad1, 5, and 8 (Kokabu *et al.* 2012). After phosphorylation, R-Smads form complexes with the co-mediator Smad4 and move into the nucleus to control transcription of osteogenic regulators, including *RUNX2* and *Osterix*, key drivers of osteoblast differentiation and matrix synthesis. (Figure 1.6 B).

Besides the Smad relevant pathway, BMP signaling also engages non-Smad pathways, including mitogen-activated protein kinase（MAPK) p38, ERK, and JNK cascades, which further modulate osteoblast function, survival, and apoptosis (Guzman *et al.*

2012, Yue and López 2020) (Figure 1.6 A). Together, these pathways coordinate to maintain the dynamic equilibrium of bone formation and resorption.

Alcohol exposure has been shown to modulate BMP signaling at multiple levels, both directly and indirectly (Klem *et al.* 2025, Lovely 2025). Experimental evidence indicates that alcohol impairs BMP-2 expression and signaling, crucial for osteogenesis and fracture repair, resulting in decreased osteoblast activity and delayed bone healing (Bratton *et al.* 2018, Eby *et al.* 2020). In hepatic cells, alcohol-induced fibrosis disrupts BMP secretion patterns, leading to altered Smad phosphorylation and reduced transcription of markers of osteoblast differentiation (Gerjevic *et al.* 2012). Moreover, changes in BMP-9 expression have been correlated with heightened osteoclast function, leading to enhanced bone resorption. (Li *et al.* 2016). Alcohol's influence on BMP pathways extends beyond the canonical Smad axis to non-Smad branches such as MAPK, further contributing to its detrimental effects on bone remodeling.

Collectively, these findings underscore the importance of BMP signaling dysregulation as a mechanistic link between liver disease, particularly alcohol-induced liver fibrosis, and impaired bone health. Understanding the modulation of BMP pathways by alcohol provides valuable insight into HOD pathogenesis and identifies potential targets for therapeutic intervention to restore bone integrity under chronic liver disease conditions.

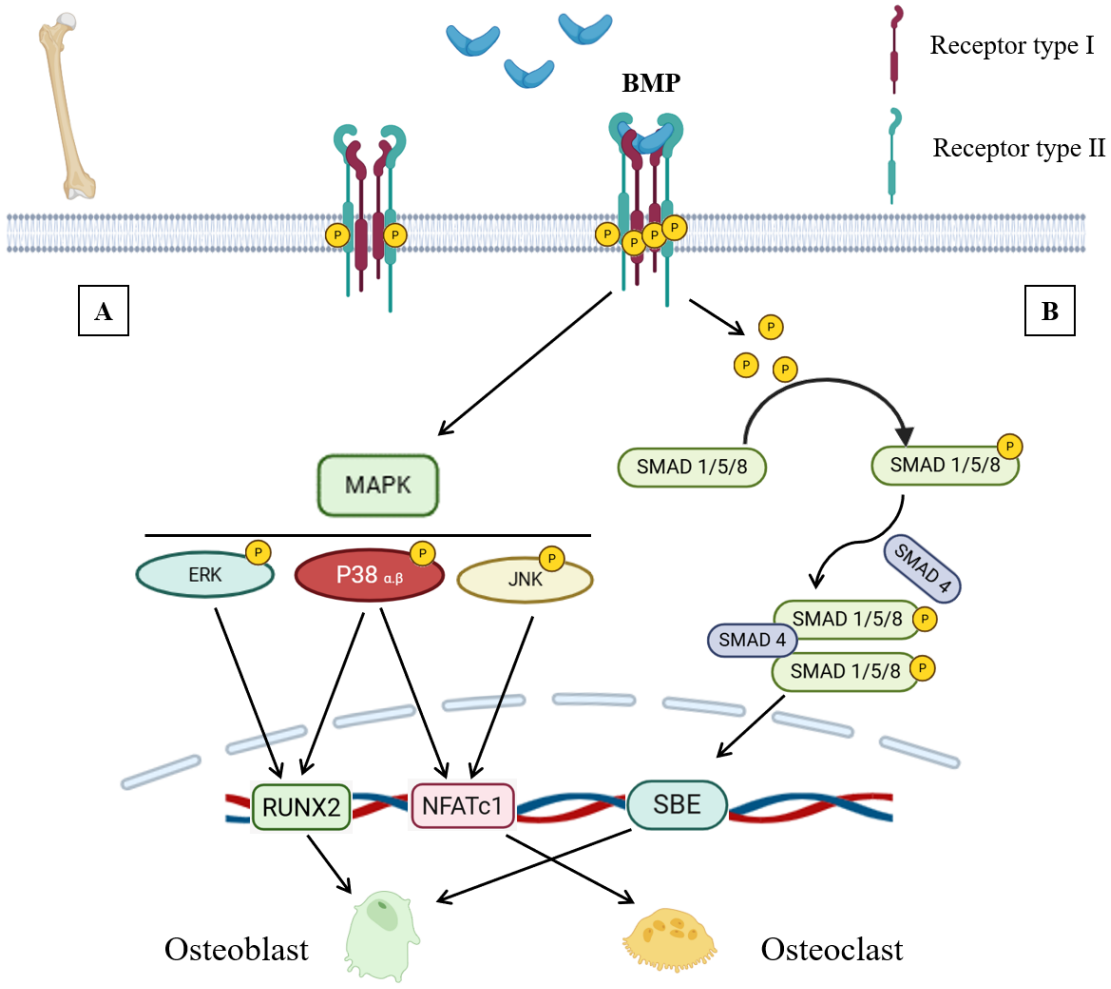

Figure 1.6 Schematic of the BMP signaling pathways in bone metabolism. On target cells, BMP signaling is initiated by the binding of BMPs to type I and type II receptors, triggering phosphorylation cascades. A. The MAPK pathway is activated through the phosphorylation of ERK, p38α/β, and JNK, resulting in the activation of downstream transcription factors RUNX2 and NFATc1. B. Within the canonical SMAD pathway, SMAD1/5/8 are phosphorylated, after which they associate with SMAD4. The resulting complex translocates to the nucleus, binds SMAD-binding elements, and modulates transcription of target genes. These pathways cooperate to regulate bone formation and resorption. Modified from Klem *et al.* 2025, Lovely 2025, Guzman *et al.* 2012, Yue and López 2020. Created by biorender.com.

1.4 Alcohol consumption and alcohol induced related disease

1.4.1 Effects of chronic alcohol use

Alcohol use is a major factor in the global burden of disease, being responsible for considerable morbidity and mortality. Currently, approximately 2.4 billion people consume alcohol, of whom 950 million are classified as heavy drinkers, defined by the

monthly consumption of over 60 g of pure ethanol at least once a month. (World Health 2018). Although potential benefits of moderate alcohol consumption were suggested in early investigations, recent analyses have challenged this view, showing that even small amounts of alcohol can cause harmful effects on health (Rumgay *et al.* 2021). According to the report, alcohol poses a significant health hazard. More than 3 million deaths in 2016, exceeding 5% of worldwide fatalities, were linked to alcohol consumption. Additionally, alcohol use contributed to 1.326 billion disability-adjusted life years. The mortality rate associated with alcohol consumption surpasses that of major diseases such as acquired immunodeficiency syndrome, tuberculosis, and diabetes (World Health 2018).

Among the numerous health problems caused by alcohol consumption, ALD stands out, resulting in approximately 372,000 deaths annually. The primary component of alcoholic beverages, alcohol, is a psychoactive and potentially toxic substance that can lead to dependence (World Health 2018). Alcohol consumption has been associated with numerous health complications, including cardiovascular disorders, metabolic diseases, infections, and injuries (Pflaum *et al.* 2016).

Alcohol-related disorders were responsible for roughly 2.6 million deaths globally in 2019, underscoring their substantial contribution to the global health burden. Among them, 1.6 million deaths were attributed to chronic non-communicable diseases (e.g., liver cirrhosis and cardiovascular disorders), 700,000 to injuries such as traffic accidents, and 300,000 to infectious diseases. Compared with 600,000 deaths in women, alcohol-related mortality in men reached 2 million, highlighting a substantial gender disparity (World Health 2024). Additionally, alcohol use disorders are a global concern. Approximately 400 million people are estimated to have alcohol use disorders, with 209 million dependent on alcohol (World Health 2024). While low levels of alcohol consumption pose relatively lower risks, the majority of alcohol-related harm is caused by long-term heavy drinking or intermittent binge drinking. Therefore, implementing effective interventions to reduce alcohol consumption, raising public awareness of its

dangers, strengthening policy management, and supporting individuals in reducing alcohol intake are critical steps.

Patterns of alcohol consumption vary significantly across regions. In North Africa and the Middle East, alcohol consumption is notably low, with some countries reporting near-zero consumption rates due to cultural and religious practices. In comparison with other regions, Europe exhibits the greatest prevalence of alcohol consumption worldwide. In the 2016 Global Burden of Disease Study, countries were stratified into five quintiles of the Socio-Demographic Index (SDI): low, low-middle, middle, middle-high, and high. The study found that alcohol consumption prevalence is highest in countries with a high SDI, where 72% of women and 83% of men consume alcohol. Conversely, low-SDI countries have the lowest prevalence, with only 9% of women and 20% of men reporting alcohol consumption. High-SDI countries exhibit the greatest daily alcohol consumption, with women consuming on average 1.9 standard drinks per day and men averaging 2.9, highlighting a marked gender difference. In comparison, daily intake is lowest among men in low-SDI countries (1.4 standard drinks) and among women in low-middle SDI countries (0.3 standard drinks). Across all SDI levels, women consistently consume less alcohol than men. However, as the SDI levels increase, the gender gap in alcohol consumption narrows (Figure 1.7). For example, in Nepal (a country with a low SDI), 1.5% of women and 21% of men consume alcohol, whereas in Sweden (a country with a high SDI), the figures are 86% for women and 87% for men (Griswold *et al.* 2018).

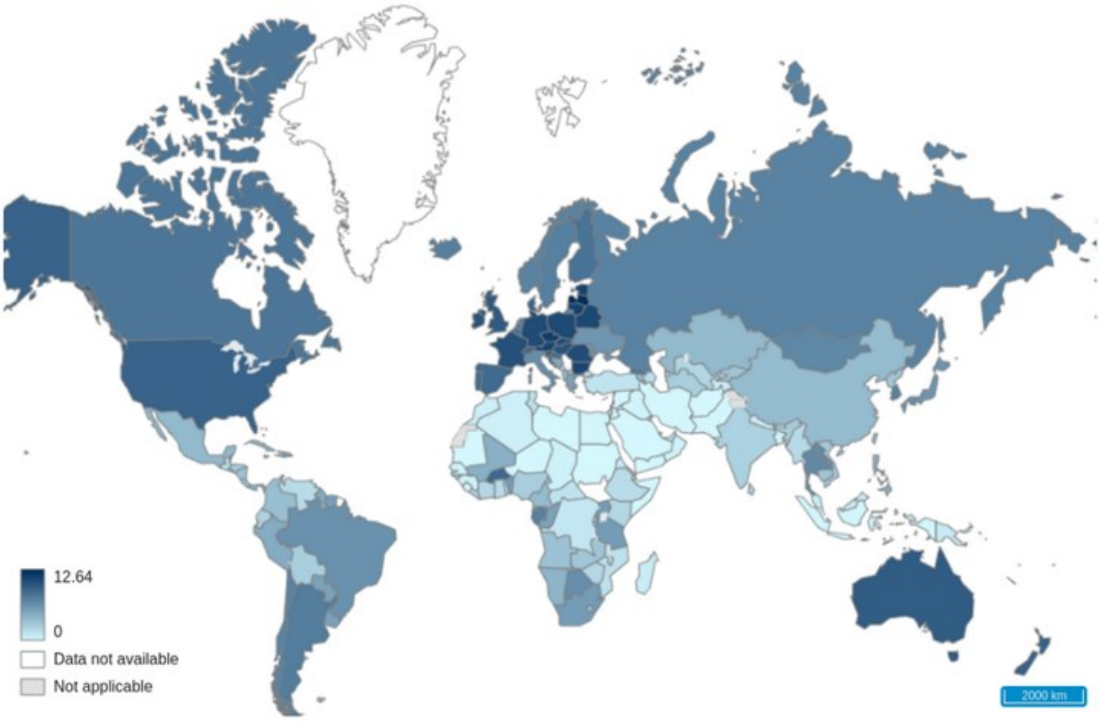

Figure 1.7 Per capita consumption of pure alcohol (L/year). The map illustrates the average per capita alcohol consumption in 2020, measured in liters of pure alcohol per person, highlighting global and regional differences across countries. Darker shades indicate higher consumption levels, with the highest rates observed in several European countries. In contrast, many countries in Africa, the Middle East, and parts of Asia report lower levels. Gray areas represent regions where data were either unavailable or not applicable. The figure is derived from the WHO's 2020 report on global per capita alcohol consumption. Reproduced with permission of the WHO. Request ID: 202506473.

1.4.2 Alcohol metabolism in the human body

The molecular structure of alcohol gives it both fat and water-soluble properties, allowing it to quickly penetrate cell membranes and be absorbed by the human body (Ingólfsson and Andersen 2011, Cederbaum 2012). Alcohol enters the bloodstream primarily through the oral mucosa, stomach, and intestines. About 90% of absorbed alcohol is directed to the liver through the portal vein, where primary metabolic processing occurs (Hyun *et al.* 2021).

The metabolism of alcohol is classified into oxidative and non-oxidative pathways, among which the oxidative pathway constitutes the predominant route (Figure 1.8). The oxidative metabolism of alcohol begins with its conversion to acetaldehyde by alcohol

dehydrogenase. Subsequently, acetaldehyde is oxidized to acetate through the activity of aldehyde dehydrogenase. Then, acetic acid is ultimately processed in peripheral tissues, producing carbon dioxide, water, and fatty acids (Zakhari 2013, Hyun *et al.* 2021). In cases of excessive drinking, CYP2E1 becomes more active in the metabolism of alcohol, generating reactive oxygen species (ROS) that further exacerbate liver injury.

Although the non-oxidative pathway constitutes only a minor portion of overall alcohol metabolism, the metabolites it produces—such as fatty acid ethyl esters, ethanol sulfate, and ethanol glucuronide—can induce toxic reactions, potentially damaging the liver, myocardium, and nervous system (Heier *et al.* 2016, Kong *et al.* 2024). These metabolic pathways and their byproducts collectively influence alcohol metabolism and its effects on overall health.

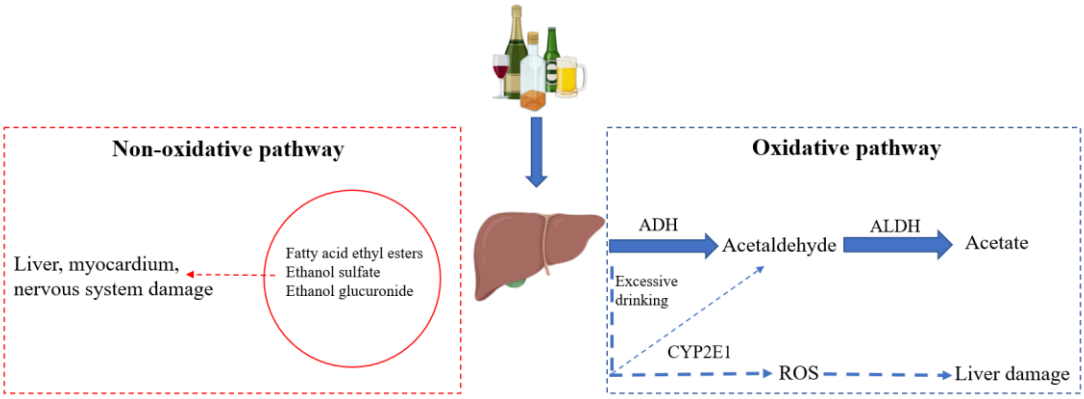

Figure 1.8 Different metabolic routes for alcohol *via* liver system. Alcohol is metabolized in the liver *via* two different ways: the oxidative and the non-oxidative pathway. ADH metabolizes most alcohol and then excreted it, but excessive drinking can promote CYP2E1 to metabolize alcohol, produce ROS, and cause liver damage. Although the non-oxidative pathway is not the primary pathway, the metabolites produced include fatty acid ethyl esters, alcohol sulfate, and alcohol glucuronide, which may impair liver function, myocardial integrity, and disrupt neural activity. Modified from Zakhari 2013, Kong *et al.* 2024. Created by biorender.com.

1.4.3 Alcohol-induced HOD

Alcohol metabolism has a complex and close relationship with liver and bone health. In cases of long-term heavy drinking, the multifaceted effects of alcohol metabolism

can significantly damage multiple systems in the body (Thomes *et al.* 2021). During hepatic metabolism, alcohol gradually inflicts irreversible damage, promoting the transition from fatty liver to alcoholic hepatitis and eventually cirrhosis. Oxidative stress and inflammatory responses generated during alcohol metabolism are the primary driving factors in this process (Dai *et al.* 2000, González-Reimers *et al.* 2015, Gao *et al.* 2024). These responses prompt hepatocytes to release large quantities of factors, including TNF-α, IL-6, and TGF-β. These inflammatory factors circulate through the bloodstream to bone tissue, profoundly impacting the homeostasis of bone metabolism.

Studies have shown that alcohol metabolites have a direct impact on bone metabolism. Among them, acetaldehyde, a key intermediate product of alcohol metabolism, is highly toxic. It reduces bone formation by directly inhibiting the function of osteoblasts and also enhances bone resorption by promoting the activity of osteoclasts (Giuliani *et al.* 1999, Turner 2000). Bone remodeling is markedly disrupted by the dual actions of acetaldehyde, resulting in lower bone density and compromised architecture, ultimately increasing the likelihood of osteoporosis and fractures (González-Reimers *et al.* 2015, Johnson *et al.* 2022). Furthermore, the large quantities of ROS produced during alcohol metabolism exacerbate oxidative stress. These free radicals not only damage liver cells, causing apoptosis and DNA damage (Wu and Cederbaum 2003), but also disrupt bone metabolism further by degrading the ECM and impairing osteoblast function, accelerating bone loss (Kimball *et al.* 2021, Iantomasi *et al.* 2023).

It is noteworthy that patients with ALD often face particularly severe bone health problems due to liver dysfunction and metabolic imbalances. These patients frequently present with osteoporosis, reduced bone strength, and an impaired mineralization capacity (Ehnert *et al.* 2019, Danford *et al.* 2020, Jadzic and Djonic 2023). Additionally, alcohol may indirectly harm bone health by affecting intestinal flora and nutrient absorption (Cheng *et al.* 2021, Guo *et al.* 2025). For instance, ALD is often associated with disrupted vitamin D metabolism and reduced calcium absorption, which further exacerbates the risk of bone hypomineralization and fragility (Kizilgul *et al.* 2016).

In summary, alcohol damages liver and bone function through the combined effects of metabolites (such as acetaldehyde and ROS), inflammatory responses, and oxidative stress, ultimately leading to the development of HOD.

1.5 Models for HOD

Although patients represent the most ideal model for studying HOD, ethical restrictions make it unrealistic to study patients directly. As a result, animal experimental models have been developed and are now widely used to explore the mechanisms of HOD, develop treatments, and evaluate drug efficacy (Nussler *et al.* 2014). Approximately 100 million experimental animals are used in related research annually, significantly advancing the understanding of the disease and facilitating the exploration of treatments (Swaminathan *et al.* 2019, Park *et al.* 2024). However, these models have some limitations. A major issue is species differences, which result in significant physiological and genetic disparities between animal and humans. These differences can limit the translatability of experimental results to clinical applications. Another challenge is the ethical controversy surrounding animal experiments, as the procedures often cause pain or discomfort to the animals (Akhtar 2015, Singh *et al.* 2016). This has raised public and scientific concerns about animal welfare. Additionally, the high costs associated with animal experiments—including animal breeding, laboratory maintenance, and post-experiment processing—pose significant challenges, particularly for research teams with limited resources. For these reasons, many researchers have adopted alternative methods, such as *in vitro* experiments and computational simulations. These approaches not only reduce reliance on animals but also provide more direct, cost-effective, and efficient research outcomes, paving the way for innovative and ethical scientific exploration (Lee *et al.* 2022, Pastorino *et al.* 2024).

Among these alternatives, *in vitro* models—especially advanced three-dimensional (3D) systems—have garnered increasing attention for their potential to more accurately replicate human physiology and disease conditions.

Compared with two-dimensional (2D) *in vitro* models, 3D models offer significant advantages for studying complex diseases (Edmondson *et al.* 2014, Lee *et al.* 2022). While 2D models are quick to establish and feature a monolayer distribution of cells, making them easy to observe and manipulate, they struggle to effectively simulate the intricate interactions between cells and the ECM. Additionally, 2D models tend to exhibit heightened sensitivity to drug responses, often failing to accurately reflect *in vivo* conditions. These limitations hinder their utility in studying the true biological behavior of diseases (Kapałczyńska *et al.* 2018). In contrast, with cell arrangements and dynamic microenvironments that closely mimic *in vivo* conditions, 3D models more accurately replicate cellular physiological functions and pathological processes. Consequently, 3D models are increasingly becoming the preferred tool for researching complex diseases.

Developing a long-term, stable in vitro 3D liver–bone co-culture system is critical to accurately replicate tissue interactions and to elucidate the mechanisms driving HOD. In liver-related studies, hepatocyte-derived lines such as HepG2, Huh7, and THLE are widely applied as substitutes for primary human hepatocytes. These cell lines approximate specific hepatocyte functions while offering practical advantages, including accessibility and ease of maintenance. Despite this, their metabolic activity is significantly lower than that of primary human hepatocytes, limiting their utility in drug toxicity screening and mechanism studies (Lin *et al.* 2012). HepaRG cells have been introduced as a prominent alternative to address these limitations in *in vitro* hepatocyte research. Unlike conventional hepatocyte cell lines, HepaRG cells possess the ability to differentiate into both mature hepatocytes and cholangiocyte-like cells in response to specific culture conditions. In addition, the expression of drug-metabolizing enzymes, particularly CYP450 family members, in HepaRG cells closely mirrors that of primary hepatocytes, making them a reliable system to model liver function under normal and disease conditions (Chen *et al.* 2025). Evidence indicates that HepaRG cells are highly versatile, being applicable to various fields such as drug metabolism research, toxicity evaluation, liver disease modeling, and viral infection studies, underscoring

their broad utility. Notably, differentiated HepaRG cells exhibit significantly enhanced functional stability, maintaining their properties over extended periods and avoiding the rapid loss of liver-specific characteristics observed in primary hepatocytes. This combination of stability and functionality makes HepaRG cells a highly reliable *in vitro* research model, offering a robust platform for advancing our understanding of complex disease mechanisms (Ruoß *et al.* 2020, Hammour *et al.* 2022, Asano *et al.* 2024). To further enhance the physiological relevance of our model and better replicate the functions of a normal liver, we incorporated human HSCs and vascular endothelial cells. By mediating ECM remodeling and modulating fibrogenesis, HSCs serve as pivotal components in maintaining the structural integrity of the liver. Meanwhile, vascular endothelial cells are essential for forming functional microvascular networks, supporting nutrient and oxygen exchange, and contributing to the overall liver microenvironment (Zahmatkesh *et al.* 2022). By including these cell types, our model aims to more accurately simulate the complex cellular interactions and dynamic microenvironment of a normal liver, thereby improving its functionality and applicability for research purposes. Notably, the presence of multiple liver cell types in our previous model enabled it to reproduce certain aspects of liver fibrosis, but this effect was only sustainable in the short term.

For the bone part, 3D biomaterials provide an ideal microenvironment for cell-based tissue and organ regeneration, with the scaffold's structure playing a crucial role in determining its functionality and performance. An optimal scaffold should possess interconnected pores and high porosity, ensuring cell adhesion, migration, and proliferation, as well as efficient diffusion of metabolic waste and degradation products—features essential for 3D tissue regeneration. Moreover, pore size must strike a precise balance: Excessively large pores may weaken cell-scaffold interactions, while overly small pores can hinder cell migration and tissue growth. In bone tissue engineering, the ideal scaffold material must combine excellent biocompatibility, biodegradability, and appropriate mechanical properties to provide structural support throughout the degradation process (Hollister 2005, Karageorgiou and Kaplan 2005,

O'Brien 2011). Scaffold materials are typically classified into three categories: natural polymers (Pina *et al.* 2015), synthetic polymers (Place *et al.* 2009), and bioactive materials (Rezwan *et al.* 2006). Although collagen and chitosan are highly biocompatible natural polymers, they typically provide inadequate mechanical support and limited regulation of degradation behavior. Synthetic polymers, like polylactic acid and polycaprolactone, exhibit superior mechanical properties and tunable degradation profiles but have low intrinsic bioactivity, often requiring functionalization or the addition of growth factors. In contrast, platelet-rich plasma (PRP) scaffolds, a type of bioactive material, stand out for their remarkable bioactivity. Rich in growth factors including platelet-derived growth factor, TGF-β, and epidermal growth factor, PRP directly promotes cell proliferation, differentiation, and angiogenesis, thereby strongly supporting repair process of the tissue (Xie *et al.* 2014, Pereira *et al.* 2023). Therefore, we use PRP scaffolds as carriers for the bone co-culture to fully leverage their exceptional bioactivity and tissue repair potential.

In vitro bone co-culture models are commonly established using cell lines derived from humans or animals. Because this experiment focuses on the pathological changes of bone tissue in HOD, employing human-derived cell lines provides a model that better represents the physiological and pathological conditions of the human body.

In selecting osteoblasts, the commonly used cell lines are Saos-2 and MG-63 (Pautke *et al.* 2004, Vandrovcova *et al.* 2014), both derived from human osteosarcoma and characterized by their osteoblast-like phenotype. In our study, we employ SCP-1 cells, a human bone marrow–derived mesenchymal stem cell line and immortalize by introducing the human telomerase reverse transcriptase (hTERT) gene (Böcker *et al.* 2008). The expression of hTERT prevents telomere shortening, thereby bypassing replicative senescence and allowing the cells to proliferate indefinitely in culture while maintaining key stem cell properties and confirmed potential for osteogenic, chondrogenic, and adipogenic differentiation (Jaiswal *et al.* 2000, Böcker *et al.* 2008). SCP-1 cells stable phenotype and multipotency make them a promising model for

studying early osteogenic commitment compared to primary MSCs, which undergo growth arrest due to senescence triggered by telomere shortening and cellular stress. Unlike tumor-derived osteoblast cell lines such as Saos-2 and MG-63, the differentiation potential and biological behavior of SCP-1 are closer to primary cells, so it can more accurately reflect the *in vivo* osteogenesis process and has a higher biological relevance (Weng *et al.* 2020). Moreover, during osteogenic differentiation, SCP-1 cells display significantly enhanced alkaline phosphatase (AP) activity, upregulated expression of osteogenic markers including osteocalcin, and pronounced mineralized nodule formation, thereby confirming their strong osteogenic differentiation capacity. In osteoclast research, peripheral blood mononuclear cells, bone marrow–derived mononuclear cells, and THP-1 cells are among the most frequently used models. The latter have unique advantages in simulating the function of osteoclasts: They can be induced to differentiate into osteoclast precursors, have the characteristics of monocytes, and can respond to the influence of multiple immunomodulatory factors (Chanput *et al.* 2014, Li *et al.* 2017). Therefore, we induce these two types of cells to differentiate into osteoblasts and osteoclasts under specific conditions, combining the system with liver components and optimizing the culture conditions to prolong the culture period, thereby get a stable long term *in vitro* liver–bone co-culture model suitable for HOD research (Chen *et al.* 2025). This model offers a valuable platform for investigating the bone pathology associated with HOD.

1.6 The aim of this study

This study aims to optimized a stable long term *in vitro* liver–bone co-culture model using human cell lines, to induce pathological changes in liver microorganoids through alcohol exposure, to simulate the interaction of the liver–bone axis under disease conditions *in vivo*, and to investigate the mechanisms by which pathological liver affects bone. The specific objectives are as follows:

1. **Establish and optimize a stable long-term *in vitro* 3D liver-bone co-culture model and simulate its pathological state.**

   a. Construct *in vitro* liver and bone tissue models separately, optimize their structure and function, and enhance their resemblance to *in vivo* conditions.

   b. Establish a stable, sustained pathological liver model by inducing fibrotic phenotype formation in liver microorganoids *via* alcohol stimulation.

   c. Co-culture the pathological liver microorganoids with bone system and assess bone function changed at specific time points to evaluate their interactions.
2. **Optimize methodological strategies for the liver-bone co-culture system.**

   Explore various co-culture approaches, including direct and indirect. Compare their feasibility and respective advantages within the liver–bone model, and identify the most suitable approach.
3. **Investigate the mechanisms by which liver pathology-related factors influence bone function.**

   Determine the mechanism by which pathological hepatocyte-derived factors induced by alcohol stimulation regulate bone formation and metabolism through modulation of the BMP signaling pathway.

Chapter 2

2. Materials and Methods

2.1. Material

2.1.1 List of chemicals

Table 2.1.1 List of used chemicals.

Substance	Company	Article No.
2-Hydroxyethylmethacrylat	Sigma	128635
3,3′-Methylene-bis(4-hydroxycoumarin)	Sigma	M1390
4-Methylumbelliferone	Sigma	M1381
4-Nitrophenyl acetate	Sigma	N8130
4-Nitrophenyl-phosphate disodium salt hexahydrate	Carl Roth	4165.1
Acetic acid	VWR	20104.298
Agarose	Genaxxon bioscience	M3044.1000
Ammonium Persulfate	Sigma	A3678-25G
Bis-Acrylamide	Carl Roth	3039.1
Bufuralol Hydrochloride	Toronto Research Chemicals	B689540
Bupropion Hydrochloride	Toronto Research Chemicals	B689625
Calcein AM	Sigma	17783
Calcium chloride (CaCl2)	Carl Roth	CN93.2
Cetylpyridinium chloride solution	Carl Roth	CN27.1
Cholecalciferol (VitD3)	Sigma	95230
Dimethyl sulfoxide (DMSO)	Carl Roth	4720.2
Di-Sodium hydrogen phosphate buffer	Carl Roth	T876.1

Di-sodium tartrate	Carl Roth	0254.1
DMEM high glucose (4.5 g/l) with L-Glutamine	Sigma	D5796
Endothelial basal medium 2	Promocell	C-22211
Ethanol	SAV	UN1170
Ethanol absolute	VWR	20821.330
Fetal calf serum	Life Technologies	10270-106
Formaldehyde solution	Carl Roth	4979.1
Glutamine	Sigma	M11-006
Glutaraldehyde	Carl Roth	3778.1
Glycine	Carl Roth	3908.2
Gelatin	Sigma	G7041
HEPES	Carl Roth	HN78.2
Hoechst 33342	Sigma	14533
Hydrocortison	Pfizer	
Hydrogen peroxide (H2O2)	Carl Roth	CP26.5
Insulin	Novo Nordisk	
Isopropanol	Honeywell	33539
L-Ascorbic acid 2-phosphate	Sigma	A8960-5G
Luminol	Carl Roth	4203.1
Magnesium chloride (MgCl2)	Carl Roth	KK36.2
Minimum Essential Medium Eagle Alpha	Sigma	M4655
P-Coumaric acid	Carl Roth	9908.1
Penicillin/Streptomycin	Sigma	P0781
Phenacetin	Sigma	77440
Phorbol 12-myristate 13-acetate	Abcam	ab120297
Phosphate-buffered saline	Merck	L182-50
Resazurin sodium salt	Sigma	199303

RPMI 1640	Sigma	R8758
S-Mephenytoin	Toronto Research Chemicals	M225000
Sodium acetate	Carl Roth	X891.2
Sodium chloride (NaCl2)	Sigma	S7653
Sodium hydroxide (NaOH)	Carl Roth	T135.1
Sulforhodamine B	Sigma	S1402
Testosterone	Sigma	T1500
Tetramethylethylenediamine (TEMED)	Carl Roth	2367.3
TRIS	Sigma	T1503
Triton-X-100	Carl Roth	3051.2
Trypsin	Sigma	T3924
Tween-20	Carl Roth	9127.1
William's E medium	Sigma	W1878
β-Glycerophosphate disodium salt hydrate	Sigma	G9422

2.1.2 List of solutions

Table 2.1.2 List of used solutions.

Buffers/Medium/Solutions	**Compounds and handing**
Acetic acid solution (1%)	500 µl Acetic acid 49.5 ml ddH_20
Agarose working solution (2%)	5 mg Agarose Adjust volume to 250 ml ddH_2O
AP activity assay buffer	3.75 g Glycine 12.11 g Tris-Base 95.21 mg $MgCl_2$ Adjust volume to 900 ml with ddH_20 Adjust pH to 10.5 with NaOH Adjust volume to 1 L with ddH_20
AP substrate solution	1.3 mg 4-Nitrophenyl phosphate disodium salt hexahydrate (pNPP)

	1 ml AP Activity Assay Buffer (pH 10.5)
APS solution (10%)	2 g Ammonium Persulfate 20 ml ddH_20
CA II activity solution	54.3 mg 4-Nitrophenyl acetate 1.5 ml Ethanol (99%)
CA II substrate buffer	75.7 mg TRIS 219.2 mg NaCl Adjust pH to 7.5 Adjust volume to 50 ml with ddH_20
Calcein AM stock solution	502 µl DMSO 1 mg Calcein AM
Calcium chloride substrate solution (1M)	11.09 g Calcium chloride Adjust volume to 100 ml with ddH_2O
Cetylpyridium chloride Solution (10%)	10 g Cetylpyridium chlorid monohydrate Adjust volume to 40 ml with tap water Heat in the water bath for dissolving the chemical
Cholecalciferol stock solution	2 mg Cholecalciferol 10 ml DMSO
Dicumarol stock solution (10 mM)	33.6 mg 3,3'-Methylene-bis(4-hydroxycoumarin) 10 ml DMSO
Di-Sodium hydrogen phosphate substrate solution (1M)	7.1 g Di-Sodium hydrogen phosphate Adjust volume to 50 ml with ddH2O
HepaRG cell differentiation medium	100 ml HepaRG cell growing medium 1.7 ml DMSO
HepaRG cell growing medium	500 ml William's E medium 5 ml Penicillin/Streptomycin 50 ml Fetal calf Serum 5 ml L-Glutamine 800 µl Insulin 200 µl Hydrocortisone
Hoechst stock solution	10 mg Hoechst 33342 5 ml DMSO
Human platelet-rich plasma (hPRP) scaffold	1320 µl pHEMA (97%) 1320 µl Bis-Acrylamid (2%) 800 µl Human platelet-rich plasma (2.4 g/L) 1952 µl ddH2O Incubate for 30 mins on ice

	2400 µl Na2HPO4 (1M) 160 µl APS (10%) 16 µl TEMED (99%) 32 µl Glutaraldehyde (25%)
Huvec cell growing medium	500 ml Endothelial basal medium 2 2.5 µl Human vascular endothelial growth factor A isoform 165 10 µl Human basic fibroblast growth factor 5 µl Human epidermal growth factor 20 µl hRIGF-R3 350 µl Heparin 2 µl Hydrocortisone 200 µl L-ascorbic acid 5 ml Antibiotic Antimycotic Solution 10 ml Fetal calf Serum
LX-2 cell growing medium	500 ml DMEM high glucose (4.5 g/l) with L-Glutamine 5 ml L- Glutamine 5 ml Penicillin/Streptomycin
NaOH solution for DNA quantification (50 mM)	1.25 ml 2 M NaOH solution 48.75 ml ddH_20
Osteogenic differentiation medium for SCP-1/THP-1 co-culture System	250 ml RPMI 1640 medium 250 ml MEM α medium 29 mg L-Ascorbic acid 2-phosphate 0.54 g β-Glycerophosphate 2.98 g HEPES 83 mg Calcium chloride 50 µl Cholecalciferol stock solution 10 ml Fetal calf serum
PMA stock solution (200 µM)	1 mg Phorbole- 12-myristate-13-acetate 8.1 ml DMSO
Resazurin stock solution (11 X)	12.5 mg Resazurin sodium salt 50 ml PBS
Resazurin working solution (1 X)	100 µl Resazurin stock solution (11X) 1 ml PBS or plain medium
SCP-1 cell growing medium	500 ml MEM α medium 25 ml Fetal calf serum
Sulforhodamine B solution (0.4%)	0.2 g Sulforhodamine B Adjust volume to 50 ml with 1% acetic acid
THP-1 cell growing medium	500 ml RPMI 1640 medium 25 ml Fetal calf serum
TRAP activity assay buffer	8.2 g Na-Acetate

	11.5 g Na2-Tartrate Adjust volume to 900 ml with ddH_2O Adjust pH to 5.5 with HCl Adjust volume to 1 L with ddH_2O
TRAP reaction stop solution	10 ml 2M NaOH 10 ml ddH_2O
TRAP substrate solution	1.3 mg 4-Nitrophenyl phosphate disodium salt hexahydrate (pNPP) 1 ml TRAP Activity Assay Buffer (pH 5.5)
TRIS solution for DNA quantification (1M)	6.06 g TRIS Adjust volume to 40 ml with ddH_20 Adjust pH to 8.0 with HCl Adjust volume to 50 mL with ddH_20
Trypan blue solution	62.5 mg Trypan blue 50 ml PBS
Unbuffered TRIS Solution for SRB staining (10 mM)	1.2 g TRIS Adjust volume to 1 L with ddH_20

2.1.3 List of consumables

Table 2.1.3 List of used consumables.

Consumable	**Manufacturer**	**Type**	**Serial number**
Cell culture flasks	Neo-lab	25 CM^2	C-8203
Cell culture flasks	Greiner bio-one	75 CM^2	658175
Cell culture flasks	Greiner bio-one	175 CM^2	660175
Cell culture plates	Greiner bio-one	96-well, flat bottom	655180
Cell culture plates	Greiner bio-one	96-well, V bottom	651101
Cell culture plates	Greiner bio-one	48-well, flat bottom	677102
Cell culture plates	Coming Inc.	6-well, flat bottom	353046
Cell culture tubes	Greiner bio-one	50 ml	227261
Cell culture tubes	Greiner bio-one	15 ml	188271

Eppendorf tubes	SARSTEDT AG	0.5 ml, white	72.699
Eppendorf tubes	Carl Roth GmbH +	1.5 ml, white	4182.1
Eppendorf tubes	Eppendorf	2.0 ml, white	2549
Pipette	Greiner bio-one	5 ml	606160
Pipette	Greiner bio-one	10 ml	607160
Pipette	Greiner bio-one	25 ml	760160
Pipette tips	Starlab	0.1-10 µl	S1111-3000
Pipette tips	Greiner bio-one	0.1-10 µl	772350
Pipette tips	Greiner bio-one	2-200 µl	775350
Pipette tips	Greiner bio-one	100-1000 µl	777350
Adhesive Film	VWR		BK497F

2.1.4 List of equipment

Table 2.1.4 List of used equipment.

Equipment	**Manufacturer**	**Type**	**Serial number**
Agitator, magnetic stirrer	IKA-Werke GmbH	RH B2	06.050357
Agitator, magnetic stirrer	Heidolph Instruments GmbH	MR Hei-Mix L	040700340
Centrifuge	Dako Deutschland GmbH	Stat Spin	620E50000693
Centrifuge	ThermoFisher Scientific	Megafuge 40 R	41307652
Centrifuge	Scientific Industries Inc.	SI DD 58	DD58-1001
Centrifuge (Mirco)	Labnet International	BN 08060235	C1301B
Centrifuge (Mirco)	HERAEUS Med GmbH	Fresco 17	41250019
CT scanner	Siemens	SOMATOM	

	Healthineers	Definition Edge	
Electrophoresis power supplies	Bio-Rad Laboratories GmbH	Power Pac 200	285BR05538
Freezer -20°C	BSH	IQ500	GS51NYW41 (01)
Freezer -20°C	Liebherr	Med Line	LGex3410-21K 001
Freezer -20°C	Liebherr	Comfort	84.175.797.2
Freezer -80 °C	Thermo Fisher Scientific	905	827860-2521
Fridge +4 °C	Liebherr	Comfort	3523-21L
Fridge +4 °C	Cool Compact Kühlgeräte G	HKMT 040-01	CC00412514
Ice maker	Scotsmen	AF 80	DD 8837 11 X
Incubator	Thermo Fisher Scientific	Heratherm OMS 60	41296334
Incubator	Binder GmbH	9040-0078	11-22649
Incubator	Binder GmbH	9040-0081	11-22190
Incubator	New Brunwick	Galaxy 14s	10042432
Laboratory pump (Bench)	Carl Roth GmbH + Co.KG	Cyclo 2	1109-065
Microscope	Peqlab Biotechnologie GmbH	EVOS-fl	91-AF-4301
Microscope	Logos Biosystems	CELENA® X High Content Imaging System	CX30000
Microscope	Zeiss	Primovert	491206-0002-000
Mixer	Corning Inc.	Vortex Mixer	804995

Mixer	Labinco BV	LD-76	76000
Multichannel Pipette	Corning Inc.	5-50 µl	151620022
Multichannel Pipette	Corning Inc.	20-200 µl	551630277
Multichannel Pipette	Thermo Electron Co.	0.5-10 µl	CH98998 4510
Multichannel Pipette	Corning Inc.	50-300 µl	151640033
PCR thermal cyclers	Thermo Fisher Scientific	Arktik	10040953
PCR thermal cyclers	Applied Biosystems GmbH	Forschungs labor	50132
pH meter	Mettler-Toledo GmbH	Five Easy FE 20	1232315296
pH meter	Mettler-Toledo GmbH	Five Easy F 20	30266626
Pipette controller	Integra GmbH	Pipetboyacu	629619
Pipette controller	Heathrow Scientific LLC	Rota-Filler 3000	HSA05119
Refrigerator	Cool Compact Kühlgeräte G	HKMT 040-01	CC 00412516
Refrigerator	Cool Compact Kühlgeräte G	HKMN 062-01	CC 00412513
Safety workbench	Thermo Fisher Scientific	Maxisave S20201.8	41293949
Safety workbench	Thermo Fisher Scientific	Maxisave S20201.8	41293948
Scale	Kern & Sohn	ABJ 120-4M	WB 1140084

	GmbH		
Shaker, laboratory	Peqlab Biotechnologie GmbH	ES-20	010111-1107-0119
Shaker, laboratory	LTF Labortechnik GmbH	DRS 12	11DE243
Shaker, laboratory	LTF Labortechnik GmbH	DRS 12	11DE090
Shaker, laboratory	Corning Inc.	LSE Vortex Mixer	1101260
Single-channel Pipette	Corning Inc.	100-1000 µl	058261237
Single-channel Pipette	Corning Inc.	20-200 µl	158250088
Single-channel Pipette	Corning Inc.	10-100 µl	158240031
Single-channel Pipette	Corning Inc.	0.5-10 µl	158220060
Single-channel Pipette	Corning Inc.	2-20 µl	158230441
Single-channel Pipette	Eppendorf	0.1-2.5 µl	P35434B
Spectrophotometer	BMG Labtech GmbH	Fluostar Omega	415-1264
Water-bath	Lauder Dr. R. Wobser GmbH	Al 25	LCB 0727-11-0094
Water-bath	Lauder Dr. R. Wobser GmbH	ECO ET 20	LY 06.1
ZwickiLine	Zwick GmbH &	2.5 TN	059003

Co. KG

2.2 Method

2.2.1. Cell lines

HepaRG cells (Biopredic International, Saint Grégoire, France), liver progenitor cells, were remained undifferentiated throughout a 2-week proliferation phase, cultured in HepaRG medium, then use HepaRG cell differentiation medium (Hammour *et al.* 2022). The medium changes performed every other day (Zahmatkesh *et al.* 2022).

LX-2 human HSC line, were propagated in LX-2 growth medium (Zahmatkesh *et al.* 2022), with all assays performed on cells between passages 5 and 14. The medium was replaced twice a week.

HUVECs were graciously provided from Professor Alexander-Friedrich (University Tübingen, department of maxillofacial surgery) and maintained in Huvec cell growing medium (Song *et al.* 2021). Experiments were carried out using passages 7–12, with medium changes twice weekly.

SCP-1 cells were generously supplied by Professor Matthias Schieker (Böcker *et al.* 2008), This MSC line used as osteoprogenitor cells, was maintained in SCP-1 cell growing medium. The growth medium was replaced twice a week.

The human monocytic leukemia cell line THP-1 was used as the precursor population for osteoclast differentiation. Cells were propagated in suspension using THP-1 growth medium (Chen *et al.* 2025). The growth medium changed twice a week.

Cells of all types were cultured under humidified conditions at 37 °C in an atmosphere containing 5% CO_2.

2.2.2 Preparation of human platelet-rich plasma (hPRP) scaffolds

Preparation of the hPRP scaffold followed methods outlined in an early publication (Häussling *et al.* 2019). hPRP was obtained by centrifuging EDTA-treated blood from healthy volunteers at 1000 *g* for 10 min. A solution of 16.0% 2-hydroxyethyl methacrylate, 0.3% bis-acrylamide, and 0.25 g/L PRP was prepared, homogenized, and

kept on ice for 30 min. To the mixture, di-sodium hydrogen phosphate buffer was added to yield a final concentration of 0.3 M. Subsequently, 0.1% glutaraldehyde, 0.2% ammonium persulfate, and 0.2% TEMED were introduced. The final mixture was transferred to molds, and incubated at −20°C (18 h). The scaffold's pore size and morphology are strongly influenced by the freezing temperature and rate. To facilitate cutting, the molds at −80°C for at least 30min. To promote calcium phosphate crystallization, scaffolds of uniform size (6 mm diameter × 4 mm height) were immersed in 1 M $CaCl_2$ and kept on a rotating shaker overnight. The following day, the $CaCl_2$ solution was removed, then put the scaffolds to 70% alcohol and incubated overnight on a rotating shaker. Subsequently, scaffolds underwent four washes with sterile phosphate-buffered saline (PBS) (30min per wash) (Memic *et al.* 2019). And stored at 4°C covered with sterile PBS until use (Figure 2.1).

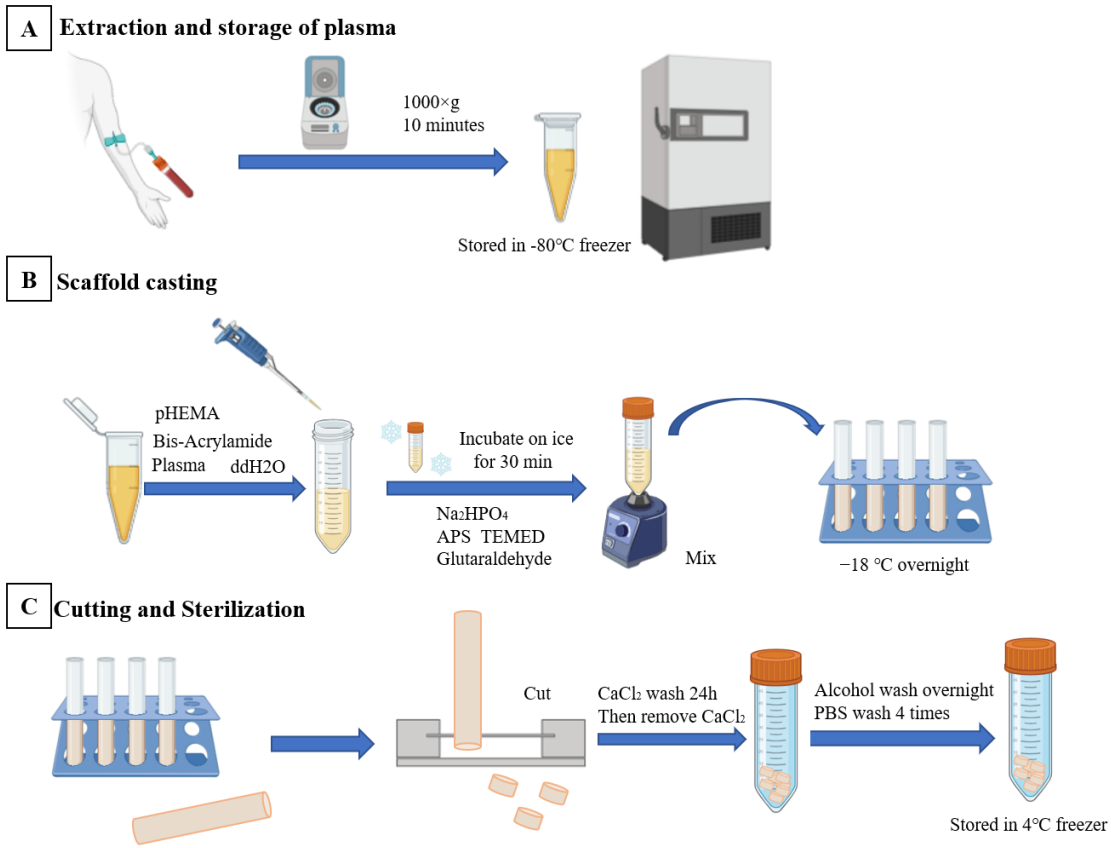

Figure 2.1 Plasma collection and PRP scaffold preparation. The procedure includes three steps: A Plasma is extracted from the upper layer following centrifugation of the collected blood. B Preparation of the scaffold. C Cutting, sterilization, and storage of the scaffold. Image created by BioRender.

2.2.3. Preparation of agarose plates

Agarose-based non-adherent microwell plates were prepared by mold replication, following established protocols (Ghezelayagh *et al.* 2022). First, 2% agarose was added to the well of a 6-well plate. A PDMS insert with 300 pyramid-shaped micropores (800 µm diameter), provided by Dr. Massoud Vosough (Royan Institute, Tehran, Iran), was placed onto the surface. Once the gel solidified, the insert was removed, creating a microporous gel plate with the corresponding pore structure (Figure 2.2). They were sterilized under ultraviolet (UV) light and microwell plates could store at 4°C to prevent drying (Chen *et al.* 2025).

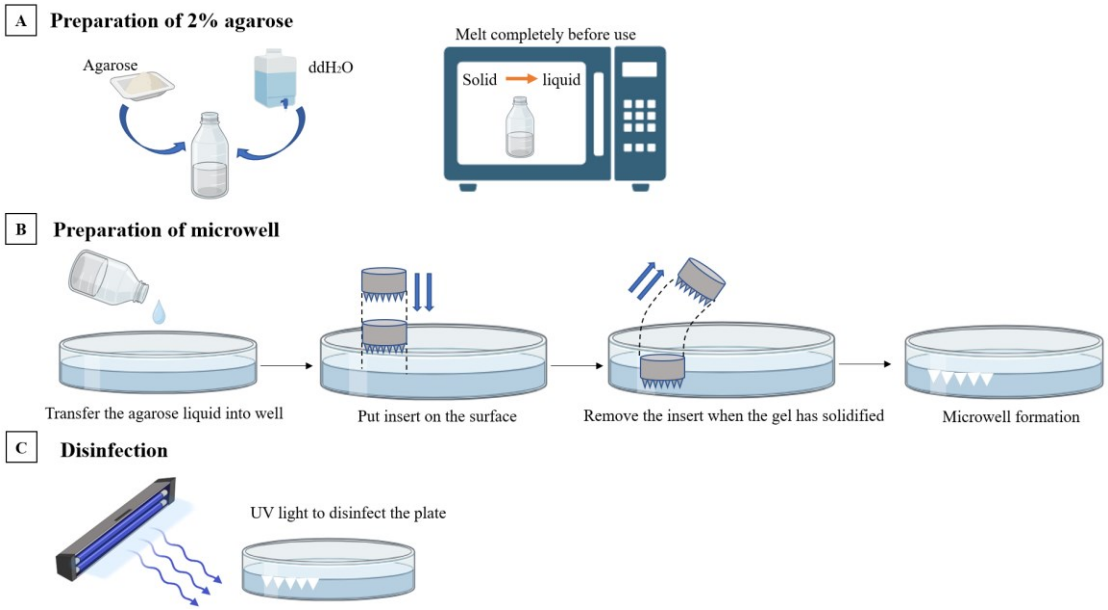

Figure 2.2 Process of the agarose plates preparation. The procedure includes three steps: A Preparation of 2% agarose. B 3.2 mL molten agarose is transferred to wells of a 6-well plate. An insert is then gently placed on the surface before gel has solidifies. Once the agarose has solidified, the insert is carefully removed, leaving behind micro-wells in the agarose surface. C Disinfect under UV light for 1 h. Image created by BioRender.

2.2.4. Seeding of cells under different conditions

2.2.4.1. Bone co-culture system

Under the 2D bone co-culture conditions, THP-1 cells were plated in a 6-well culture plate in growth medium with 200 nM PMA (7.2×10^5 cells). One day later, the medium

was removed at first and SCP-1 cells (9×10^4 cells) were added to 3 mL of bone differentiation medium (Weng *et al.* 2023). The differentiation medium was changed two times a week.

To establish the 3D bone co-culture, THP-1 and SCP-1 cells were plated on the hPRP scaffold. Prior to use, the scaffold was incubated in THP-1 culture medium for at least 48 h for pre-conditioning and to ensure sterility. Then the medium was removed from the scaffold, and it was positioned in the center of each well of a 48-well plate. (8×10^4 cells/ per scaffold) THP-1 cells were seeded onto the scaffold in the medium which contains 200 nM PMA. To ensure that cells adhesion, the scaffold was incubated for 4 h in the incubator. 500 µL of THP-1 culture medium with 200 nM PMA was gently applied to each well. The following day, the culture medium was removed from the wells prior to adding SCP-1 cells (1×10^4 cells/ per scaffold) onto the same scaffold. The SCP-1 cells are incubated for 4 h to allow for adhesion, after which time 500 µL of bone differentiation medium was carefully added to each scaffold (Chen *et al.* 2025). The differentiation medium was also changed two times a week.

2.2.4.2. Liver system

Monoculture 2D liver cells lines

In the 2D assay, the density of 7.2×10^4 cells per well was employed for differentiated HepaRG cells in a 96-well plate. To facilitate the differentiation process, HepaRG cultures received 100 µL of medium supplemented with 1.7% DMSO (Hammour *et al.* 2022).

For LX-2, the density of 0.5×10^4 cells per well was used in 96-well plates, with 100 µL of medium provided for culture and renewed twice a week.

For HUVECs, 0.5×10^4 cells were seeded to each well in a 96-well plate (with wells that had been pre-coated with gelatin), with 100 µL of medium provided for culture and renewed twice a week

Co-culture liver cell lines 2D

Under the 2D liver co-culture system, each well of a 96-well plate was seeded with a

total of 7.2 × 10^4 cells, with Diff HepaRG, LX-2, and HUVECs seeded at a ratio of 4:2:1. After seeding, a 50:50 mixture of HepaRG medium containing 1.7% DMSO and HUVEC medium was added to each well. The medium was changed twice a week.

Co-culture liver cell lines 3D (microorganoids)

For the 3D liver microorganoid model, the three cell types (differentiated HepaRG, LX-2, and HUVEC) were seeded at a ratio of 4:2:1 in 6-well plates (with wells that have been pre-prepared with agarose microwells). First, each well was filled with 2 mL of a 50:50 mixture of HepaRG medium (with 1.7% DMSO) and HUVEC medium. Then, 1 mL of cell suspension 3.0 × 10^5 cells/mL (1,000 cells per microwell), was added to each well to promote liver microorganoids formation. To achieve uniform cell distribution in the microwells, the plate was immediately centrifuged at 1200 rpm for 3 min (Zahmatkesh *et al.* 2022). Cell cluster distribution in the microwells was then examined under a light microscope. The medium changes performed every other day.

2.2.4.3. Direct 3D liver-bone co-culture model

When liver microorganoids were formed, the side of the agarose without cells was carefully hollowed out to form a pocket for the scaffold. The ratio of liver microorganoids to bone co-culture in scaffolds was 300:3. After combining the liver and bone components, the co-culture was sustained in differentiation medium for 28 days (with or without alcohol exposure). The medium changes performed every other day.

2.2.4.4. Indirect 3D liver-bone co-culture model

Bone scaffolds (3) and liver microorganoids (300) were cultured in different wells of a 6-well plate to establish an indirect co-culture system. Liver microorganoids were maintained in L-B medium (with or without alcohol exposure), conditioned medium was collected daily, and transferred to the corresponding bone scaffold cultures to provide liver-derived soluble factors without direct cell–cell contact. Fresh medium was applied each day to the liver compartment throughout the experimental period. The

co-culture system was maintained under standard incubator conditions (37 °C, 5% CO_2, humidified atmosphere) for a maximum of 28 days.

2.2.5. Stimulation liver–bone system with alcohol

Absolute alcohol was stored at a 4°C. Based on calculations, 1 mL of complete medium containing 3, 6, 9 or 12 μL sterilized absolute alcohol would have an alcohol concentration of approximately 50, 100, 150 and 200 mM, respectively. Each day, alcohol was added to the system. Immediately following alcohol exposure, the well was sealed with gas permeable cell culture film to prevent alcohol evaporation.

For the direct 3D liver-bone co-culture model, where the liver microorganoids and the bone system were seeded into one well, alcohol was added directly to the culture well (Figure 2.3 A).

For the indirect 3D liver-bone co-culture model, where bone scaffolds and liver microorganoids were cultured in separate wells, alcohol was added only to the liver compartment. Conditioned medium from alcohol treated microorganoids was collected after 2 hours daily, and transferred to the bone compartment. The liver compartment was then replenished with fresh alcohol free medium (indirect system I) or medium containing alcohol (indirect system II), thereby maintaining continuous alcohol exposure for the liver microorganoids throughout the experiment (Figure 2.3 B.C).

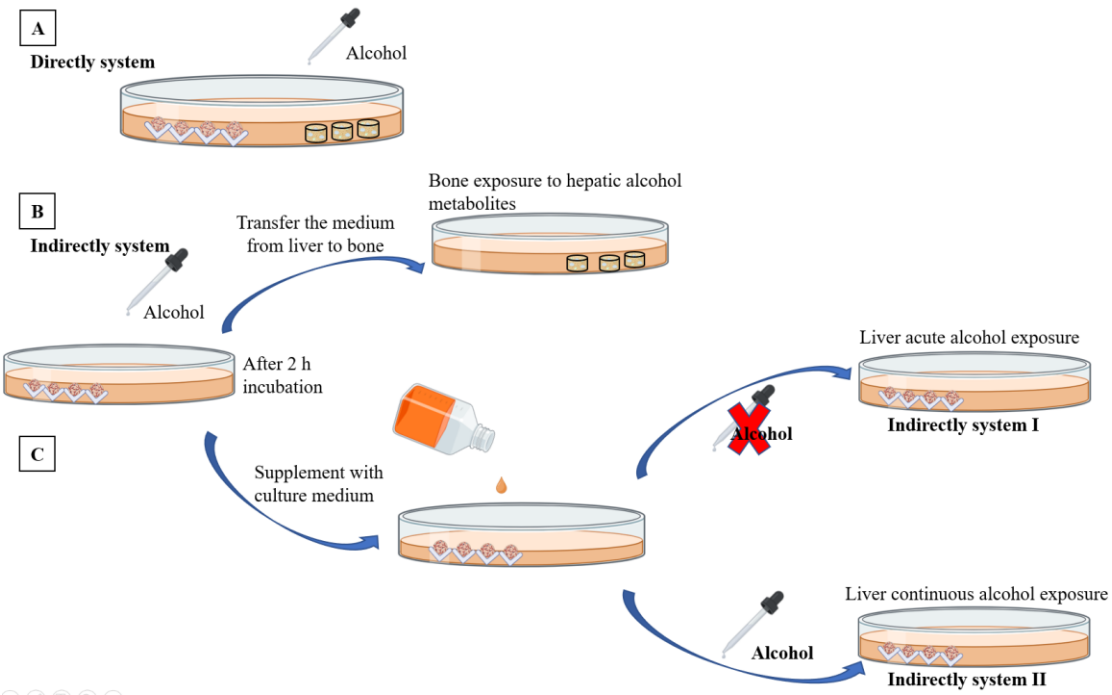

Figure 2.3 The establishment and differences between different systems. A. Direct culture system – Co-culture of liver and bone, with daily stimulation using alcohol. B. Indirect culture system – After alcohol stimulation of the liver, the medium from the liver is transferred to the bone culture. C. After transferring the medium, the liver culture was replenished with fresh medium. Indirect system I – Liver medium was replenished only with fresh medium. Indirect system II – Liver medium was replenished with fresh culture medium containing the same concentration of alcohol.

2.2.6. Mitochondrial Activity Assessment

Mitochondrial activity in liver and bone cells was evaluated using a resazurin assay, an indicator of cell viability (Zhu *et al.* 2021). In the 2D liver cell experiments, the culture medium was aspirated and the cells were rinsed three times with PBS, 100 µL of resazurin working solution (0.0025%) was transferred to each well (it was also added to the wells without cells as a blank control). For the liver microorganoids, which were carefully harvested from agarose and rinsed 3 times with PBS prior to analysis. 300 µL of resazurin working solution was used for a total of 300 liver microorganoids. From this, three 100 µL aliquots of liver microorganoids in the resazurin working solution were transferred into individual wells of a 96-well culture plate. For blank controls, 100 µL of solution lacking cells was incubated under identical conditions. Following

incubation at 37 °C, resorufin fluorescence was detected at 544 nm excitation and 590 -10 nm emission. after 30, 60, 90, and 120 min with microplate reader.

For the bone part, the scaffolds underwent three PBS washes before transferred to 48-well plate. Then, 500 µL of resazurin working solution was added promptly to the scaffolds. Scaffolds free of cells were used as background. After 2 h of incubation at 37 °C, 100 µL × 4 replicates of each scaffold sample were dispensed into a 96-well plate for fluorescence detection (excitation: 544 nm; emission: 590-10 nm). (Chen *et al.* 2025).

2.2.7. Assessment of UDP-glucuronosyltransferase (UGT) activity

A fluorescence-based assay using 4-methylumbelliferone was performed to assess the activity of UGT, representative of phase II enzyme (Hammour *et al.* 2022). A total of 200 µL 4-MU, prepared with plain medium, was applied to 300 liver microorganoids. From this mixture, 100 µL was added into new wells of a 96-well culture plate containing the liver microorganoids to generate duplicate samples. To establish a negative control, 100 µL of the working solution was added to a well without cells (Hammour et al. 2022). The plate was incubated, and fluorescence was measured at excitation/emission wavelengths of 355 /460 nm at 30, 60, 90, and 120 min by microplate reader. Data from liver microorgnaodis were normalized by DNA content.

2.2.8. Assessment of AP activity

Detection of AP activity can reflect osteogenic differentiation and cell function (Aspera-Werz *et al.* 2018). Scaffolds were washed three times at first with PBS, moved to a new 48-well plate, the reaction was carried out by incubating the samples in 500 µL of AP reaction buffer at 37 °C for 2 h. Absorbance at 405 nm was used to quantify the conversion of 4-nitrophenyl-phosphate into 4-nitrophenol. The experimental values were adjusted using a background control (consisting of cell-free scaffolds incubated in AP working solution). Data from bone scaffolds were normalized by DNA content. (Chen *et al.* 2025).

2.2.9. Assessment of Tartrate-resistant acid phosphatase (TRAP) activity

The functional activity of osteoclasts was determined through analysis of TRAP (a late-stage marker of osteoclast activity) (Zhu *et al.* 2020). Assays were performed by combining 30 μL of supernatant with 90 μL of TRAP reagent, followed by a 6-hour incubation at 37 °C. To terminate the reaction, 90 μL of 1 M NaOH was added to each well. The generated 4-nitrophenol was measured spectrophotometrically at 405 nm. Experimental readings were corrected by subtracting background values obtained from cell-free scaffolds. Data from bone scaffolds were normalized by DNA content (Chen *et al.* 2025).

2.2.10. Assessment of Carbonic anhydrase II (CAII) activity

As an early marker, CAII activity was assessed to indicate osteoclast differentiation (Zhu *et al.* 2020). Scaffolds were washed with PBS, moved to a new 48-well plate, and incubated in 500 μL of substrate solution at 37 °C for 15 min. After incubation, 100 μL of the reaction mixture containing 4-nitrophenol was measured at 405 nm with a microplate reader. Experimental readings were corrected by subtracting background values obtained from cell-free scaffolds. Data from bone scaffolds were normalized by DNA content (Chen *et al.* 2025).

2.2.11. Assessment of Total Protein *via* Sulforhodamine B (SRB) Staining

To quantify total protein, samples was determined using SRB staining. After being washed three times with PBS, cells were fixed by ethanol at −20 °C for a minimum of 1h. Then, removed the ethanol and washed with tap water once, for 30 min at room temperature, cells were incubated in 0.4% (w/v) SRB under dark conditions. To remove excess SRB, then to wash samples with 1% (v/v) acetic acid until no further dye release was observed. After solubilization of bound SRB with TRIS, absorbance was determined at 565 nm using a plate reader (Ehnert *et al.* 2018).

2.2.12. Assessment of DNA content

The DNA content was used both to determine cell numbers and for normalization of enzyme activity data (Häussling *et al.* 2019). After collection from the agarose microplate and PBS washing, liver microorganoids were incubated with 100 µL of 50 mM NaOH at 98 °C for 5 min. The solution was incubated at –20 °C for at least 24 h. The following day, they were thawed at 98 °C for 30 min and mixed with 0.1 M Tris (110 µL). Subsequently, 100 µL of the sample mixture was dispensed into a V-type 96-well plate and centrifuged for 10 min at 20,000 g. For the bone portion, scaffolds were collected first, then washed with PBS 3 times, and 98 °C 50 mM NaOH (250 µL) was added to each scaffold. After 5 min of incubation, the scaffolds were transferred to –20 °C for overnight storage. The next day, 0.1 M Tris (275 µL) was added to the thawed samples. After thorough mixing, the sample was collected, transferred into a V-type 96-well plate, and centrifuged (20,000 g, 10 min).

DNA content was quantified by absorbance in a two-step analysis using a plate reader. First, 2 µL of DNA isolation buffer was set aside as a blank control. Next, 2 µL of each DNA sample was analyzed in duplicate. Using Omega MARS analysis software (absorbance at 260 nm).

2.2.13. LC-HPLC/MS-Based analysis of CYP450 activities in liver microorganoids

Enzymatic activities of CYP2B6, CYP2D6, CYP2C9, CYP3A4, CYP1A2, and CYP2C19 were determined on days 7, 14, and 21 *via* LC–HPLC/MS-based detection. (Hoffmann *et al.* 2012, Chen *et al.* 2025). Specific CYP450 activities were determined by quantifying the metabolites formed from well-characterized substrates. Two substrate cocktails were used: Cocktail C1 contained phenacetin, testosterone, bupropion hydrochloride, and diclofenac. Cocktail C2 contained S-mephenytoin and bufuralol hydrochloride. All compounds were prepared as 10 mM stock solutions in methanol, which was subsequently evaporated. The residues were reconstituted in HepaRG plain culture medium to achieve a final dilution of 1:1000. Then, the liver microorganoids were incubated with 100 µL of both cocktails (Table 2.1 for the

substrates, reactions, incubation times, and concentration). After incubation, culture supernatants were harvested and stored at –80 °C, while cells were collected for DNA quantification. Samples from three independent experiments were pooled. Normalization of CYP450 activities to the DNA content of liver microorganoids was performed to enable comparability across samples.

Table 2.1. The substrates, reactions, incubation times, and concentration for liver microorganoids Phase I CYP enzyme activities

Enzyme	Substrate→Metabolites	Incubation time(h)	Concentration (µM)
CYP1A2	Phenacetin→ Acetaminophen	1.5	28
CYP2B6	Bupropion→ Hydroxybupropion	1.5	111
CYP2C9	Diclofenac→4'-hydroxydiclofenac	1.5	10
CYP3A4	Testosterone→ 6β- Hydroxytestosterone	1.5	55
CYP2D6	Bufuralol→ 1-OH-Bufuralol	3	10
CYP2C19	S-Mephenytion→ 4-OH-Mephenytoin	3	22

2.2.14. Semi-Quantitative reverse-transcription polymerase chain reaction (RT-PCR) analysis

To assess gene expression, RT-PCR was always performed (Zahmatkesh *et al.* 2022). Total RNA was isolated with TriFast from the 2D cells culture (30 µL), liver microorganoids (100 µL), and scaffolds (500 µL). Sample purity was ensured by centrifugation at 14,000 g for 10 min (3 times), followed by chloroform/phenol extraction. The concentration of RNA was quantified with the Omega Plate Reader, and complementary DNA was generated using a cDNA synthesis kit. According to the manufacturer's protocol, PCR amplification was performed with Biozym Red HS Taq Master Mix. The primer sequences and PCR parameters for the target genes are provided in Table 2.2. 18S rRNA served as the internal reference gene. A 1.5% (w/v) agarose gel with ethidium bromide was employed for PCR product visualization. Electrophoresis was performed at 90 V for 50 min, and band intensities were quantified with ImageJ software.

Table 2.2. Details of primer for gene analysis

Gene	Accession Number	Forward Primer (5'–3')	Reverse Primer (3'–5')	Length (bp)	Temperature (◦C)
FAPα	NM_004460.5	CATCTGGAAAAAT GAAGACTTGGGT	CCGATCAGGTGA TAAGCCGT	338	60
CYP2E1	NM_000773.3	GACTGTGGCCGA CCTGTT	ACTACGACTGTG CCCTTGG	296	59
SNAIL1	NM_005985.3	ACCACTATGCCGC GCTCTT	GGTCGTAGGGCT GCTGGAA	115	62
SNAIL2	NM_003068.5	ACAGCGAACTGG ACACACAT	GAGAGAGGCCA TTGGGTAGC	168	60
RUNX2	NM_001024630.4	CTGTGGTTACTGT CATGGCG	GGGAGGATTTGT GAAGACGGT	170	60
PPARγ	NM_138712.5	TCGAGGACACCG GAGAGGG	AAGTTGGTGGGC CAGAATGG	162	62
SOX9	NM_000346.3	GAAGGACCACCC GGATTACA	GCCTTGAAGATG GCGTTGG	120	60
18S	NR_003286	GGACAGGATTGA CAGATTGAT	AGTCTCGTTCGT TATCGGAAT	111	56

2.2.15. Dot blot analysis

Proteins released into the culture supernatant were identified by dot blot analysis (Häussling *et al.* 2019). Using a 96-well dot blotter, to perform the assay, 100 µL of supernatant was loaded onto a moistened nitrocellulose membrane with the aid of a vacuum pump. Ponceau S staining was performed to detect protein spots on the membrane and to provide a loading control for normalization. Membranes were washed with TBS-T (3 times) and subsequently kept in 5% bovine serum albumin (BSA) prepared in TBS-T for 1 h to block nonspecific protein interactions. The appropriate

primary antibody was applied to the membranes and incubated overnight at 4 °C. The antibody details are summarized in Table 2.3. After TBS-T washes, incubation with secondary antibody was performed for 2 h, and signals were detected by chemiluminescence, using 90 mM p-coumaric acid in 30% (v/v) hydrogen peroxide, and quantified by ImageJ.

2.2.16. Western blotting

On days 7, 14, and 21, samples from the bone co-culture system were collected for protein analysis. Following PBS washing, cells were incubated with freshly prepared ice-cold RIPA buffer with added protease and phosphatase inhibitors to achieve lysis. The concentration of protein was detected by Lowry. Proteins (50 µg per sample) were fractionated by SDS–PAGE based on molecular weight and then transferred onto membranes. Membranes were incubated for 1 h at room temperature in 5% (v/v) BSA in TBS-T to block nonspecific interactions. Then, the appropriate primary antibody was applied to the membranes and incubated overnight at 4 °C. The antibody details were recorded in Table 2.3. The following day, after three washes with TBS-T, membranes were incubated with HRP-conjugated secondary antibody for 2 h at room temperature. For signal detection, the membranes were treated with enhanced chemiluminescence substrate for 1 min. Chemiluminescent signals were visualized using a CCD camera system, and densitometric analysis was performed by using ImageJ (Zahmatkesh *et al.* 2022).

Table 2.3. List of antibodies used in this study

Primary antibody	Host	Company	Cat. No	Dilution
TGFβ-1	Mouse	Santa Cruz Biotech	sc-130348	1:1000
PINP	Rabbit	Abbexa	abx131414	1:1000
TNAP	Goat	Santa Cruz Biotech	sc-23430	1:1000
TRAP	Rabbit	Abcam	ab191406	1:1000
NTX	Rabbit	Cloud clone corp	PAA639H401	1:1000
MMP9	Mouse	Santa Cruz Biotechnology, Heidelberg, Germany	sc-21733	1:1000
BMP2	Mouse	Santa Cruz Biotechnology, Heidelberg, Germany	sc-137087	1:1000
BMP9	Mouse	Santa Cruz Biotechnology, Heidelberg, Germany	sc-514211	1:1000
BMP13	Mouse	Santa Cruz Biotechnology, Heidelberg, Germany	sc-374184	1:1000
CYP2E1	Rabbit	Santa Cruz Biotechnology, Heidelberg, Germany	sc-133491	1:200
Phospho-Smad 1/5	Rabbit	Cell Signaling	9516	1:1000
Phospho-p38	Rabbit	Cell Signaling	4511	1:1000
HPRT	Mouse	Santa Cruz Biotechnology,	sc-376938	1:1000
Secondary antibody		**Company**	**Cat. No**	**Dilution**
Mouse anti-rabbit IgG-		Santa Cruz Biotechnology,	sc-2357	1:10000
Anti-Mouse IgG HRP-		Santa Cruz Biotechnology,	7076	1:10000
Donkey Anti Goat IgG		Santa Cruz Biotechnology,	sc-2020	1:10000

2.2.17. Mineral content of bone scaffolds

After being collected, scaffolds were rinsed with PBS, fixed in 4% formaldehyde and stored in PBS until further analyses. Bone scaffold mineralization was evaluated with a clinical 128-slice computed tomography (CT) scanner. Scans were acquired with 80 kV tube voltage, 500 mA current, 16 × 0.3 mm collimation, 0.4 mm slices, and a pitch of 0.4. Data were reconstructed using a V80u high-resolution kernel with level-5 iterative reconstruction and displayed in bone window mode. The axial field of view was about 10 × 10 cm with a resolution of 512 × 512 pixels. For image processing, DICOM files were managed in ImageJ using the 'DICOM Sort' plugin. To evaluate mineralization, image stacks were cropped to the ROI, and the mean integrated density of each scaffold was determined and normalized to a calibration block (Phantom EFP-06-96) (Weng *et al.* 2020, Chen *et al.* 2025).

2.2.18. Stiffness of bone scaffold

The stiffness of the scaffolds was evaluated by calculating the Young's modulus (Weng *et al.* 2020). Scaffolds were compressed uniaxially to 10% of their original height at a speed of 5 mm/min for four cycles using a ZwickiLine Z 2.5TN material testing machine. The applied load was measured in real time with an X-force HP 5N sensor, and stress–strain curves were generated from load–deformation data using the scaffold's initial height and area. To evaluate scaffold stiffness, Young's modulus was derived from the linear elastic portion of the stress–strain curve using the following equation:

$$\text{Young's modulus [MPa]} = \frac{applied\ force\ [N]\ \times initial\ scaffold\ height\ [mm]}{area\ of\ the\ scaffold\ [mm^2]\ \times change\ in\ height\ [mm]}$$

2.2.19. Statistical methods

Box plots were used to present the data, with the median, interquartile range, and minimum and maximum values indicated. All experiments were independently

repeated a minimum of three times, each with 2–3 technical replicates. Statistical analysis was performed with GraphPad Prism version 9.0. Differences between two groups were assessed with the Mann–Whitney U test. Comparisons among multiple groups were carried out with the non-parametric Kruskal–Wallis test, and significant differences were further analyzed using Dunn's multiple comparisons test. **Selection of statistical methods was carried out in consultation with Dr. Johann Jacoby, Institute of Clinical Epidemiology and Applied Biometry, University of Tübingen.**

Chapter 3

3. Results

3.1 *In vitro* liver microorganoids maintain the viability and function for a minimum 21 days

Mitochondrial activity and total DNA content were measured on days 7, 14, and 21 of culture to determine the viability of the *in vitro* liver microorganoid model. The results demonstrated a progressive increase in both parameters over time, indicating sustained viability of the liver microorganoids for at least 21 days (Figure 3.1 a, b). Regarding the functional assessment, UGT activity increased continuously over time.

We also tested the activity of related CYP 450s, CYP2C9 (Figure 3.1 c) activity exhibited a steady increase from day 7 to day 21. CYP2B6 activity (Figure 3.1 d) showed a slight decline on day 14, followed by a notable rise on day 21. In contrast, CYP1A2 and CYP2C19 activity (Figure 3.1 g, h) peaked on day 14 before declining on day 21. CYP3A4 and CYP2D6 activity showed a continuous downward trend. Although not all CYP450s showed sustained upregulation over time, the presence of functional activity indicates preserved metabolic capacity, enabling further experimental applications.

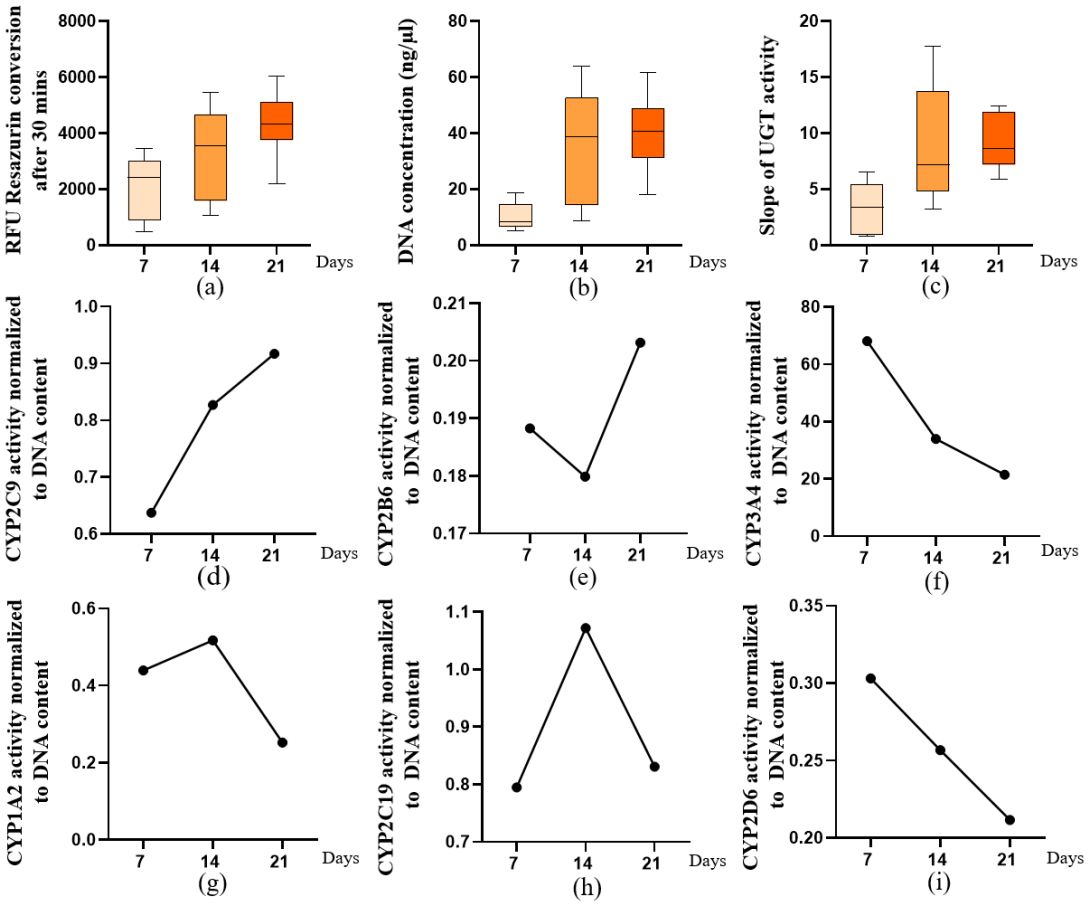

Figure 3.1 Viability and function of liver microorganoids. Liver microorganoids were generated with differentiated HepaRG, LX-2, and HUVEC using aggrewell technology. Viability and function of liver microorganoids were evaluated at days 7, 14, and 21. Cell viability was assessed by (a) mitochondrial activity determined by resazurin conversion (expressed as relative fluorescence units) and (b) total DNA content. UGT activity, normalized to DNA content, was used to evaluate phase II metabolic function as an indicator of the functional capacity of liver microorganoids. Differences among groups were evaluated using the Kruskal–Wallis test with Dunn's post hoc test for multiple comparisons. Results are presented as box plots displaying the median, interquartile range (25th–75th percentile), and extreme values (minimum and maximum). N = 3, n = 3. Phase I enzyme activities were assessed by measuring CYP2C9 (d), CYP2B6 (e), CYP3A4 (f), CYP1A2 (g), CYP2C19 (h), and CYP2D6 (i), with activities normalized to DNA content. Data were derived from pooled samples (N = 3, n = 2) collected from three independent experiments.

3.2 Differential cytotoxic effects of alcohol on human liver cell lines on day 7

To detect the cytotoxicity by different concentration of alcohol, we exposed cells to alcohol (50–200 mM) each day for 7 days. After this alcohol stimulation, the

mitochondrial activity of differentiated HepaRG cells (Figure 3.2 a) indicated a dose-dependent decrease in viability, which was significantly reduced at 200 mM alcohol ($p = 0.037$) . Correspondingly, SRB staining (Figure 3.2 b) showed a slight decrease in total protein content, but it was not significant. For LX-2 cells, both mitochondrial activity and total protein content tended to decline with higher alcohol concentrations (Figure 3.2c, d); however, these differences did not reach statistical significance. HUVEC cells results were similar to the differentiated HepaRG cells results: The mitochondrial activity assay (Figure 3.2 e) showed a significant decrease at the150 and 200 mM alcohol concentrations ($p = 0.0163$ and $p = 0.0003$). SRB staining (Figure 3.2 f) demonstrated a continuous decline in the protein content, particularly at 200 mM alcohol. The findings indicate potential hepatotoxic effects of alcohol at elevated concentrations. Notably, alcohol exerted differential toxicity across the tested cell types. HUVECs showed a significant decrease in mitochondrial activity starting at an alcohol concentration of 150 mM, indicating higher sensitivity. In contrast, HepaRG cells only exhibited a comparable significant decline at 200 mM, suggesting they are more resistant to alcohol-induced toxicity. This differential response underscores the varying susceptibility of different cell types to alcohol exposure.

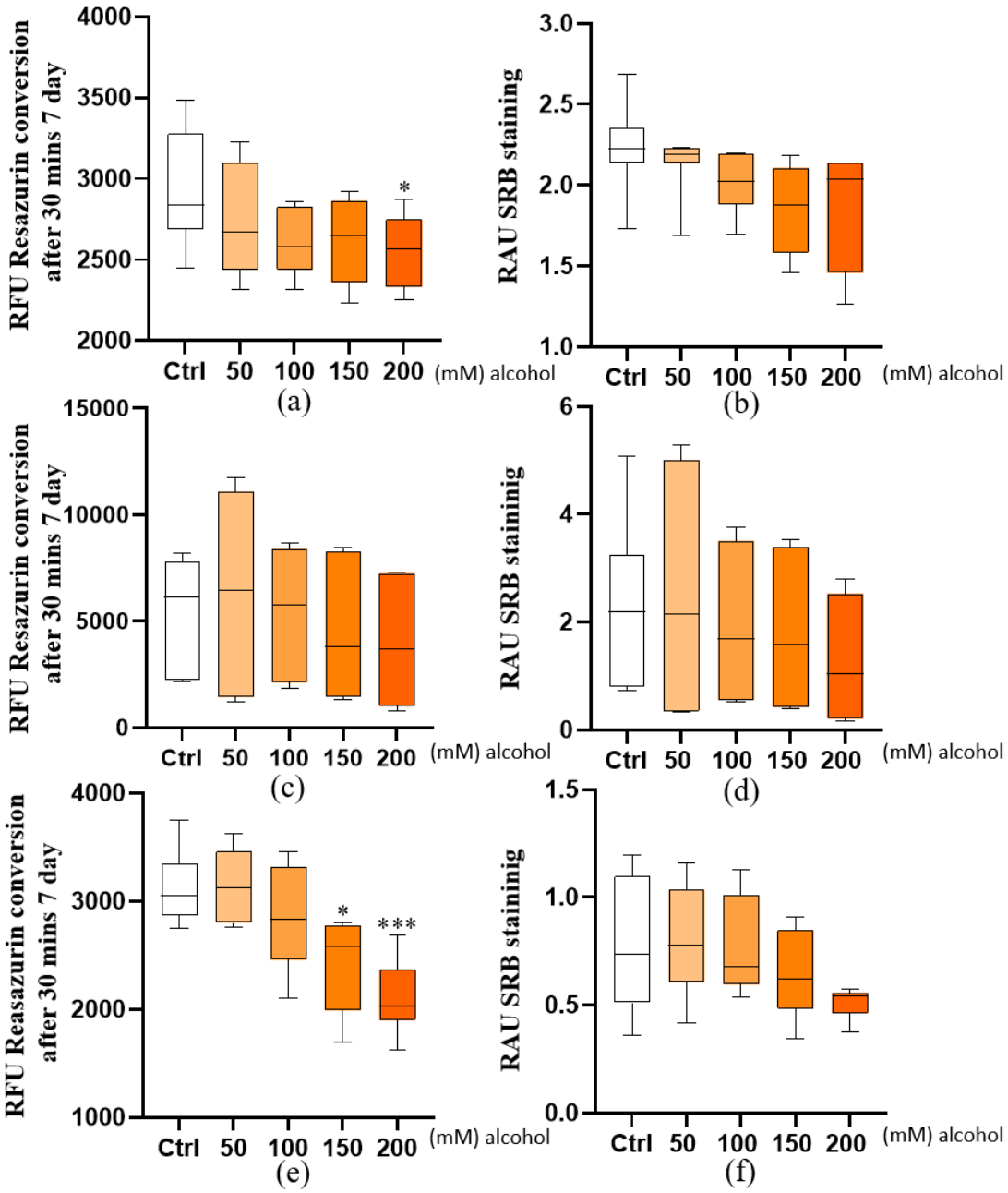

Figure 3.2 Liver cell types specific response to alcohol exposure. Differentiated HepaRG (a, b), LX-2 (c, d), and HUVEC (e, f) cells were exposed daily to alcohol at concentrations of 50, 100, 150, and 200 mM. Cell viability was assessed based on mitochondrial activity (a, c, e) and total protein (b, d, f). Differences among groups were evaluated using the Kruskal–Wallis test with Dunn's post hoc test for multiple comparisons. Results are presented as box plots displaying the median, interquartile range (25th–75th percentile), and extreme values (minimum and maximum). Significance levels were indicated as: * $p < 0.05$, *** $p < 0.001$ (compared with the control group). N = 3, n = 3.

3.3 2D and 3D liver co-culture system exhibit different responses to alcohol

concentrations

Although the 150 and 200 mM alcohol concentrations exerted toxic effects on individual cell types, we wanted to evaluate whether those effects also occurred in the co-culture system. Thus, we exposed both the 2D and 3D liver co-culture models to alcohol (50–200 mM) each day for 7 days. In 2D cultures, mitochondrial activity measured by the resazurin assay (Figure 3.3 a) showed a modest decline at higher alcohol concentrations, while SRB staining was used to quantify the total protein content (Figure 3.3 b) remained relatively stable, with no significant changes. In contrast, the 3D models exhibited a marked decrease in cell viability. was significantly reduced in a dose-dependent manner, with 200 mM alcohol inducing a profound loss of viability ($p = 0.0001$). DNA quantification (Figure 3.3 d) further confirmed reduced cellular content at higher doses.

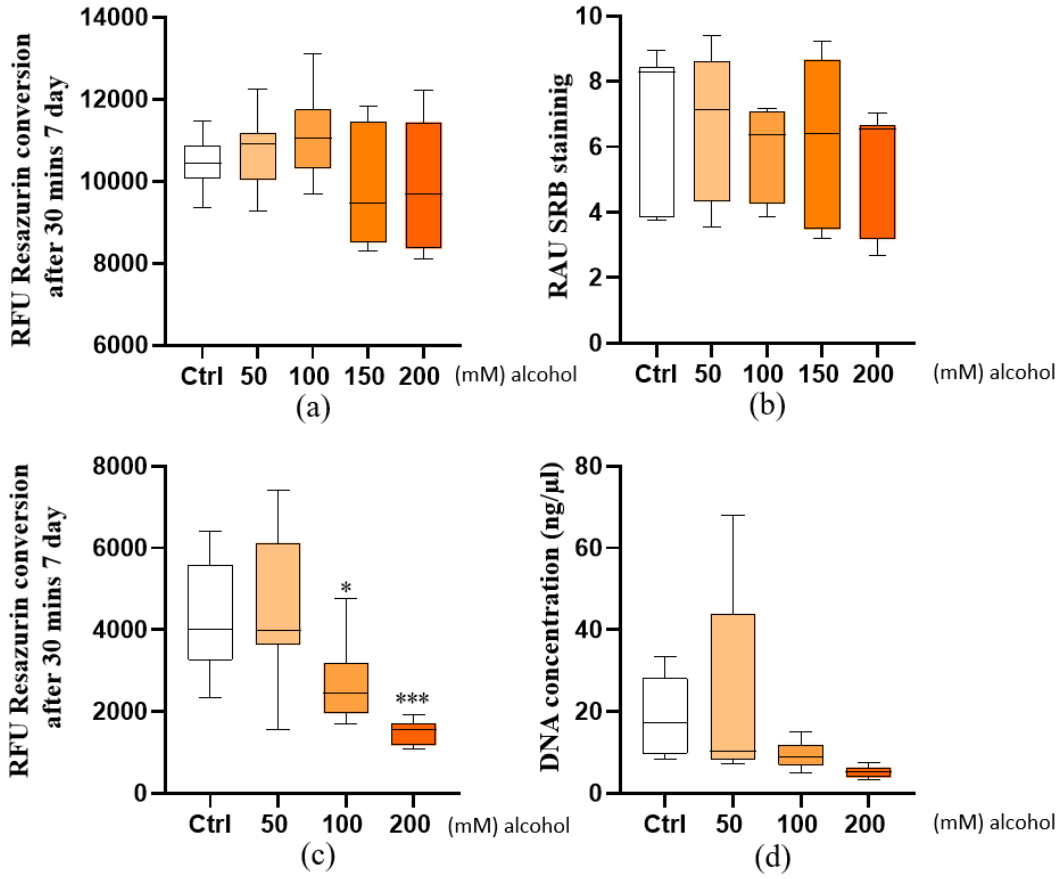

Figure 3.3 Alcohol toxicity on liver 2D and 3D co-culture systems. Liver co-culture systems were daily exposed to different alcohol concentrations for 7 days. Cell viability was assessed using mitochondrial activity in 2D (a) and 3D (c), total protein in 2D (b) and total DNA (c). Differences among groups were evaluated using the Kruskal–Wallis test with Dunn's post hoc test for

multiple comparisons. Results are presented as box plots displaying the median, interquartile range (25th–75th percentile), and extreme values (minimum and maximum). Significance levels were indicated as: * $p < 0.05$, *** $p < 0.001$ (compared with the control group). N = 3, n = 3.

3.4 Effects of Daily Alcohol Exposure on the Bone Co-Culture System

We investigated the effects of alcohol on the bone system by culturing the 3D bone co-culture model under different alcohol concentrations for 14 days. The viability and function of the bone system were determined at 2, 7, and 14 days after treatment. Mitochondrial activity (Figure 3.4 a) showed no significant changes across the different alcohol concentrations. Although, the DNA content (Figure 3.4 b) increased over time in all groups, indicating cellular proliferation, it was not affected by alcohol exposure. Bone system function was further evaluated through AP activity (Figure 3.4c), a marker of osteoblastic function, which revealed no significant differences between control and alcohol-treated groups. Likewise, TRAP activity (Figure 3.4 d), indicative of osteoclast function, remained unchanged. These results suggest that alcohol had no measurable effect on the viability and function of the bone co-culture system under the tested conditions.

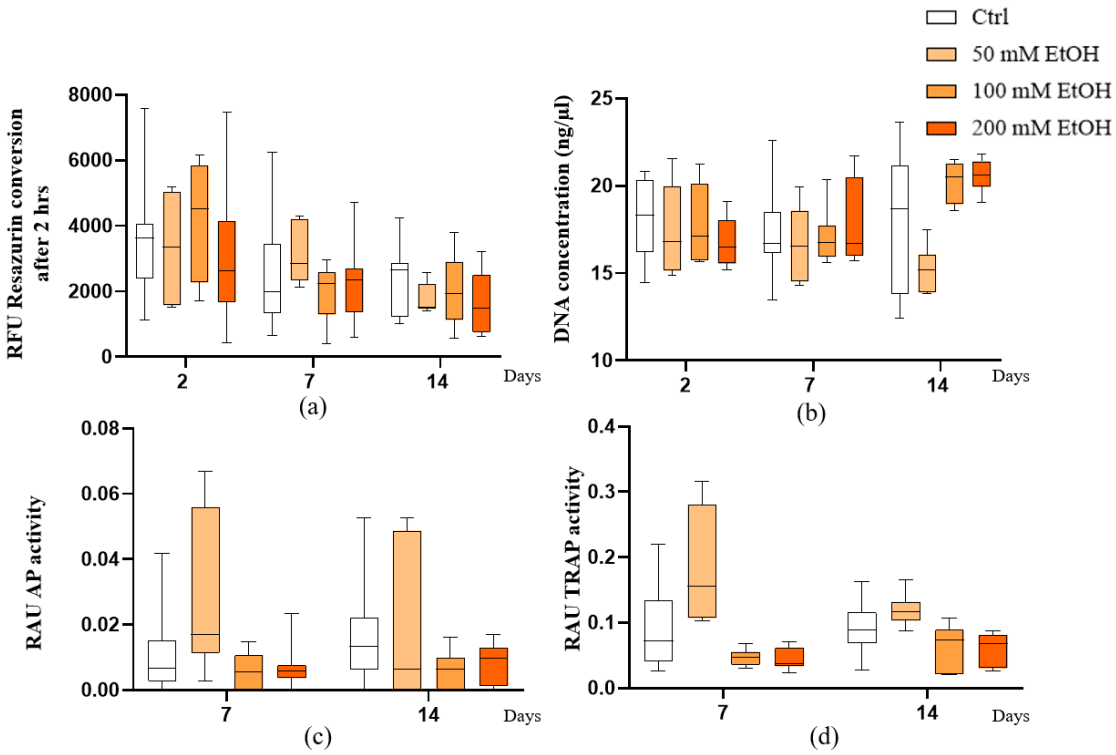

Figure 3.4 Alcohol-induced toxic effects in 3D bone co-culture systems. To monitor viability of the bone co-culture system under varying alcohol concentrations, mitochondrial activity and DNA content (a, b) were measured at days 2, 7, and 14. For the osteoblast function, AP activity (c) was used as a marker of early osteogenic differentiation. For osteoclast function, TRAP activity (d) was assessed as an indicator of bone resorption activity. Differences among groups were evaluated using the Kruskal–Wallis test with Dunn's post hoc test for multiple comparisons. Results are presented as box plots displaying the median, interquartile range (25th–75th percentile), and extreme values (minimum and maximum). Data all compared with control group. N = 3, n = 3.

3.5 Effects of daily exposure to 100 mM alcohol on the *in vitro* liver-bone system

According to the alcohol toxicity results, we selected 100 mM alcohol to stimulate the *in vitro* liver–bone co-culture system. Viability of liver and bone cells was assessed at days 7, 14, and 21, alongside evaluation of the effects of hepatic alcohol metabolism on bone function. In the liver compartment, mitochondrial activity and the DNA content (Figure 3.5 a, b) increased progressively over time in the control group, whereas both parameters remained consistently low in the alcohol-treated group starting from day 7. Similarly, in the bone part, mitochondrial activity in controls peaked on day 14, whereas in the alcohol-treated group, it declined significantly throughout the experiment (Figure

3.5 c). The DNA content (Figure 3.5 d) in the bone cells also showed a tendency to decrease in response to alcohol exposure, especially on day 14. For the bone co-culture system, no significant differences in osteoblast activity were observed between control and alcohol-treated groups, and osteoblast function in the alcohol-treated group remained relatively constant throughout the study (Figure 3.5 e). Conversely, alcohol exposure markedly suppressed osteoclast function (Figure 3.5f) across all examined time points ($p < 0.0001$). Based on results, 100 mM alcohol exerted significant cytotoxicity to the liver–bone co-culture system. Therefore, we used a lower alcohol concentration of 50 mM in subsequent experiments to better preserve cell viability while still modeling alcohol-induced effects.

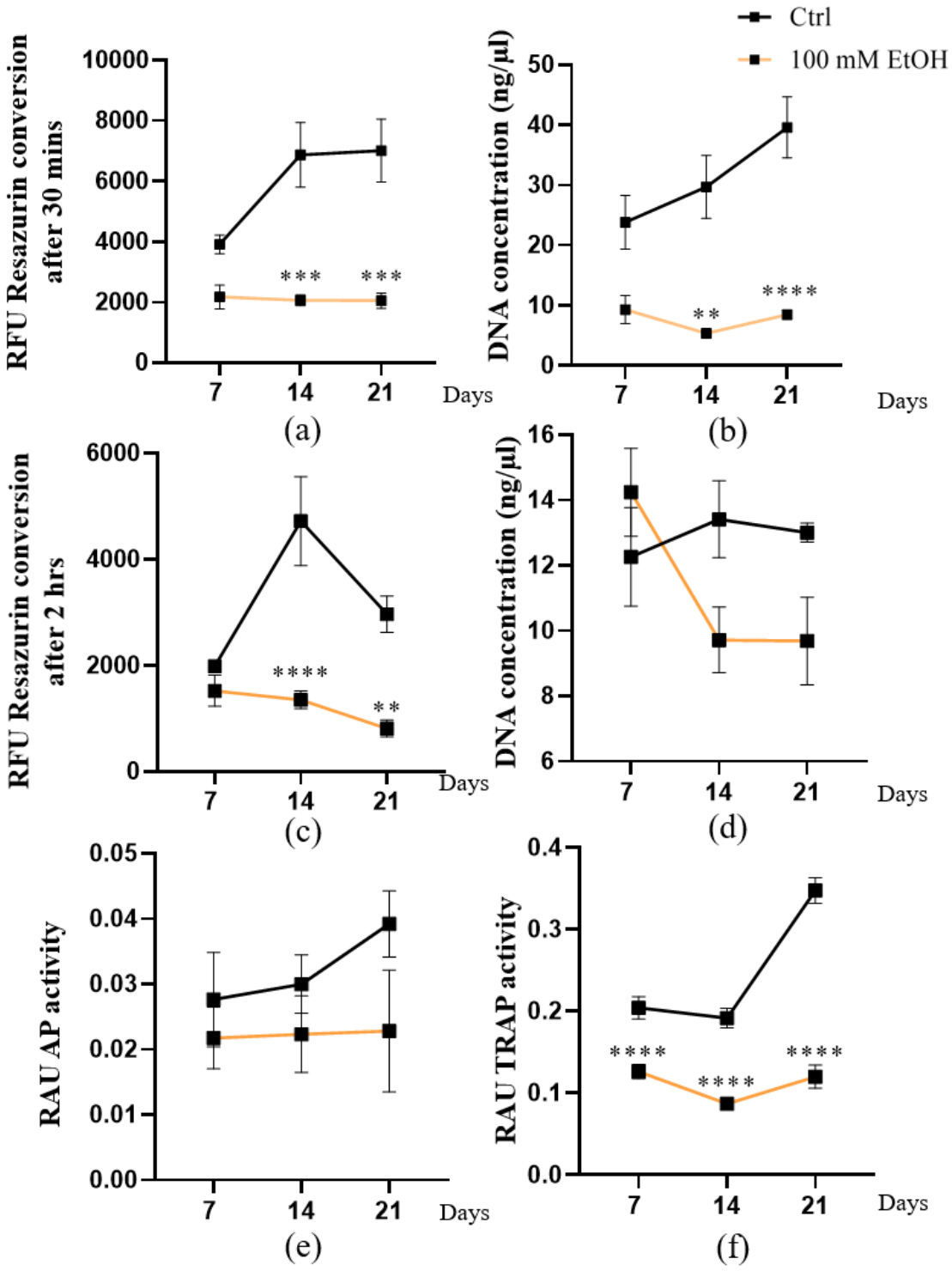

Figure 3.5 The *in vitro* liver–bone co-culture system was exposed to 100 mM alcohol daily for 21 consecutive days. Viability of the liver (a, b) and bone (c, d) systems was assessed on days 7, 14, and 21 by measuring mitochondrial activity and total DNA content. To investigate the effects of alcohol on bone function following hepatic metabolism, AP and TRAP activities (e, f) were measured as functional markers of osteoblasts and osteoclasts, respectively, at each time point. Differences were evaluated by two-way ANOVA with Tukey's post hoc test. Results are displayed as line charts and reported as mean ± SEM, Significance levels were indicated as: ** p

< 0.01, *** p < 0.001, and **** p < 0.0001 (compared with the control group). N = 3, n = 3.

3.6 Sustained viability of the liver–bone co-culture system exposed to 50 mM alcohol

Next, exposure of the co-culture system to 50 mM alcohol was carried out to examine its effects on the individual components of the liver–bone system. Mitochondrial activity (Figure 3.6a), used as a marker of bone viability in the co-culture system, showed a time-dependent increase in both the control and alcohol-treated groups. However, a significant reduction was observed in the alcohol-treated group on day 21 ($p = 0.0017$). In contrast, no significant differences in DNA content (Figure 3.6b) or LDH release (Figure 3.6c) were observed between the two groups at any time point. These results indicate that in the liver–bone co-culture system, liver-derived factors produced under alcohol exposure may impair the viability of bone cells without causing obvious cytotoxicity. For liver microorganoids, mitochondrial activity (Figure 3.6 d), DNA content (Figure 3.6 e), and LDH release (Figure 3.6 f) showed similar trends between the control and alcohol-treated groups over 21 days. These results indicate that the activity of the liver part of the co-culture is stabilized when exposed to 50 mM alcohol. Overall, these results demonstrate that the liver–bone co-culture system maintains cellular viability and integrity under daily exposure to 50 mM alcohol at least 21 days.

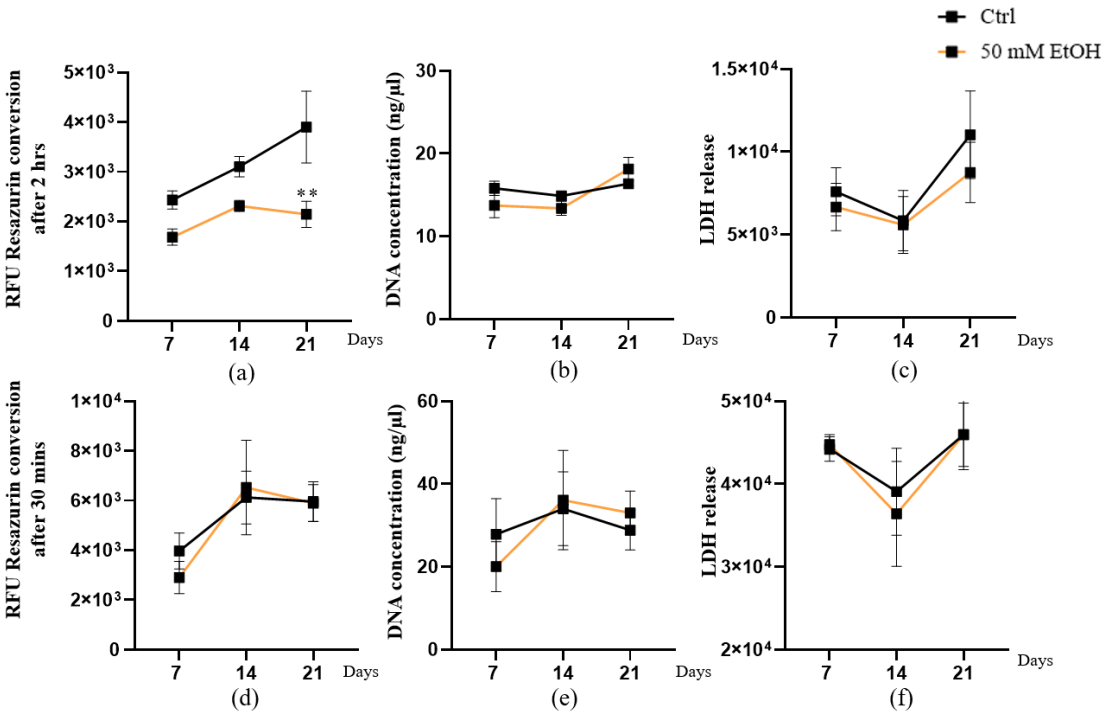

Figure 3.6 Effects of 50 mM alcohol exposure over 21 days on the viability of liver and bone in the co-culture system. Mitochondrial activity, total DNA content, and LDH release were determined on days 7, 14, and 21 after daily exposure to 50 mM alcohol to assess changes in the viability of the respective components of the bone (a–c) and liver (d–f) in the coculture system. Differences were evaluated by two-way ANOVA with Tukey's post hoc test. Results are displayed as line charts and reported as mean ± SEM. Significance levels were indicated as: **p < 0.01 (compared with the control group). N = 3, n = 3.

3.7 Daily alcohol exposure induces LX-2 cell activation and fibrotic features in liver microorganoids

After continuous exposure of liver microorganoids to 50 mM alcohol, there were significant changes in metabolic and fibrotic markers over time. The expression of CYP2E1 (Figure 3.7a), a major enzyme in alcohol metabolism, showed a gradual rise in the alcohol-treated group, reaching a significant increase by day 21 ($p = 0.0188$). Consistently, CYP2E1 protein levels (Figure 3.7b) were elevated in the alcohol-treated group across all time points, reaching statistical significance on day 21 ($p < 0.0001$). These results suggest that alcohol is metabolized within the liver microorganoids *via* the CYP2E1. Within 48 h of alcohol stimulation, *FAPα* (Figure 3.7 c), a marker gene associated with HSC activation, showed significant upregulation in the alcohol-treated group ($p = 0.0039$). As alcohol was metabolized in the liver, TGF-β1 secretion—a

central mediator of HSC activation and ECM deposition—was markedly increased at all time points in the alcohol-treated group (Figure 3.7 d) ($p = 0.0045$, $p = 0.0003$, and $p < 0.0001$). We focused on this target because TGF-β plays a central role in liver fibrosis, driving HSC activation and ECM deposition, which are critical processes in alcohol-induced liver injury. Moreover, SNAIL1 and SNAIL2, encoding central epithelial-mesenchymal transition (EMT) transcription factors, showed time-dependent changes in expression. In the alcohol-treated group, *SNAIL1* expression (Figure 3.7 e) showed a slight increase on day 7, a decrease on day 14 ($p = 0.0013$), and a significant upregulation on day 21 ($p < 0.0001$). *SNAIL2* showed a similar pattern (Figure 3.7 f), which also displayed a significant increase by day 21 ($p < 0.0001$).

To evaluate the downstream effects and validate of alcohol-induced liver damage, we examined tissue non-specific alkaline phosphatase (TNAP) and procollagen type I N-terminal propeptide (PINP) protein expression. TNAP is a clinically relevant biomarker commonly used to assess liver damage, particularly in conditions such as cholestasis and hepatocellular injury. In such pathological states, TNAP typically remains elevated in the serum (Zeng *et al.* 2023, Thakur *et al.* 2024). In parallel, PINP, a recognized serum biomarker of collagen synthesis, is widely used to indicate fibrogenesis and liver fibrosis progression (Gressner *et al.* 2007, Veidal *et al.* 2010). Together, these markers provide insight into both functional liver injury and early fibrotic responses following alcohol exposure. Alcohol exposure significantly elevated PINP protein expression at multiple time points, especially on day 21 (Figure 3.7 g), indicating enhanced type I collagen synthesis in the liver part ($p = 0.0319$). At the same time, TNAP was also upregulated, showing an increasing trend on days 7 and 14, and marked elevation on day 21 (Figure 3.7 h), suggesting the advancement of fibrogenic remodeling and further establishment of the pathological model ($p = 0.0012$). In contrast, the protein expression of matrix metalloprotein 9 (MMP9)-an enzyme involved in the breakdown of ECM-was significantly reduced in the alcohol-treated group on day 21 (Figure 3.7i), suggesting decreased matrix degradation and a progressive accumulation of ECM ($p < 0.0001$). MMP9 was specifically assessed because it is involved in the breakdown of

ECM components; its downregulation is commonly associated with impaired matrix turnover and the progression of liver fibrosis (Wang *et al.* 2024). These findings suggest that 50 mM alcohol can induce sustained fibrotic signaling and collagen deposition in liver microorganoids, supporting our subsequent exploration of the liver–bone axis.

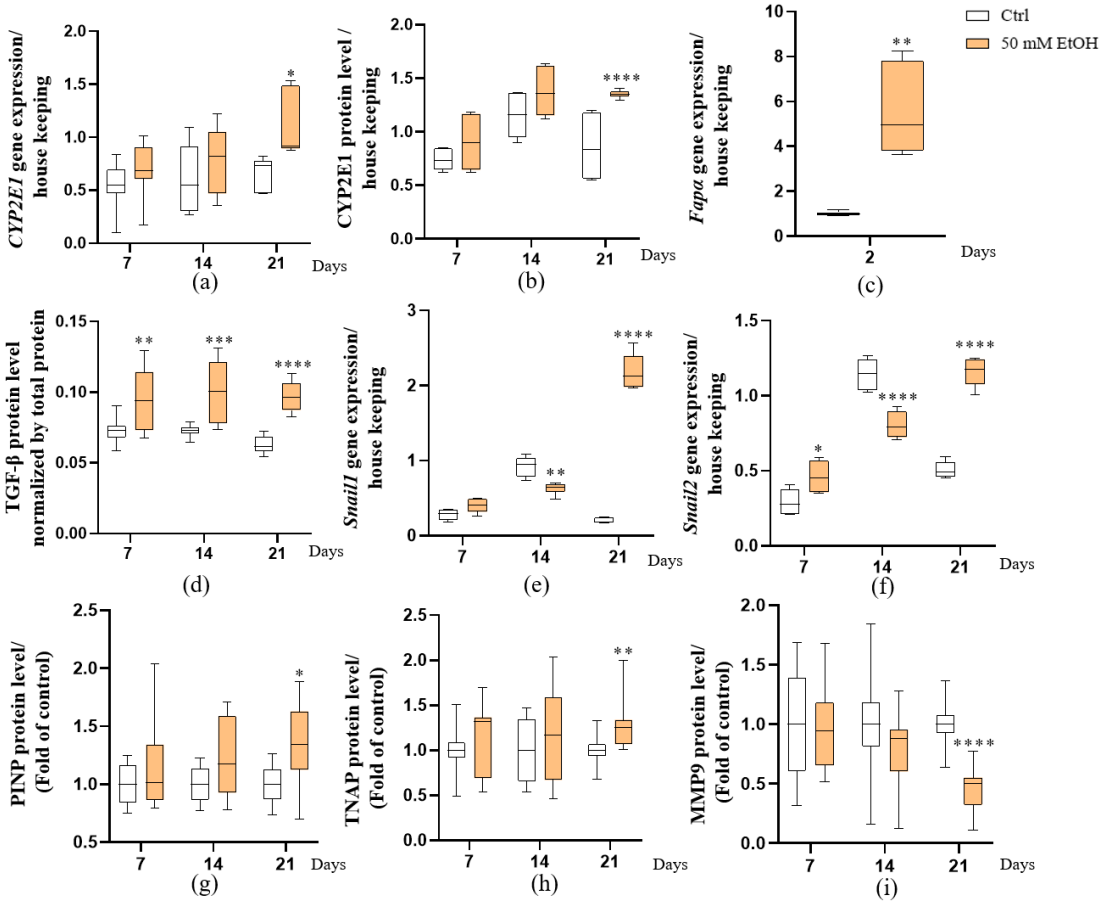

Figure 3.7 Long-term exposure to 50 mM alcohol induces a fibrotic phenotype in liver microorganoids. The gene (a) and protein (b) expression of *CYP2E1*, the primary alcohol-metabolizing enzyme in the liver, was assessed at days 7, 14, and 21. TGF-β1 protein levels (c) in the supernatant were measured as an indicator of fibrosis. Activation of hepatic stellate cells was evaluated by detecting fibroblast activation protein alpha (*FAPα*) (d) after 48 hours alcohol stimulation. Markers of EMT *snail1, snail2* (e, f) in liver microorganoids were analyzed on days 7, 14, and 21. Additionally, protein levels of PINP (g), TNAP (h), and MMP9 (i) were measured over time to assess collagen accumulation, inflammation and fibrosis progression, and ECM deposition, respectively. Differences among groups were evaluated using the Kruskal–Wallis test with Dunn's post hoc test for multiple comparisons. Results are presented as box plots displaying the median, interquartile range (25th–75th percentile), and extreme values (minimum and maximum). Significance levels were indicated as: *p < 0.05, ** p < 0.01, ***p < 0.001, and **** p < 0.0001 (compared with the control group). N = 3, n = 3.

3.8.1 Bone response to alcohol metabolism in the direct and indirect liver–bone co-culture systems

We determined osteoblast and osteoclast activity as well as the DNA content to investigate the effects of alcohol in direct/indirect liver–bone co-culture systems on bone cells function.

In the direct system (Figure 2.3), AP activity (Figure 3.8.1 1a), an indicator of osteoblast function, increased steadily from day 7 to day 21 in both groups, reaching its highest level on day 21. In contrast, AP activity was consistently reduced in the alcohol-treated group, reaching significance on day 21 ($p = 0.0105$), indicating impaired osteoblast function. CAII and TRAP activities (Figure 3.8.1 1b, c), which represent osteoclast function, increased moderately from day 7 to day 14 in both groups but showed different trends on day 21 in the alcohol-treated group. On day 21, CAII was significantly reduced in the alcohol-treated group ($p = 0.0005$), while TRAP showed a downward trend, suggesting that alcohol exposure also suppressed osteoclast activity.The DNA content (Figure 3.8.1 1d) increased over time in both groups, reflecting continued proliferation or activity of the cells, suggesting that alcohol affected only bone function.

In indirect system I (Figure 2.3), AP activity (Figure 3.8.1 2a) in the alcohol-treated group showed a downward trend on days 14 and 21. CAII activity (Figure 3.8.1 2b) remained relatively stable compared with the control group. However, TRAP activity (Figure 3.8.1 2c) was significantly reduced, particularly on day 14 ($p = 0.0383$). The DNA content (Figure 3.8.1 2d) also remained relatively stable. In indirect system II (Figure 2.3), the changes in osteoblast and osteoclast activity were mostly similar to those in indirect system I, and the relative AP activity (Figure 3.8.1 3a) in the alcohol-treated group also showed a downward trend on days 14 and 21. CAII activity remained unchanged throughout the experiment (Figure 3.8.1 3b). However, TRAP activity (Figure 3.8.1 3c) decreased significantly on day 21 ($p = 0.0044$), and the DNA content (Figure 3.8.1 3d) remained relatively stable. Together, the results indicate that indirect stimulation may attenuate the activity of both osteoblasts and osteoclasts.

These results demonstrated that osteoblast and osteoclast activities were all higher in the direct system than in the two indirect systems. Adding alcohol to the direct system

promotes stronger liver–bone responses, while the indirect system may not be able to fully stimulate cell function under the current situation.

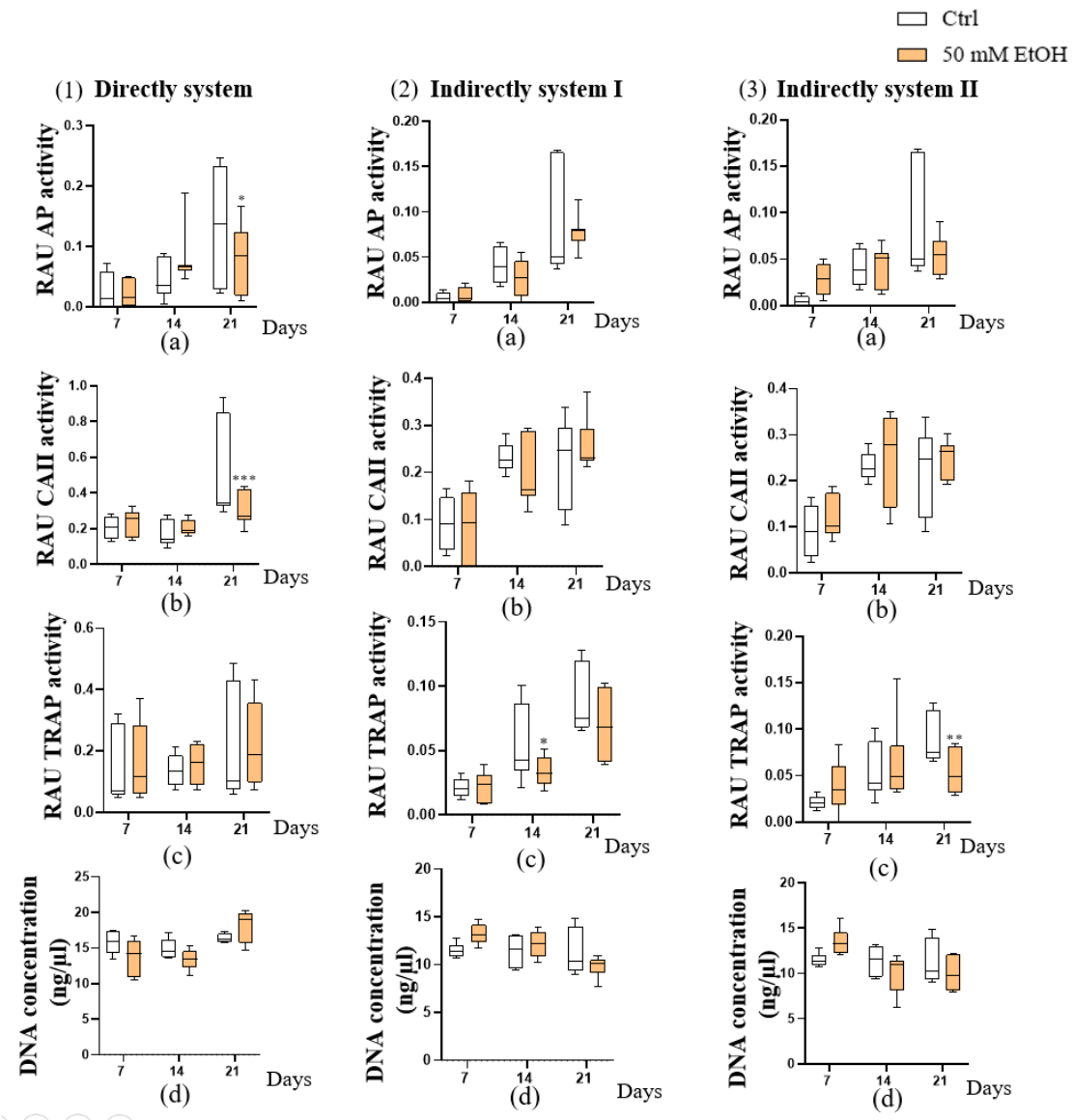

Figure 3.8.1 Construction of different model systems and evaluation of bone function. Direct system—liver spheroids and bone scaffolds were co-cultured in the same well. Indirect system—liver and bone cultures were cultured in separate wells, liver was stimulated with alcohol for 2h, and the supernatant was transferred to the bone culture while the liver received medium containing alcohol Indirect system I or fresh medium Indirect system II. Functional assessments of bone cells performed across the three experimental systems at days 7, 14, and 21: (a) AP activity for osteoblast function; (b) CAII activity and (c) TRAP activity for osteoclast function; and (d) DNA concentration. Differences among groups were evaluated using the Kruskal–Wallis test with Dunn's post hoc test for multiple comparisons. Results are presented as box plots displaying the median, interquartile range (25th–75th percentile), and extreme values (minimum and maximum). Significance levels were indicated as: *$p < 0.05$, ***$p < 0.001$ (compared with the control group). N $\geqslant$3, n $\geqslant$ 3.

3.8.2 Daily exposure of the liver–bone system to 50 mM alcohol induce osteoporotic characteristics in bone scaffolds

Bone scaffold stiffness and mineral density were assessed on day 28 after daily exposure to 50 mM alcohol in the liver–bone co-culture system. This exposure significantly reduced both the mineral density and stiffness of the bone scaffolds in the directly system (Figure 3.8.2 a, b). Both indirect co-culture systems also exhibited a downward trend (Figure 3.8.2 c, d). In contrast, the bone co-cultures exposed to alcohol alone showed no significant changes (Figure 3.8.2 e, f). These findings suggest that the observed deterioration in bone quality within the liver–bone system is likely mediated by liver-derived alcohol metabolites, rather than due to the direct effect of alcohol on bone co-culture system. Since the direct system more closely mimics *in vivo* conditions, we employed it in the following experiments.

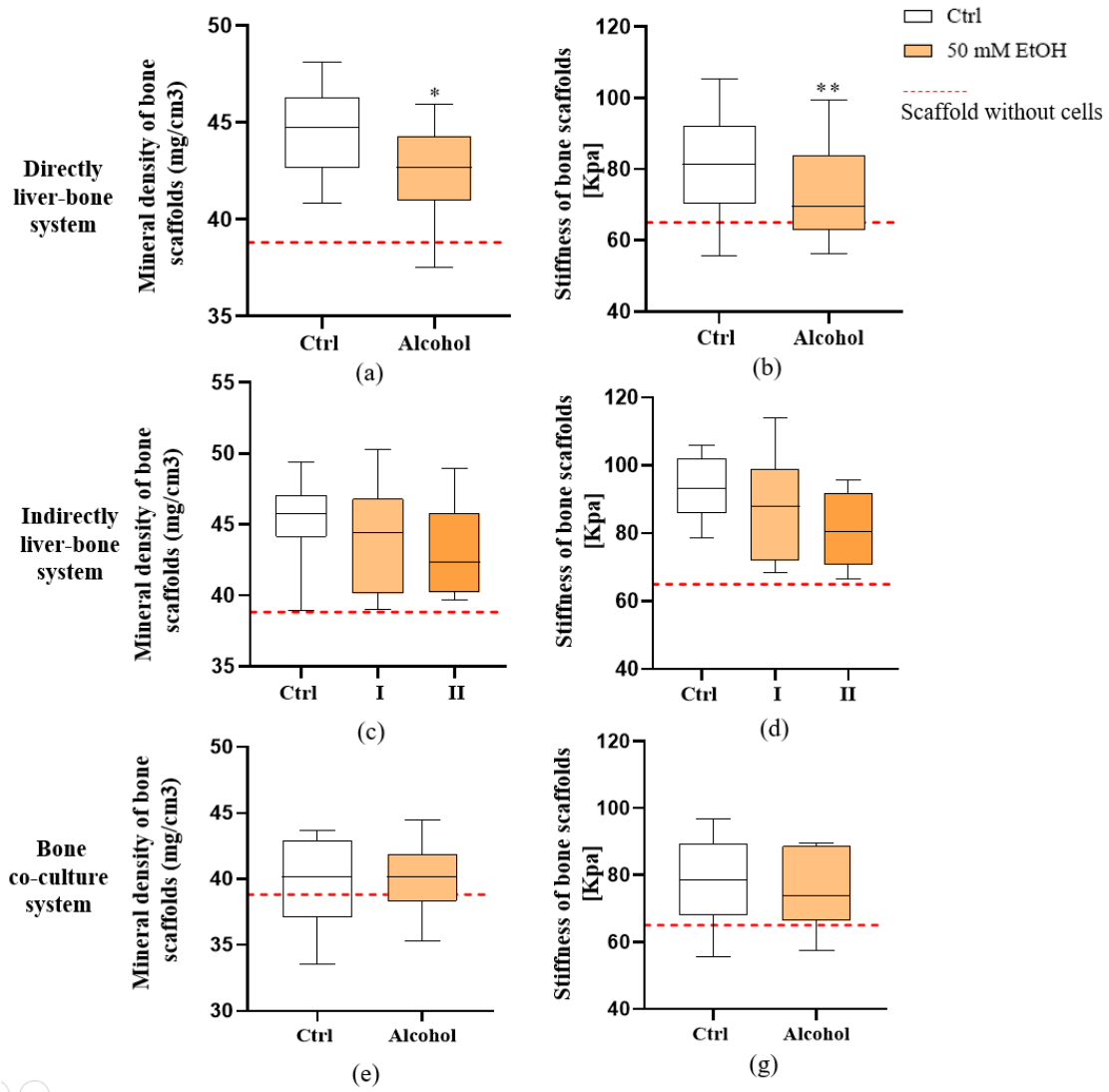
Directly liver-bone system
Indirectly liver-bone system
Bone co-culture system
Mineral density of bone scaffolds (mg/cm3)
Stiffness of bone scaffolds [Kpa]
Ctrl
50 mM EtOH
Scaffold without cells
Ctrl
Alcohol
I
II
(a)
(b)
(c)
(d)
(e)
(g)

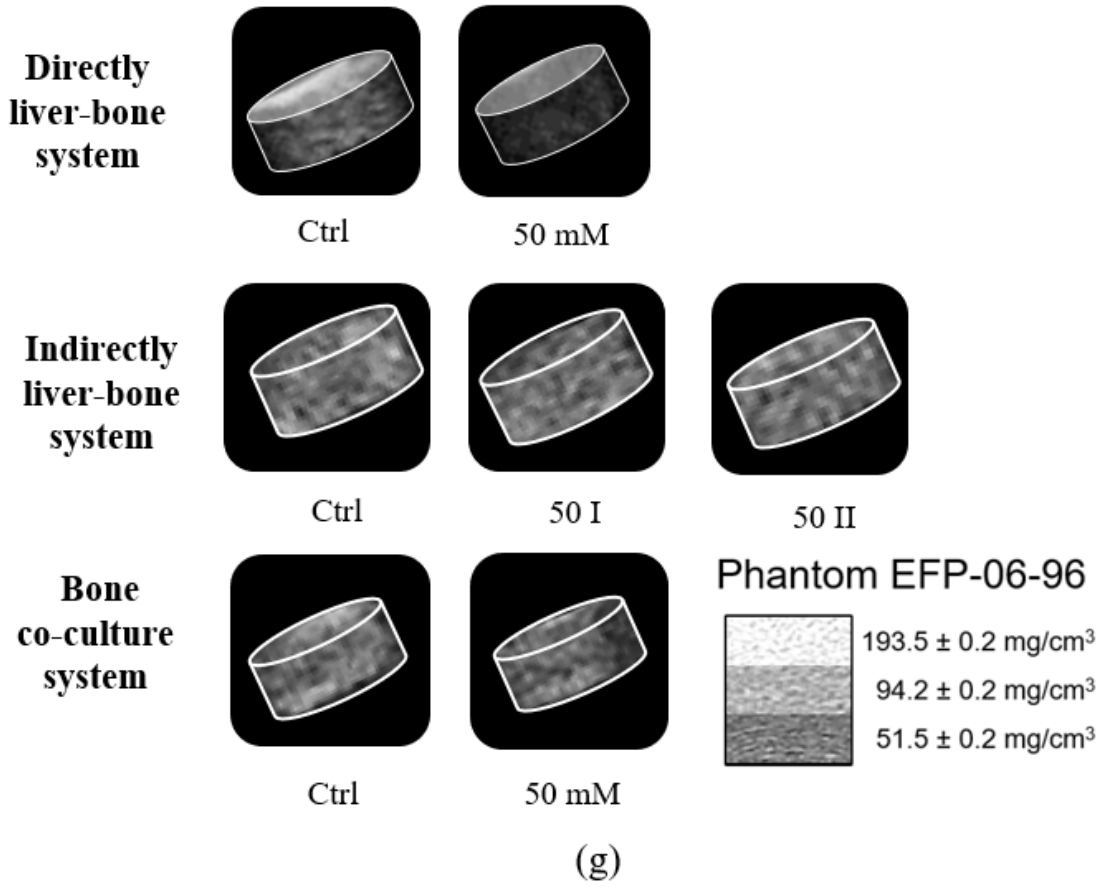

Figure 3.8.2 Effects of different exposure methods of liver-bone system culture on bone homeostasis. To detect the mineral density (mg/cm³) and stiffness (Kpa) for bone system. Direct system (a, b), indirect system I, II (c, d) and bone co-culture alone (e, f). Reconstruction of representative 3D scaffold structures (g) was performed following CT scanning. Differences among groups were evaluated using the Kruskal–Wallis test with Dunn's post hoc test for multiple comparisons. Results are presented as box plots displaying the median, interquartile range (25th–75th percentile), and extreme values (minimum and maximum). Significance levels were indicated as: *$p < 0.05$, **$p < 0.01$(compared with the control group). N ⩾3, n ⩾ 3.

3.8.3 Daily exposure of the liver–bone system to 50 mM alcohol decreases type I collagen production in bone scaffolds

To gain deeper insight into how alcohol affects bone collagen metabolism, we determined PINP and N-terminal telopeptide (NTX) protein expression in the supernatant on days 7, 14, and 21. PINP (Gillett *et al.* 2021) expression was significantly reduced in the alcohol-treated group compared with the control group on

day 14 (p = 0.0005) and day 21 (p = 0.0297) (Figure 3.8.3 a). In contrast, NTX (a marker of collagen degradation and bone resorption (Franke *et al.* 1998)) was not significantly changed at the tested time points (Figure 3.8.3 b). These results indicate that alcohol appears to impair the activity of bone-forming cells by suppressing collagen synthesis, thereby inhibiting bone matrix formation, while exerting minimal influence on collagen degradation

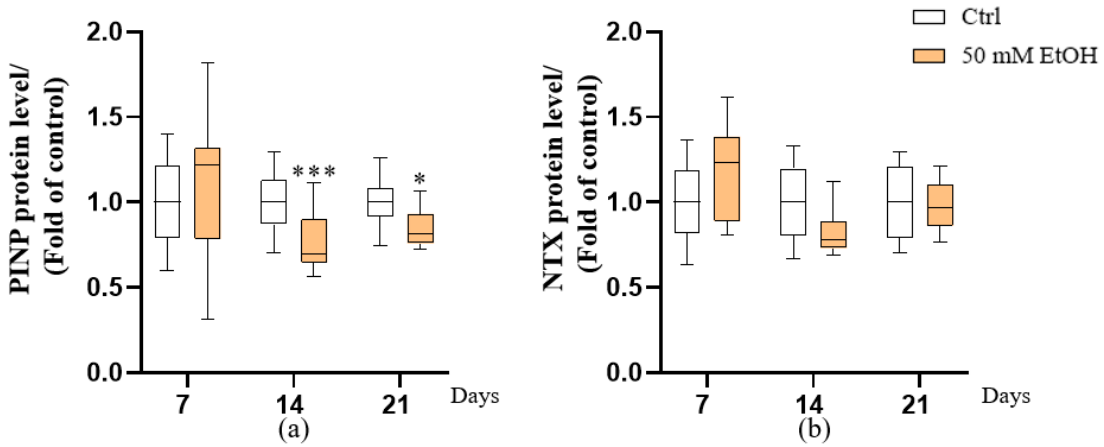

Figure 3.8.3 Assessment of bone remodeling markers. To quantify bone formation and resorption markers. PINP protein (a) levels as a marker of collagen synthesis and bone formation. (b) NTX protein levels as a marker of collagen degradation and bone resorption. Differences among groups were evaluated using the Kruskal–Wallis test with Dunn's post hoc test for multiple comparisons. Results are presented as box plots displaying the median, interquartile range (25th–75th percentile), and extreme values (minimum and maximum). Significance levels were indicated as: *p < 0.05, ***p < 0.001 (compared with the control group). N ⩾3, n ⩾ 3.

3.9 Effects of alcohol on liver-derived BMP secretion in liver–bone system

The previous results suggested that reduce mineral content and stiffness may be related to impaired osteoblast function in our system. BMPs are critical signaling molecules that regulate osteoblast differentiation, matrix synthesis, and overall bone formation. Emerging evidence suggests that chronic alcohol exposure alters hepatic function, leading to reduced production and secretion of key BMP family members. For instance, it was demonstrated that alcohol impairs BMP-2 expression in liver cells, which consequently diminishes their endocrine support to bone tissue (Bratton *et al.* 2018). Thus, we measured BMP-2, BMP-9, and BMP-13 protein expression in the supernatant

after exposure to 50 mM alcohol for 24 h. BMP-2, BMP-9, and BMP-13 were selected due to their importance as signaling molecules for bone biology and are significantly secreted by liver cells (Chung *et al.* 2018, Peschl *et al.* 2022, Chen *et al.* 2024). Compared with the control group, BMP-2 expression (Figure 3.9 a) was significantly reduced in the alcohol-treated group ($p = 0.026$). In contrast, BMP-13 (Figure 3.9 c) was significantly increased ($p = 0.026$) at the same time point. BMP-9 expression showed no significant change (Figure 3.9 b). In summary, these findings highlight differential regulation of BMP ligands in response to alcohol, characterized by a strong inhibition of BMP-2 and a transient early increase in BMP-13. The results suggest that BMP signaling plays an active role in the liver–bone axis under alcohol exposure, highlighting the need to explore downstream mechanisms.

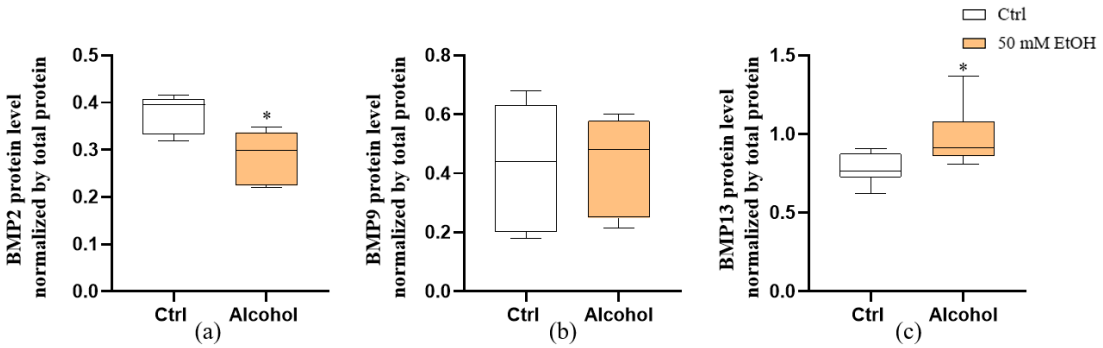

Figure 3.9 Changes in BMP levels released by the liver microorganoids under alcohol stimulation. Protein levels of BMP2 (a), BMP9 (b) and BMP13 (c) were assessed in liver microorganoids treated with or without 50Mm alcohol for 24hs. Differences among groups were evaluated using the Kruskal–Wallis test with Dunn's post hoc test for multiple comparisons. Results are presented as box plots displaying the median, interquartile range (25th–75th percentile), and extreme values (minimum and maximum). Significance levels were indicated as: *$p < 0.05$ (compared with the control group). $N = 3$, $n \geqslant 3$.

3.10 Activation of bone BMP signaling by liver-derived BMPs in liver–bone axis

Since alcohol disrupts liver-derived BMPs secretion levels that influence bone formation. We examined Smad-dependent and Smad-independent pathways (Figure 3.10 a) to investigate whether alcohol affects BMP signaling in the bone system after liver metabolism. We employed western blotting (Figure 3.10 b) to detect the phosphorylation of the Smad1/5 and P38 proteins in the control and alcohol-treated

groups on days 7, 14, and 21. Over time, the level of p-Smad1/5 exhibited an overall decreasing trend, while p-P38 showed a progressive increase. When comparing between groups, the p-Smad1/5 and p-P38 levels were consistently higher in the alcohol-treated group compared with the control group at all time points. Quantitative analysis (Figure 3.10 c) further confirmed that p-Smad1/5 levels were elevated in the alcohol-treated group across all time points, especially on day 7 ($p < 0.0001$). On the other hand, p-P38 demonstrated a time-dependent increase, with a significantly higher level in the alcohol-treated group compared with the control group on day 21 ($p = 0.0166$). These findings suggest that alcohol exposure activates Smad-dependent signaling at earlier stages, whereas Smad-independent signaling *via* p-P38 is engaged at later stages.

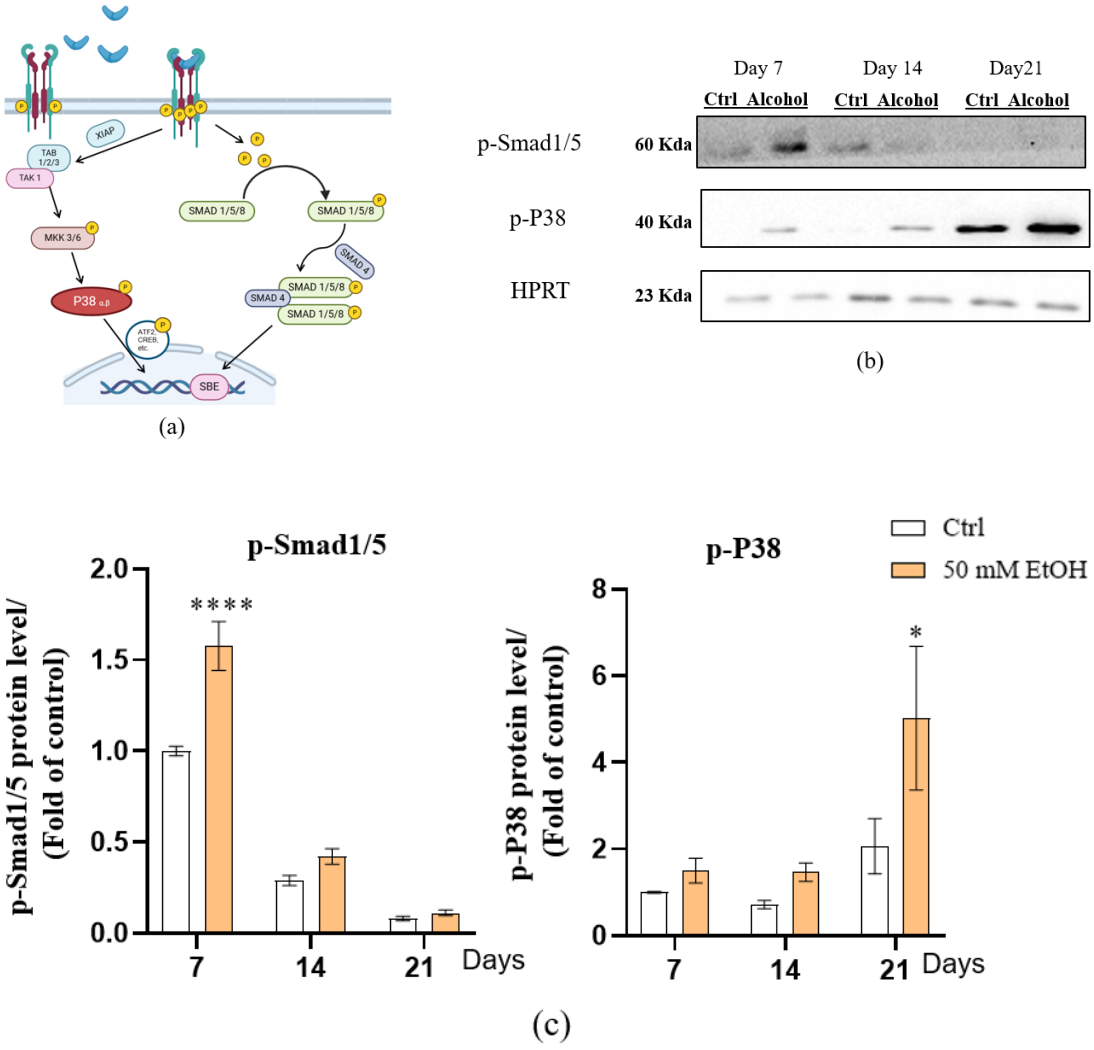

Figure 3.10 BMP Signaling in bone part on liver-bone system. (a). BMPs initiate signaling by binding to homomeric type II receptors, which in turn transphosphorylate type I receptors.

This activates both Smad-dependent and Smad-independent pathways. In the Smad-dependent pathway, phosphorylated Smad1, 5, and 8 form heteromeric complexes with Smad4 and translocate into the nucleus. There, they interact with transcriptional cofactors and RUNX2 to regulate the expression of osteogenic target genes. Alternatively, in the Smad-independent pathway, activated TAK1 recruits TAB1 to initiate downstream signaling cascades, including MKK-p38 MAPK or MKK-ERK1/2 pathways. These MAPK pathways modulate osteogenic gene expression by phosphorylating and regulating RUNX2, thereby influencing osteoblast differentiation. To confirm activation of the BMP signaling pathway, the phosphorylation levels of Smad1/5 and P38 (b) were assessed at days 7, 14, and 21, HPRT was used as an internal reference in the experiment. The results (c) were subsequently quantified and all fold of 7 days control. Statistical differences were assessed by two-way ANOVA followed by Tukey's multiple comparisons test. Data are presented as mean ± SEM. Significance levels were indicated as: *$p < 0.05$, ****$p < 0.0001$ (compared with the control group). N = 4, n = 2.

3.11 Alcohol affects gene expression of transcriptional factor *via* the liver–bone axis

BMPs play a pivotal role in directing MSCs toward specialized lineages, including osteoblasts, chondrocytes, and adipocytes. For example, BMP-2 and BMP9 are potent inducers of osteogenic differentiation (Lamplot *et al.* 2013, Marupanthorn *et al.* 2017), and BMP-13 promotes chondrogenesis (Shen *et al.* 2009). However, exposure to alcohol can disrupt the expression of BMPs by the liver, thereby interfering with their normal signaling functions. Therefore, we assessed the effect of alcohol on the differentiation of SCP-1 cells *via* the liver–bone axis by measuring the gene expression of osteogenic (*RUNX2*), chondrogenic (*SOX9*) and adipogenic (*PPAR γ)* transcription factors on days 7, 14, and 21. *RUNX2* (Figure 3.11 a), a critical transcription factor that drives osteoblast differentiation, was significantly downregulated in the alcohol-treated group on day 7 ($p = 0.0060$). However, on days 14 and 21, its expression was not significantly different compared with the control group. *PPARγ* (Figure 3.11 b), The key adipogenesis regulator was expressed at significantly lower levels in the alcohol-treated group on day 7 ($p < 0.0001$) and day 14 ($p = 0.0010$). The expression of *SOX9* (Figure 3.11 c), a transcription factor associated with chondrogenesis, showed an increasing trend on day 7 in the alcohol-treated group ($p = 0.0487$), and no significant differences at the subsequent time points. These results indicate that alcohol exposure stimulates the liver–bone axis, which in turn downregulates *RUNX2* and *PPARγ*

expression in SCP-1 cells, ultimately interfering with their differentiation into osteoblastic and adipocyte lineages.

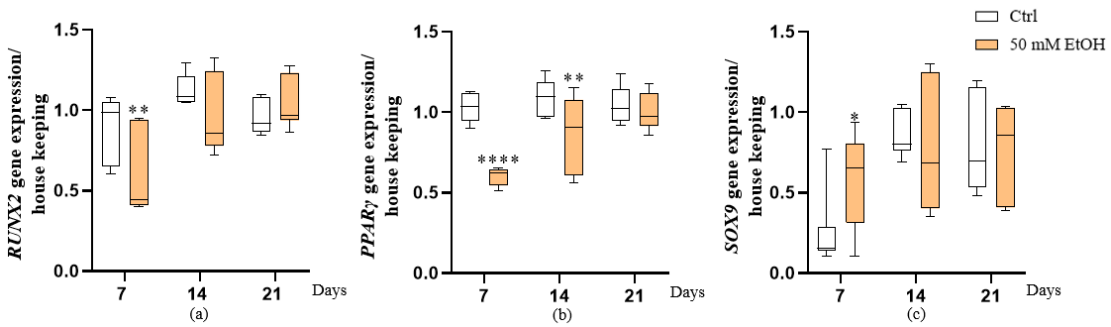

Figure 3.11 Gene expression of osteoblast differentiation, osteogenic, adipogenic, and chondrogenic transcriptional factors changes under alcohol stimulation. To detect the specific differentiation direction of SCP-1, the relative expression levels of *RUNX2* (a), *PPARγ* (b), and *SOX9* (c) genes in SCP-1 cells were measured at 7, 14, and 21 days of L-B co-system under the stimulation of alcohol. Gene expression has been normalized to housekeeping genes. Differences among groups were evaluated using the Kruskal–Wallis test with Dunn's post hoc test for multiple comparisons. Results are presented as box plots displaying the median, interquartile range (25th–75th percentile), and extreme values (minimum and maximum). Significance levels were indicated as: *p < 0.05, **p < 0.01, and ****p < 0.0001 (compared with the control group). N ⩾3, n ⩾ 3.

Chapter 4

4. Discussion

ALD is a significant contributor to chronic liver disease throughout the world, with HOD being a notable complication. Studies indicate that 22%–50% of chronic alcohol consumers experience varying degrees of bone metabolism abnormalities, reduced bone density, and elevated fracture susceptibility, all of which detrimentally impact quality of life and prognosis (Kizilgul *et al.* 2016, Song *et al.* 2018). Nonetheless, the precise pathological mechanisms, particularly signal regulation within the liver–bone axis, warrant further investigation. While animal models offer insights into the relationship between liver injury and bone metabolism disorders (van der Merwe *et al.* 2003, Nussler *et al.* 2014, Lu *et al.* 2022), they are limited by lengthy model establishment, intervention challenges, and constraints in molecular mechanism investigations. Consequently, *in vitro* cell models serve as valuable tools to investigate the mechanisms underlying HOD (Chen *et al.* 2025).

When constructing the model, we utilized a 3D co-culture system in spheroid form to improve the physiological relevance of the system. Unlike standard 2D cultures, a cell sphere model better mimics liver tissue by preserving 3D spatial architecture, cell polarity, and interactions between cells and the extracellular matrix. (Chaicharoenaudomrung *et al.* 2019, Polidoro *et al.* 2021). To more accurately simulate liver function, we are continuing to optimize our liver model. In previous studies, we developed a liver–bone co-culture system by combining HepaRG cell spheroids with bone to explore the development of an *in vitro* platform for evaluating drug effects on the liver–bone axis (Chen *et al.* 2025). Although this model provides a preliminary foundation for simulating liver–bone interactions, the use of only a single hepatocyte type limits its ability to replicate the full process of HSC activation and the subsequent progression of fibrosis following liver stimulation. Furthermore, we established a short-term liver microorganoid model using HepaRG cells, LX-2 cells, and HUVECs, in which a fibrotic phenotype is induced *via* the addition exogenous TGF-β1 to investigate the mechanisms of liver fibrosis progression (Zahmatkesh *et al.* 2022). However, the

model's short culture duration, combined with the pronounced functional alterations that exogenous TGF-β induces in bone tissue, limits its suitability for long-term mechanistic studies of HOD.

To address the limitations of previous models, this project optimized stimulation conditions and culture methods based on previous liver microorganoids, successfully establishing a long-term, stable liver fibrosis model. Compared with the earlier models, this system more accurately reproduces the liver microenvironment and simulates the pathological responses of liver tissue to stimuli by alcohol. Furthermore, the liver–bone co-culture system presents alcohol-induced changes in osteoblast function. This platform also facilitated the investigation of BMP-related signaling pathways in HOD, providing a more reliable and physiologically relevant *in vitro* model for studying disease mechanisms and screening potential therapeutic agents.

Compared with HepG2 and HuH-7 cells, HepaRG cells, a human hepatoma cell line, exhibit drug metabolism capabilities and functional characteristics more akin to primary human hepatocytes (Nelson *et al.* 2017). Particularly noteworthy is their expression and activity CYP450s (*e.g.,* CYP3A4, CYP1A2, and CYP2E1), which closely resemble the human physiological state (Andersson *et al.* 2012, Hammour *et al.* 2022). In addition, HepaRG cells may be induced to acquire a biphenotypic state, exhibiting features of both liver parenchymal and bile duct–like cells, thereby broadening the functional relevance of the model (Parent *et al.* 2004). These attributes render HepaRG cells promising for applications in liver toxicity assessment, drug metabolism studies, and complex liver disease modeling.

LX-2 cells are a human-derived immortalized HSC line that stably express stellate cell markers such as alpha-smooth muscle actin (α-SMA) and collagen I, and exhibit fibrotic characteristics upon activation (Xu *et al.* 2005). In co-culture systems, LX-2 cells secrete ECM components to support the stability of liver microstructures and regulate the functions of hepatocytes and endothelial cells through the secretion of various cytokines, including TGF-β (Zahmatkesh *et al.* 2022). Therefore, LX-2 cells serve as an indispensable cell component for modeling the liver microenvironment and

are particularly valuable for studying liver fibrosis and related disease models.

HUVECs are endothelial cells derived from the human umbilical vein, widely used to model vascular endothelium structure and function. By secreting vascular active factors and various inflammatory cytokines (Medina-Leyte *et al.* 2020), they facilitate the exchange of substances and signal communication between hepatocytes and HSCs. As a result, the model more closely reflects the physiological and pathological conditions of the liver.

Overall, our long-term *in vitro* model of alcohol-induced liver fibrosis using HepaRG, LX-2, and HUVEC spheroids offers high translational value, recapitulates progressive fibrogenesis, and enables mechanistic investigation, unlike classic 2D or rodent-only models. HepaRG cells possess drug metabolizing abilities similar to those of human liver cells and can effectively metabolize alcohol (Andersson *et al.* 2012). The metabolites then activate LX-2 cells through various signaling pathways, causing them to become activated and produce collagen and ECM, which mimics liver fibrosis. At the same time, HUVECs improve communication between cells. Together, the three cell types work in harmony to make the liver fibrosis model closer to a real liver in both structure and function.

We established the bone system with SCP-1/THP-1 co-culture, in which SCP-1 cells, representing human MSCs, contribute to osteogenic differentiation (Sreekumar *et al.* 2018, Chen *et al.* 2025), while THP-1 cells, representing the osteoclast lineage, capturing the *in vivo* balance between bone formation and resorption. (Owen and Reilly 2018, Zhu *et al.* 2020). This co-culture system closely mimics bone tissue dynamics, encompassing both osteoblast and osteoclast activity, as well as the cytokine interactions that are essential for bone remodeling (Guo *et al.* 2022). Incorporation of a PRP scaffold enriches the model with growth factors that promote cell proliferation, differentiation, and matrix mineralization, further replicating the physiological bone environment. This model is particularly relevant to investigate HOD, as it enables the assessment of metabolic bone alterations similar to those observed in patients with chronic liver disease—such as disrupted bone turnover and impaired mineralization—

thereby offering a translational platform for mechanistic investigation. Given these advantages, the combination of these two models offers a more robust and controllable platform for studying the pathogenesis of alcohol-induced HOD and for developing targeted intervention strategies.

Because the liver is a key regulator of systemic bone metabolism, alcohol-induced hepatocellular damage can indirectly affect bone tissue function through multiple signaling pathways (Liu 2014, Gao *et al.* 2024), making it a significant contributor to the development and progression of HOD. Under conditions of long-term or high-dose alcohol intake, the toxic damage to liver cells involves multiple intertwined biological processes. First, alcohol metabolism, particularly through CYP2E1, generates significant ROS, inducing oxidative stress and leading to oxidative damage to proteins, lipids, and nucleic acids (Koop 2006, Lai *et al.* 2024). Second, alcohol interferes with mitochondrial function, inhibiting ATP synthesis and increasing mitochondrial membrane permeability, further activating apoptotic signaling pathways (Hoek *et al.* 2002, Thoudam *et al.* 2024). Furthermore, alcohol significantly disrupts lipid metabolism in hepatocytes, promoting lipid synthesis and inhibiting fatty acid oxidation, ultimately leading to the accumulation of lipid droplets within hepatocytes and the development of alcoholic fatty liver disease (You and Arteel 2019, Jeon and Carr 2020). Alcohol exposure can stimulate Kupffer cells, inducing the production of inflammatory mediators like TNF-α and IL-6, which in turn amplify liver inflammation and hepatocellular damage (Kawaratani *et al.* 2013). As the exposure time increases, HSCs are continuously activated, a large amount of ECM is deposited, and liver fibrosis and even cirrhosis gradually develop (Osna *et al.* 2017).

To better simulate the *in vivo* environment, we further considered the structural and functional advantages of the 3D culture system. In liver microorganoids, alcohol induces stronger cytotoxic responses compared with traditional 2D co-culture systems, highlighting the superior ability of liver microorganoids to mimic the *in vivo* microenvironment. Unlike flat monolayer cultures, 3D models allow different cells to aggregate into tissue-like structures, promoting cell–cell adhesion, the establishment of

polarity, and cell–ECM interactions that more closely resemble physiological conditions (Chaicharoenaudomrung *et al.* 2019, Lee *et al.* 2023). This structural complexity facilitates the formation of *in vivo*–like microenvironmental gradients, such as those of oxygen, nutrients, drugs, and their metabolites, thereby eliciting more physiologically relevant biological and toxicological responses (Serras *et al.* 2021). Studies have shown that hepatic metabolic activity is significantly enhanced in 3D spheroids, particularly the expression and activity of alcohol-metabolizing enzymes (*e.g.,* CYP2E1) and drug transporters (Schyschka *et al.* 2013, Bachmann *et al.* 2015, Lee *et al.* 2023), which are markedly higher than in 2D systems. This functional enhancement increases the uptake and processing of drugs and toxic substances, leading to the rapid accumulation of alcohol metabolites (*e.g.,* acetaldehyde and ROS) within cells (Wang *et al.* 2020). Consequently, 3D models show elevated oxidative stress, lipid peroxidation, mitochondrial damage, and activation of inflammatory signaling, leading to enhanced apoptosis and greater overall toxicity. Moreover, 3D models offer notable advantages in maintaining liver-specific cellular functions (Tutty *et al.* 2022). For example, compared with 2D models, 3D spheroids can sustain key physiological activities—such as albumin secretion and glucose metabolism—for longer durations, making them more suitable for modeling the pathological processes associated with chronic alcohol exposure (Takahashi *et al.* 2015, Urzì *et al.* 2023). Importantly, due to diffusion limitations within the 3D spheroids, alcohol and its metabolites form concentration gradients that result in heterogeneous cellular damage across different layers of the spheroid (Białkowska *et al.* 2020). This spatially distinct toxicity is often overlooked in monolayer cultures. As a result, 3D models provide an overall assessment of toxicity and enable a deeper investigation into stress responses of cells exposed to alcohol within diverse microenvironments. Additionally, 3D models exhibit greater cell viability and structural stability, making them more appropriate for long-term experiments, repeated-dose exposures, and combination toxicity studies. In drug development and toxicological evaluation, the greater physiological relevance and sensitivity of 3D systems offer a more reliable experimental platform for predicting

toxicity risks in humans.

This study employed different liver–bone systems to explore the interplay of liver and bone cells under alcohol stimulation to better simulate the metabolic process of alcohol after entering the human body. Each system offers diverse experimental viewpoints and unique advantages that enhance our comprehension of alcohol's impact on liver–bone co-cultures. The primary experimental platform we utilized is the direct system, which offers advantages in terms of simplicity and cost-effectiveness. This system eliminates the need for sophisticated equipment and technical assistance, enabling a swift and direct evaluation of the interaction between liver and bone system (Chen *et al.* 2025). Co-culturing liver microorganoids and bone co-culture creates an optimal setting to investigate direct cellular signaling and interactions. Hepatocytes respond quickly to alcohol stimulation, so this system, allows us to observe the early effects of alcohol—including the generation of ROS and inflammatory factors by hepatocytes— on liver–bone interactions (Allameh *et al.* 2023). Thus, the direct system is particularly advantageous for simulating alcohol-induced alterations in cellular function.

On the other hand, the conditional medium system offers indirect stimulation of bone system by factors secreted by hepatocytes, presenting an approach for precise experimental control. This system involves the transfer of factors from alcohol-stimulated liver microorganoids to the bone co-culture system through conditioned media, thereby replicating indirect liver–bone interactions. While this model facilitates the study of liver–bone interactions and the biological responses of hepatocytes, certain challenges warrant further exploration. For example, the duration required for liver cells to metabolize alcohol is a critical consideration. In our experimental framework, we selected a 2 h incubation period to simulate the early metabolic phase following alcohol exposure. This choice is based on the average human ethanol clearance rate of approximately 7 g/h for a 70-kg individual, which translates to about one drink per hour (Cederbaum 2012). This timeframe allows sufficient hepatic metabolism while preserving intermediate metabolites, such as acetaldehyde, that may affect bone cells (Hugbart *et al.* 2020, Iturrospe *et al.* 2023). Furthermore, the potential instability of

cytokines produced by liver microorganoids during culture transfer may influence their downstream effects on bone cells. For instance, TNF-α has been reported to have a short plasma half-life of approximately 18 min in whole blood models, primarily due to rapid cellular uptake and degradation (Oliver *et al.* 1993). In addition, studies have shown that IL-1, IL-2, IL-3, and IL-6 exhibit rapid clearance from circulation after injection, with distribution half-lives measured in minutes (Bocci 1991). Hence, although the conditional medium system allows for precise control over experimental conditions, careful attention is necessary when considering the temporal aspects of liver metabolism and factor transfer to ensure accurate simulation.

As a commonly used central nervous system depressant, long-term alcohol consumption is widely recognized as a major contributor to bone homeostasis disorders, primarily through liver–bone axis (Sampson 1998, González-Reimers *et al.* 2015). Chronic alcohol intake induces liver injury and fibrosis, which in turn disrupts hepatic endocrine and inflammatory signaling pathways—such as those involving BMPs and cytokines—that are crucial for maintaining bone remodeling balance (Kawaratani *et al.* 2013). After intake, approximately 90% of alcohol is metabolized by the liver (Paton 2005, Seitz *et al.* 2023), while the remaining 5%–10% may directly affect other organs, including bone tissue. Although in vitro studies have reported that alcohol treatment of MC3T3 E1 osteoblasts can induce cell cycle arrest, downregulate the expression of osteogenic marker genes such as AP and COL1A1(Guo *et al.* 2021), inhibit RUNX2, and promote apoptosis (Luo *et al.* 2017, Hong *et al.* 2020), these findings may not fully reflect the physiological condition. One limitation of these studies is that they do not account for the predominant liver metabolism of alcohol. In contrast, our model incorporates liver microorganoids that can metabolize alcohol and release relevant hepatic factors, providing a more physiologically relevant platform to investigate how alcohol-induced liver injury indirectly affects bone homeostasis. Indeed, evidence from animal models also supports the involvement of the liver in alcohol-related bone disorders, highlighting the importance of studying the liver–bone axis.

An *in vivo* experiment in a mouse model of chronic alcohol consumption showed a

reduction in bone density, trabecular thinning, and an increase in IL-6 levels and osteoclast activity (Dai *et al.* 2000, Jia *et al.* 2019). Notably, these effects were markedly reduced in IL-6–deficient mice, indicating a critical role of IL-6 in alcohol-induced bone resorption. On the other hand, a large amount of clinical data shows that alcohol-related bone disease is often accompanied by liver damage, and bone metabolism disorders are correlated with hepatic inflammatory factors (Díez-Ruiz *et al.* 2010, Neuman *et al.* 2015, Gao *et al.* 2024). In our experiment, we constructed a liver-bone co-culture system and compared the bone system responses in alcohol-treated and co-cultured states. Alcohol did not significantly inhibit osteogenic differentiation without the participation liver microorganoids. However, in the liver–bone co-culture system, alcohol reduced the AP activity, PINP expression, bone mineral density, and stiffness, suggesting that its inhibitory effect on osteoblasts is mediated by liver microorganoids. This mechanism may include alcohol metabolism in the liver production of acetaldehyde and ROS, which induce hepatocytes to release BMPs during the early stage of injury (Gerjevic *et al.* 2012, Chung *et al.* 2018, Thayer *et al.* 2020), and also activate inflammation-related pathways, including the upregulation of IL-6, TNF-α, RANKL, and Fibroblast Growth Factor 21 (FGF21), thereby disrupting bone homeostasis (Luo *et al.* 2017, Li *et al.* 2023). In addition, growing evidence indicate that hepatocytes can secreted microRNAs in extracellular vesicles (*e.g.*, miR-122), which regulate post-transcriptional expression of *osterix* and impair osteogenesis (Bala *et al.* 2012, Le *et al.* 2025). Overall, our results further strengthen the core position of the liver-bone axis in alcohol-related bone metabolic abnormalities, which simulates the interaction between liver and bone cells in the context of alcohol metabolism and is closer to the complex pathological state of clinical HOD.

In the regulation of bone homeostasis, osteoblasts and osteoclasts exhibit a tightly coupled functional relationship: A reduction in osteoblast activity can disrupt this coupling and lead to a relative increase in osteoclast activity, thereby contributing to bone resorption and remodeling imbalance (Chen *et al.* 2018, Kim *et al.* 2020). The classical RANKL/OPG signaling axis plays a central role in mediating this coupling

(Borciani *et al.* 2020, Kim *et al.* 2020). In our liver–bone co-culture system, we also observed a significant reduction in the osteogenic capacity of osteoblast-like cells, while the function of osteoclast-like cells did not exhibit marked changes. This result is consistent with previous findings indicating that impaired osteogenesis can occur independently of osteoclast overactivation in certain pathological contexts (Marie 2015). However, the absence of a direct increase in osteoclast activity may be attributed to multiple interacting factors. First, RANKL—a key signal for inducing THP-1 differentiation into mature osteoclasts—is primarily expressed by osteoblasts. Following exposure to alcohol-stimulated liver microorganoids secretions, osteoblast like cells exhibit insufficient RANKL expression or relatively increased OPG expression, thereby suppressing osteoclast lineage initiation. Second, when metabolizing alcohol, the liver can secrete various immunomodulatory and inflammatory factors, such as TGF-β_1 (Tokunaga *et al.* 2020), and exosomal miRNAs (Li et al. 2021)(miR-503-3p (Chen *et al.* 2014) and miR-155 (Song *et al.* 2019)), some of which may directly inhibit osteoclast and interfere with their differentiation. Finally, our detection time points—days 7, 14, and 21—span the typical osteogenic differentiation timeline but may not fully capture the osteoclastogenic timeline, which could be delayed relative to that of osteoblasts (Sun *et al.* 2021). In summary, our study suggests that in the context of alcohol-induced liver damage, hepatocytes in liver microorganoids inhibit the differentiation ability of osteoblasts by regulating their secretion profile and also delay, weaken, or offset osteoclast signals, resulting in no immediate enhancement of osteoclast activity.

To further investigate the molecular mechanisms underlying liver-derived regulation of bone metabolism, we turned our attention to BMPs, which are well-known for their critical roles in regulating osteoblast differentiation and bone formation (Bordukalo-Nikšić *et al.* 2022). In the context of liver–bone interactions, we specifically focused on BMP2 (Chung *et al.* 2018), BMP9 (Chen *et al.* 2024), and BMP13 (Peschl *et al.* 2022), as these factors are functionally involved in osteogenic signaling and detectable in the liver under physiological or pathological conditions. Hence, they are suitable

candidates to investigate how liver-derived signals may influence bone metabolism in our co-culture system. Among them, BMP-2 and BMP-9 are well established as a potent pro-osteogenic factor (Halloran *et al.* 2020, Park *et al.* 2023), while BMP-13 is predominantly involved in chondrogenic differentiation and may negatively regulate osteogenesis by inhibiting osteoblast maturation (Nochi *et al.* 2004, Shen *et al.* 2009). In our direct culture system, BMP-2 expression was significantly decreased, while BMP-13 was significantly increased. These results suggest that alcohol may affect changes in bone homeostasis by selectively regulating the secretion of different BMP isoforms. Although both BMP-2 and BMP-13 signal through type I BMP receptors to activate the Smad1/5/8 pathway (Wu *et al.* 2016), they exhibit distinct receptor binding preferences that may contribute to their divergent biological functions (Sanchez-Duffhues *et al.* 2020), as previously discussed. BMP-2 binds with comparable affinity to both activin receptor-like kinase3 (ALK3) and ALK6, allowing it to efficiently induce osteogenic differentiation across a broad range of cellular environments (Jang *et al.* 2012). In contrast, BMP-13 displays a stronger preference for ALK6 over ALK3, which restricts it signaling to cells expressing high levels of ALK6, which have different tissue distributions and affinities, resulting in distinct biological outcomes(Berasi *et al.* 2011, Lin *et al.* 2016). This receptor selectivity may help explain why BMP-13 primarily promotes tenogenic or chondrogenic programs, while BMP-2 robustly induces osteogenesis. Moreover, BMP-13 can exhibit context-dependent antagonism toward BMP-2 by competing for type II receptors without effectively activating ALK3-mediated signaling in certain cellular settings. There are significant differences in receptor selectivity, downstream targets, and tissue distribution. This subtype-specific regulatory mechanism may be an important molecular basis for cell fate deviation. Furthermore, the interaction of different BMP ligands with distinct receptor subtypes may influence the strength and duration of downstream phosphorylation events, ultimately resulting in divergent gene expression patterns. These variations may underlie the complex or even opposing roles of BMP signaling in regulating the liver–bone axis under chronic alcohol exposure.

Several *in vivo* studies have reported that alcohol exposure can impair BMP-2 function by inhibiting BMP receptor activity (Gerjevic *et al.* 2012). In addition, evidence indicates that BMP-2 expression is markedly reduced as fibrosis progresses (Thayer *et al.* 2020). Since BMP-2 is crucial for maintaining bone homeostasis by driving osteoblast differentiation and bone formation, alcohol-mediated suppression of BMP-2 could compromise liver tissue repair and disrupt bone remodeling, ultimately lowering bone density through the liver–bone axis. In contrast, BMP-13 appears to be upregulated during liver fibrosis, although there has been limited research in this area(Kersten *et al.* 2023). Consistent with these reports, our model also showed similar BMPs expression patterns, supporting its reliability. Further analysis of protein-level signaling revealed that p-Smad1/5 levels increased significantly on day 7, coinciding with the upregulation of *SOX9*. These results suggest that alcohol may initiate chondrogenic gene programs *via* the BMP-13–Smad1/5–*SOX9* signaling axis, rather than promoting osteogenic differentiation through the canonical BMP-2–Smad1/5-*RUNX2* pathway. In contrast, p-P38 expression did not show a significant increase on day 7, it rose gradually up to day 21, suggesting it may function as a regulatory factor in maintaining *SOX9* expression or promoting chondrocyte maturation at later stages. In summary, these results indicate that alcohol-related HOD may involve the selective activation of specific BMP subtypes and the coordinated regulation of Smad and P38 signaling pathways, ultimately driving MSC fate toward chondrogenic rather than osteogenic.

Researchers have recently found that in inflammatory or stress microenvironments, the activation of Smad signals may no longer directly lead to osteogenic differentiation; rather, it may be reprogrammed into atypical signal outputs and even associated with abnormal bone formation (Chen *et al.* 2024, Wang and Luo 2025). In addition, the significant increase in p-P38 suggests the involvement of the non-classical MAPK pathway. p38 MAPK is a recognized inflammatory response and stress regulation pathway and has also been shown to play a synergistic role in promoting cartilage lineage differentiation. p38 can enhance *SOX9* activity and induce MSCs to

differentiate into cartilage (Ma *et al.* 2019, Sahu *et al.* 2020). Therefore, we speculate that under alcohol induction, the factors released by hepatocyte-like cells from liver microorganoids activate the P38-*SOX9* axis, guiding osteoblast-like cells in the bone co-culture system to differentiate into the cartilage lineage, which is generally manifested as decreased osteogenic function and increased cartilage characteristics.

We also considered the possible role of BMP-9, a member of the BMP family derived from the liver, and known to be involved in regulating bone metabolism. Total BMP-9 expression did not change significantly in our liver–bone co-culture system after alcohol stimulation. However, the biological activity of BMP-9 is also closely related to its structural configuration (Chen *et al.* 2024). Specifically, dimeric D-type BMP9 has a stronger ability to phosphorylate Smad1/5 than the monomeric M-type, and the stability of the dimer depends on the formation of disulfide bonds (Chen *et al.* 2024, Gaither *et al.* 2025). Alcohol can impair the function of protein disulfide isomerase in hepatocytes, a phenomenon that may lead to a decrease in the ability of BMP-9 to form dimers, thereby reducing the D/M ratio and weakening functional activity. This may explain why a shift in cell lineage—such as osteogenic suppression and chondrogenic preference—still occurs despite unchanged BMP-9 expression, highlighting the importance of dimeric structural integrity for maintaining its biological function.

In the liver–bone co-culture system, alcohol also influence MSC lineage commitment. Under long-term alcohol exposure, the osteogenic and adipogenic differentiation abilities of SCP-1 cells were significantly inhibited, while the chondrogenic differentiation potential was significantly enhanced. This shift in differentiation preference reflects a competitive imbalance among MSC lineage fates, potentially driven by oxidative stress resulting from alcohol metabolism and inflammatory factors released by the liver. From a metabolic perspective, both osteogenesis and adipogenesis are energy-intensive processes that are highly dependent on mitochondrial function (Li *et al.* 2017). Mitochondrial integrity, oxidative phosphorylation levels, and a sufficient ATP supply are essential for the expression and activity of transcription factors *RUNX2* and *PPARγ*. Alcohol is mainly metabolized by CYP2E1 in the liver, accompanied by

the production of a large amount of ROS, which can lead to loss of the mitochondrial membrane potential, blocked ATP production, and result in an imbalance in the NAD+/NADH ratio, leading to a disordered redox state in the cell (Koop 2006, Zorov *et al.* 2014). These metabolic stresses not only inhibit the expression of *RUNX2*, an osteogenic initiation transcriptional factor, and *PPARγ*, a regulator of adipogenesis, but also weaken their mediated lineage maintenance and transcriptional activity, thereby significantly reducing the differentiation efficiency of osteogenic and adipogenic lineages. In contrast, the chondrogenic differentiation program is relatively less dependent on oxygen metabolism and has an adaptive advantage because it can be initiated under adverse conditions such as hypoxia, low energy, and chronic inflammation. *SOX9*, a key transcription factor that dominates chondrogenesis, is more easily activated under stress conditions, especially in a hypoxic or inflammatory environment (Gilbert *et al.* 2000, Jiang *et al.* 2019). In addition, *SOX9* and *RUNX2* exhibit functional antagonism, where *SOX9* can suppress *RUNX2* expression and its downstream signaling pathways involved in bone formation, thus tipping the balance in favor of *SOX9* during lineage commitment. This type of interaction mechanism may further amplify this trend. Moreover, this enhancement of cartilage formation may represent a stress-induced adaptive response and a compensatory mechanism for MSCs in the face of long-term metabolic load and immune stimulation (Chen *et al.* 2023). Studies have shown that in an environment driven by oxidative stress, impaired mitochondrial function, or inflammation, MSCs are more inclined to initiate the chondrogenic program and enhance the stability of the local microenvironment by secreting a protective ECM (Thoudam *et al.* 2024). In summary, our results suggest that alcoholic liver injury not only directly impairs bone cell function through metabolic toxicity and inflammatory mechanisms, but also reshapes the lineage fate of MSCs, shifting in a direction that is not conducive to osteogenesis. This lineage imbalance may ultimately lead to osteopenia and decreased bone quality and increase the risk of bone metabolic disorders in patients with ALD, revealing a pathological mechanism in the liver–bone axis that has not been fully recognized.

This study has some limitations. In addition to BMPs, a variety of other cytokines—such as TNF-α and IL-6 family members—may be significantly altered when liver microorganoids are exposed to alcohol. These altered cytokine levels could potentially disrupt bone cell homeostasis and lead to changes in bone density, underscoring the need for further investigation. Although all experimental cells used in this study were of human origin, the inherent limitations of *in vitro* cell models remain, making it difficult to fully mimic the complex internal environment of the human body. Our liver microorganoids included only three basic cell types and did not incorporate immune-related cells, such as Kupffer cells. The absence of these cells may have limited the model's capacity to secrete inflammatory mediators. Similarly, the bone model lacked several essential cell types required for the maintenance of bone tissue homeostasis, including chondrocytes, immune cells, and bone lining cells. Therefore, to more accurately investigate the mechanisms underlying alcohol-induced HOD, 3D co-culture system incorporating Kupffer cells shall be implemented in the next step, allowing for a more realistic representation of the immune-inflammatory state in the liver and its regulation of bone metabolism-related signals. In addition, the traditional static culture model is difficult to simulate the dynamic blood flow and mechanical stimulation environment of liver and bone *in vivo*.

In future experiments, a dynamic liver–bone co-culture system is planned to be implemented, in which liver cells are first exposed to alcohol and the resulting conditioned medium is subsequently transferred to bone cells. This setup is expected to more accurately reflect the sequential nature of alcohol metabolism and to allow for a more physiologically relevant simulation of metabolite exposure along the liver–bone axis (Figure 4). This type of system enables shear stress and metabolite gradients to be more precisely modeled and based on the optimized dynamic co-culture system, we can systematically analyze the key intercellular communication and signaling pathways in the microenvironment of alcohol-induced HOD, which will provide an important theoretical basis for the development of targeted intervention strategies.

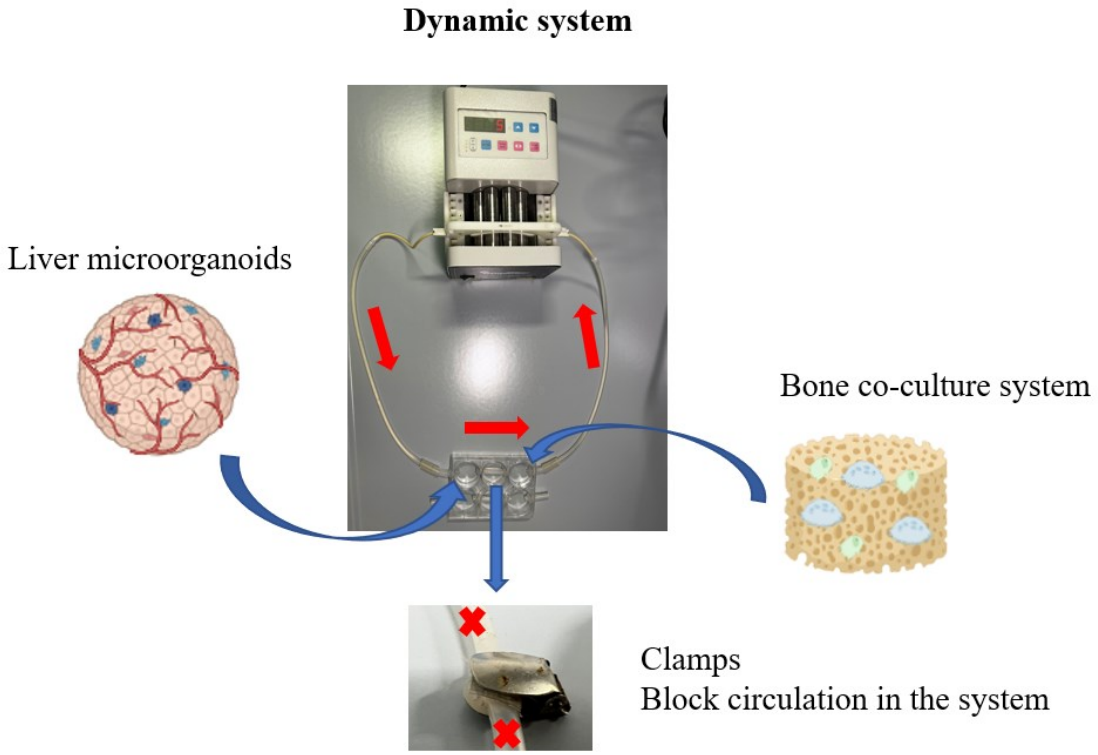

Figure 4. Possible future experimental setup of a dynamic liver–bone co-culture system. The system is designed to simulate the exposure of bone co-culture to alcohol metabolites produced by the liver microorganoids. Liver microorganoids are cultured in the left chamber, and bone co-culture systems are seeded in the right chamber. The chambers are initially filled with culture medium and connected by a tube. A clamp is used to block flow between compartments during the first 2-hour incubation, during which only the liver microorganoids are exposed to alcohol. After this period, the clamp is released and the pump is activated, enabling unidirectional circulation of conditioned medium (as indicated by red arrows). This setup mimics the physiological transfer of liver-derived metabolites to the bone microenvironment, while also allowing the modeling of flow-induced shear stress and concentration gradients.

Chapter 5

5. Summary

In this study, we established a novel three-dimensional *in vitro* liver–bone co-culture system that simulated the physiological interactions between liver and bone tissues at the tissue structural and functional levels. The model consists of liver microorganoids composed of hepatocytes (HepaRG), hepatic stellate cells (LX-2), and human umbilical vein endothelial cells (HUVECs) in a 4:2:1 ratio, co-cultured with scaffolds embedded with a human monocytic cell line (THP-1) and mesenchymal stem cell line (SCP-1) on agarose plate. This system demonstrated stable viability and functional for at least 28 days, offering a reliable platform for studying liver–bone crosstalk *in vitro*.

Numerous clinical and animal studies have demonstrated that alcohol intake induces osteoporosis and delays fracture healing. However, the underlying pathological mechanisms remain unclear. Since alcohol mainly affects the liver, and hepatic dysfunction is closely associated with osteodystrophy, it is plausible that liver-driven mechanisms are key contributors to alcohol-related bone disease. This study provides a systematic evaluation of how alcohol exposure affects the liver–bone axis. Specifically, we simulated alcohol exposure by exposing our system to an alcohol concentration that would result from drinking more than four beers (50 mM). This exposure significantly inhibited the bone-forming capacity, as evidenced by a decrease in AP and PINP expression, accompanied by downregulation in the expression of a key osteogenic transcription factor, *RUNX2*, and upregulation of the chondrogenic marker gene *SOX9*. Further mechanistic investigation revealed that this effect may be closely related to alteration of the BMP signaling pathway. Specifically, liver microorganoids exposed daily to alcohol showed significantly reduced expression and secretion of BMP-2, which is closely associated with osteogenesis, and markedly increased expression of BMP-13, a change that drives the shift from osteogenic toward chondrogenic differentiation. Although BMP-9 did not show significant changes, this protein exists in different forms stabilized by disulfide bonds, and the correct formation

of these bonds is crucial for its biological activity. Alcohol intake has been reported to alter the expression and activity of protein disulfide isomerases in the liver, which are essential for the proper formation of disulfide bonds in secreted proteins. This suggests that, even if the total level of BMP-9 remains unchanged, alcohol exposure may disrupt the balance between its different molecular forms by affecting disulfide bond formation, thereby altering the ratio of D-form BMP-9 to M-form BMP-9. Overall, these findings suggest that these changes affect bone homeostasis along the liver–bone axis and highlight the key role of liver-derived factors in modulating bone metabolism under alcohol-induced pathological state.

In conclusion, we have established a long-term, stable *in vitro* liver fibrosis model by exposing the liver microorganoids to alcohol and have determined the potential molecular mechanism by which alcohol disrupts bone homeostasis through the liver–bone axis. These findings provide a new explanation for alcohol-related bone metabolism disorders and offer a theoretical basis and potential therapeutic targets for the clinical management of alcoholic hepatic osteodystrophy. In addition, our in vitro liver–bone co-culture model can be stably maintained for up to 28 days, offering a controllable and expandable research platform. This model has broad application prospects, including the screening of drug-induced osteotoxicity, investigation of the etiology of liver dysfunction-associated bone diseases, and personalized efficacy and toxicity prediction studies.

Chapter 6

6. Zusammenfassung

In dieser Studie etablierten wir ein neuartiges dreidimensionales *in vitro* Leber-Knochen-Kokultursystem, das die physiologischen Wechselwirkungen zwischen Leber- und Knochengewebe sowohl auf struktureller als auch funktioneller Ebene nachbildete. Das Modell besteht aus Lebermikroorganoiden, die aus Hepatozyten (HepaRG), hepatischen Sternzellen (LX-2) und humanen Nabelvenen-Endothelzellen (HUVECs) im Verhältnis 4:2:1 zusammengesetzt sind, und wird zusammen mit Gerüsten, die mit einer humanen monozytischen Zelllinie (THP-1) und einer mesenchymalen Stammzelllinie (SCP-1) versehen sind, auf einer Agaroseplatte kultiviert. Dieses System zeigte über mindestens 28 Tage hinweg eine stabile Lebensfähigkeit und Funktionalität und bietet damit eine zuverlässige Plattform zur Untersuchung des Leber-Knochen-Crosstalks *in vitro*.

Zahlreiche klinische und tierexperimentelle Studien haben bestätigt, dass Alkoholkonsum zu Osteoporose führen und die Frakturheilung beeinträchtigen kann. Die zugrunde liegenden pathologischen Mechanismen sind jedoch bislang unklar. Da Alkohol in erster Linie die Leber betrifft und Leberfunktionsstörungen eng mit hepatischer Osteodystrophie assoziiert sind, könnten lebervermittelte Signalwege eine zentrale Rolle bei alkoholinduzierten Knochenerkrankungen spielen. In dieser Studie bewerteten wir systematisch die Auswirkungen einer Alkoholexposition auf die gesamte Leber-Knochen-Achse. Konkret simulierten wir die Alkoholexposition, indem wir unser Leber-Knochen-Kokultursystem einer Alkoholkonzentration aussetzten, die dem Konsum von mehr als vier Bieren entspricht (50 mM). Diese Exposition hemmte die Knochenbildungsfähigkeit signifikant, was sich in einer Abnahme der Aktivität der alkalischen Phosphatase (AP) und der Expression des Prokollagen-Typ-I-N-terminalen Propeptids (PINP) zeigte. Begleitet wurde dies von einer Herunterregulation der Expression des zentralen osteogenen Transkriptionsfaktors RUNX2 sowie einer Hochregulation des chondrogenen Marker-Gens SOX9. Weitere mechanistische Untersuchungen zeigten, dass dieser Effekt eng mit Veränderungen des Signalwegs der

knochenmorphogenetischen Proteine (BMP) verbunden sein könnte. Insbesondere wiesen Lebermikroorganoide, die täglich Alkohol ausgesetzt waren, eine deutlich verringerte Expression und Sekretion von BMP-2 auf, das eng mit der Osteogenese verknüpft ist, sowie eine deutlich erhöhte Expression von BMP-13 – eine Veränderung, die den Übergang von osteogener zu chondrogener Differenzierung fördert. Obwohl bei BMP-9 keine signifikanten Veränderungen festgestellt wurden, liegt dieses Protein in unterschiedlichen, durch Disulfidbrücken stabilisierten Formen vor, und die korrekte Ausbildung dieser Bindungen ist entscheidend für seine biologische Aktivität. Es wurde berichtet, dass Alkoholkonsum die Expression und Aktivität von Protein-Disulfid-Isomerasen in der Leber verändert, die für die ordnungsgemäße Ausbildung von Disulfidbrücken in sezernierten Proteinen unerlässlich sind. Dies deutet darauf hin, dass selbst bei unverändertem Gesamtspiegel von BMP-9 die Alkoholexposition das Gleichgewicht zwischen seinen verschiedenen molekularen Formen durch Beeinflussung der Disulfidbrückenbildung stören und somit das Verhältnis von D-Form-BMP-9 zu M-Form-BMP-9 verändern könnte. Zusammenfassend weisen diese Ergebnisse darauf hin, dass solche Veränderungen zu einer Beeinträchtigung der Knochenhomöostase innerhalb der Leber-Knochen-Achse beitragen und die zentrale Rolle leberabgeleiteter Faktoren bei der Regulation des Knochenstoffwechsels unter alkoholinduzierten pathologischen Bedingungen unterstreichen.

Zusammenfassend haben wir ein langfristig stabiles *in vitro* Leberfibrosemodell etabliert, indem wir die Lebermikroorganoide Alkohol aussetzten, und den potenziellen molekularen Mechanismus ermittelt, durch den Alkohol über die Leber-Knochen-Achse die Knochenhomöostase stört. Diese Ergebnisse liefern eine neue Erklärung für alkoholbedingte Störungen des Knochenstoffwechsels und bieten eine theoretische Grundlage sowie potenzielle therapeutische Ziele für das klinische Management der alkoholischen hepatischen Osteodystrophie. Darüber hinaus kann unser *in vitro* Leber-Knochen-Kokulturmodell bis zu 28 Tage stabil aufrechterhalten werden und stellt damit eine kontrollierbare und erweiterbare Forschungsplattform dar. Dieses Modell hat ein breites Anwendungspotenzial, einschließlich des Screenings von

arzneimittelinduzierter Osteotoxizität, der Untersuchung der Ätiologie von leberfunktionsstörungsassoziierten Knochenerkrankungen sowie von Studien zur personalisierten Wirksamkeits- und Toxizitätsvorhersage.

7. Bibliography

Aguilar, A., et al. (2023). "Pathophysiology of bone disease in chronic kidney disease: from basics to renal osteodystrophy and osteoporosis." Front Physiol **14**: 1177829.

Akhtar, A. (2015). "The flaws and human harms of animal experimentation." Camb Q Healthc Ethics **24**(4): 407-419.

Allameh, A., et al. (2023). "Oxidative Stress in Liver Pathophysiology and Disease." Antioxidants (Basel) **12**(9).

Andersson, T. B., et al. (2012). "The HepaRG cell line: a unique in vitro tool for understanding drug metabolism and toxicology in human." Expert Opin Drug Metab Toxicol **8**(7): 909-920.

Arriazu, E., et al. (2014). "Extracellular matrix and liver disease." Antioxid Redox Signal **21**(7): 1078-1097.

Asano, R., et al. (2024). "Unveiling dynamic hepatocyte plasticity in HepaRG cells with a dual CYP reporter system." PLoS One **19**(11): e0308694.

Aspera-Werz, R. H., et al. (2018). "Nicotine and Cotinine Inhibit Catalase and Glutathione Reductase Activity Contributing to the Impaired Osteogenesis of SCP-1 Cells Exposed to Cigarette Smoke." Oxid Med Cell Longev **2018**: 3172480.

Bachmann, A., et al. (2015). "3D Cultivation Techniques for Primary Human Hepatocytes." Microarrays (Basel) **4**(1): 64-83.

Bala, S., et al. (2012). "Circulating microRNAs in exosomes indicate hepatocyte injury and inflammation in alcoholic, drug-induced, and inflammatory liver diseases." Hepatology **56**(5): 1946-1957.

Bedossa, P. and V. Paradis (2003). "Liver extracellular matrix in health and disease." The Journal of Pathology **200**(4): 504-515.

Beederman, M., et al. (2013). "BMP signaling in mesenchymal stem cell differentiation and bone formation." J Biomed Sci Eng **6**(8a): 32-52.

Berasi, S. P., et al. (2011). "Divergent activities of osteogenic BMP2, and tenogenic BMP12 and BMP13 independent of receptor binding affinities." Growth Factors **29**(4):

128-139.

Bhattarai, H. K., et al. (2020). "Vitamin D, Calcium, Parathyroid Hormone, and Sex Steroids in Bone Health and Effects of Aging." J Osteoporos **2020**: 9324505.

Białkowska, K., et al. (2020). "Spheroids as a Type of Three-Dimensional Cell Cultures-Examples of Methods of Preparation and the Most Important Application." Int J Mol Sci **21**(17).

Blanco, A. and G. Blanco (2017). "Metabolism in Some Tissues." Medical Biochemistry: 447-463.

Bocci, V. (1991). "Interleukins. Clinical pharmacokinetics and practical implications." Clin Pharmacokinet **21**(4): 274-284.

Böcker, W., et al. (2008). "Introducing a single-cell-derived human mesenchymal stem cell line expressing hTERT after lentiviral gene transfer." J Cell Mol Med **12**(4): 1347-1359.

Böcker, W., et al. (2008). "Introducing a single-cell-derived human mesenchymal stem cell line expressing hTERT after lentiviral gene transfer." Journal of Cellular and Molecular Medicine **12**(4): 1347-1359.

Bonnardel, J., et al. (2019). "Stellate Cells, Hepatocytes, and Endothelial Cells Imprint the Kupffer Cell Identity on Monocytes Colonizing the Liver Macrophage Niche." Immunity **51**(4): 638-654.e639.

Borciani, G., et al. (2020). "Co–culture systems of osteoblasts and osteoclasts: Simulating in vitro bone remodeling in regenerative approaches." Acta Biomaterialia **108**: 22-45.

Bordukalo-Nikšić, T., et al. (2022). "The Role Of BMPs in the Regulation of Osteoclasts Resorption and Bone Remodeling: From Experimental Models to Clinical Applications." Front Immunol **13**: 869422.

Bratton, A., et al. (2018). "Effects of Episodic Alcohol Exposure on BMP2 Signaling During Tibia Fracture Healing." J Orthop Trauma **32**(6): 288-295.

Cederbaum, A. I. (2012). "Alcohol metabolism." Clin Liver Dis **16**(4): 667-685.

Chaicharoenaudomrung, N., et al. (2019). "Three-dimensional cell culture systems as

an in vitro platform for cancer and stem cell modeling." World J Stem Cells **11**(12): 1065-1083.

Chanput, W., et al. (2014). "THP-1 cell line: an in vitro cell model for immune modulation approach." Int Immunopharmacol **23**(1): 37-45.

Chen, C., et al. (2014). "MiR-503 regulates osteoclastogenesis via targeting RANK." J Bone Miner Res **29**(2): 338-347.

Chen, C., et al. (2024). "Activation of BMP4/SMAD pathway by HIF-1α in hypoxic environment promotes osteogenic differentiation of BMSCs and leads to ectopic bone formation." Tissue Cell **88**: 102376.

Chen, G., et al. (2012). "TGF-β and BMP signaling in osteoblast differentiation and bone formation." Int J Biol Sci **8**(2): 272-288.

Chen, G., et al. (2025). "Establishment of a human 3D in vitro liver-bone model as a potential system for drug toxicity screening." Arch Toxicol **99**(1): 333-356.

Chen, H., et al. (2024). "Unveiling the Impact of BMP9 in Liver Diseases: Insights into Pathogenesis and Therapeutic Potential." Biomolecules **14**(8): 1013.

Chen, H., et al. (2024). "Unveiling the Impact of BMP9 in Liver Diseases: Insights into Pathogenesis and Therapeutic Potential." Biomolecules **14**(8).

Chen, N., et al. (2023). "Hypertrophic chondrocytes at the junction of musculoskeletal structures." Bone Rep **19**: 101698.

Chen, X., et al. (2018). "Osteoblast-osteoclast interactions." Connect Tissue Res **59**(2): 99-107.

Cheng, M., et al. (2021). "Gut Microbiota Is Involved in Alcohol-Induced Osteoporosis in Young and Old Rats Through Immune Regulation." Front Cell Infect Microbiol **11**: 636231.

Chung, Y.-H., et al. (2018). "BMP-2 restoration aids in recovery from liver fibrosis by attenuating TGF-β1 signaling." Laboratory Investigation **98**(8): 999-1013.

Colucci, S., et al. (2021). "Liver Sinusoidal Endothelial Cells Suppress Bone Morphogenetic Protein 2 Production in Response to TGFβ Pathway Activation." Hepatology **74**(4): 2186-2200.

Dai, J., et al. (2000). "Chronic alcohol ingestion induces osteoclastogenesis and bone loss through IL-6 in mice." J Clin Invest **106**(7): 887-895.

Danford, C. J., et al. (2020). "Bone Health in Patients With Liver Diseases." J Clin Densitom **23**(2): 212-222.

David, S. and J. P. Hamilton (2010). "Drug-induced Liver Injury." US Gastroenterol Hepatol Rev **6**: 73-80.

de Paula, F. J. A. and C. J. Rosen (2013). "Bone Remodeling and Energy Metabolism: New Perspectives." Bone Research **1**(1): 72-84.

Devarbhavi, H., et al. (2023). "Global burden of liver disease: 2023 update." Journal of Hepatology **79**(2): 516-537.

Devarbhavi, H., et al. (2023). "Global burden of liver disease: 2023 update." J Hepatol **79**(2): 516-537.

Díez-Ruiz, A., et al. (2010). "Bone mineral density, bone turnover markers and cytokines in alcohol-induced cirrhosis." Alcohol Alcohol **45**(5): 427-430.

Dreyer, T. J., et al. (2023). "Novel insights on the effect of sclerostin on bone and other organs." J Endocrinol **257**(2).

Dunn, W. and V. H. Shah (2016). "Pathogenesis of Alcoholic Liver Disease." Clin Liver Dis **20**(3): 445-456.

Eby, J. M., et al. (2020). "Impact of Alcohol on Bone Health, Homeostasis and Fracture repair." Curr Pathobiol Rep **8**(3): 75-86.

Edmondson, R., et al. (2014). "Three-Dimensional Cell Culture Systems and Their Applications in Drug Discovery and Cell-Based Biosensors." ASSAY and Drug Development Technologies **12**(4): 207-218.

Edwards, C. M. and G. R. Mundy (2008). "Eph receptors and ephrin signaling pathways: a role in bone homeostasis." Int J Med Sci **5**(5): 263-272.

Ehnert, S., et al. (2019). "Hepatic Osteodystrophy-Molecular Mechanisms Proposed to Favor Its Development." Int J Mol Sci **20**(10).

Ehnert, S., et al. (2018). "Co-Culture with Human Osteoblasts and Exposure to Extremely Low Frequency Pulsed Electromagnetic Fields Improve Osteogenic

Differentiation of Human Adipose-Derived Mesenchymal Stem Cells." Int J Mol Sci **19**(4).

Ferron, M., et al. (2010). "Insulin signaling in osteoblasts integrates bone remodeling and energy metabolism." Cell **142**(2): 296-308.

Filipovic, B., et al. (2025). "A Closer Look into Autoimmune Liver Diseases." International Journal of Molecular Sciences **26**(5): 1863.

Florencio-Silva, R., et al. (2015). "Biology of Bone Tissue: Structure, Function, and Factors That Influence Bone Cells." Biomed Res Int **2015**: 421746.

Föger-Samwald, U., et al. (2020). "Osteoporosis: Pathophysiology and therapeutic options." EXCLI J **19**: 1017-1037.

Franke, S., et al. (1998). "PICP as bone formation and NTx as bone resorption marker in patients with chronic renal failure." Eur J Med Res **3**(1-2): 81-88.

Gaither, K. A., et al. (2025). "Effects of Chronic Alcohol Intake on the Composition of the Ensemble of Drug-Metabolizing Enzymes and Transporters in the Human Liver." Journal of Xenobiotics **15**(1): 20.

Gan, C., et al. (2025). "Liver diseases: epidemiology, causes, trends and predictions." Signal Transduct Target Ther **10**(1): 33.

Gan, C., et al. (2025). "Liver diseases: epidemiology, causes, trends and predictions." Signal Transduction and Targeted Therapy **10**(1): 33.

Gao, H., et al. (2024). "Emerging role of liver-bone axis in osteoporosis." Journal of Orthopaedic Translation **48**: 217-231.

Gao, H., et al. (2024). "Emerging role of liver-bone axis in osteoporosis." J Orthop Translat **48**: 217-231.

Garbuzenko, D. V. (2022). "Pathophysiological mechanisms of hepatic stellate cells activation in liver fibrosis." World J Clin Cases **10**(12): 3662-3676.

Gerjevic, L. N., et al. (2012). "Alcohol Activates TGF-Beta but Inhibits BMP Receptor-Mediated Smad Signaling and Smad4 Binding to Hepcidin Promoter in the Liver." Int J Hepatol **2012**: 459278.

Ghezelayagh, Z., et al. (2022). "Improved Differentiation of hESC-Derived Pancreatic

Progenitors by Using Human Fetal Pancreatic Mesenchymal Cells in a Micro-scalable Three-Dimensional Co-culture System." Stem Cell Reviews and Reports **18**(1): 360-377.

Gilbert, L., et al. (2000). "Inhibition of osteoblast differentiation by tumor necrosis factor-alpha." Endocrinology **141**(11): 3956-3964.

Gilboa, L., et al. (2000). "Bone morphogenetic protein receptor complexes on the surface of live cells: a new oligomerization mode for serine/threonine kinase receptors." Mol Biol Cell **11**(3): 1023-1035.

Gillett, M. J., et al. (2021). "The Role of PINP in Diagnosis and Management of Metabolic Bone Disease." Clin Biochem Rev **42**(1): 3-10.

Giuliani, N., et al. (1999). "Ethanol and acetaldehyde inhibit the formation of early osteoblast progenitors in murine and human bone marrow cultures." Alcohol Clin Exp Res **23**(2): 381-385.

González-Reimers, E., et al. (2015). "Bone changes in alcoholic liver disease." World J Hepatol **7**(9): 1258-1264.

Gressner, O. A., et al. (2007). "Biomarkers of hepatic fibrosis, fibrogenesis and genetic pre-disposition pending between fiction and reality." J Cell Mol Med **11**(5): 1031-1051.

Griswold, M. G., et al. (2018). "Alcohol use and burden for 195 countries and territories, 1990–2016: a systematic analysis for the Global Burden of Disease Study 2016." The Lancet **392**(10152): 1015-1035.

Guengerich, F. P. (2001). "Common and Uncommon Cytochrome P450 Reactions Related to Metabolism and Chemical Toxicity." Chemical Research in Toxicology **14**(6): 611-650.

Guo, H., et al. (2025). "Alcohol-induced bone loss driven by dysregulated spatial distribution of gut microbiota and PGD2-IL17 pathway-mediated osteoclast activation." Front Microbiol **16**: 1551028.

Guo, H., et al. (2022). "Maqui Berry and Ginseng Extracts Reduce Cigarette Smoke-Induced Cell Injury in a 3D Bone Co-Culture Model." Antioxidants **11**(12): 2460.

Guo, M., et al. (2021). "Chronic Ethanol Consumption Induces Osteopenia via

Activation of Osteoblast Necroptosis." Oxid Med Cell Longev **2021**: 3027954.

Guzman, A., et al. (2012). "SMAD versus non-SMAD signaling is determined by lateral mobility of bone morphogenetic protein (BMP) receptors." J Biol Chem **287**(47): 39492-39504.

Halloran, D., et al. (2020). "Bone Morphogenetic Protein-2 in Development and Bone Homeostasis." J Dev Biol **8**(3).

Hammour, M. M., et al. (2022). "Optimisation of the HepaRG cell line model for drug toxicity studies using two different cultivation conditions: advantages and limitations." Archives of Toxicology **96**(9): 2511-2521.

Hammour, M. M., et al. (2022). "Optimisation of the HepaRG cell line model for drug toxicity studies using two different cultivation conditions: advantages and limitations." Arch Toxicol **96**(9): 2511-2521.

Handzlik-Orlik, G., et al. (2016). "Osteoporosis in liver disease: pathogenesis and management." Ther Adv Endocrinol Metab **7**(3): 128-135.

Häussling, V., et al. (2019). "Impact of Four Protein Additives in Cryogels on Osteogenic Differentiation of Adipose-Derived Mesenchymal Stem Cells." Bioengineering **6**(3): 67.

Häussling, V., et al. (2019). "Impact of Four Protein Additives in Cryogels on Osteogenic Differentiation of Adipose-Derived Mesenchymal Stem Cells." Bioengineering (Basel) **6**(3).

Heier, C., et al. (2016). "Nonoxidative ethanol metabolism in humans-from biomarkers to bioactive lipids." IUBMB Life **68**(12): 916-923.

Herrera, B., et al. (2018). "BMP Signalling at the Crossroad of Liver Fibrosis and Regeneration." International Journal of Molecular Sciences **19**(1): 39.

Hoek, J. B., et al. (2002). "Alcohol and mitochondria: a dysfunctional relationship." Gastroenterology **122**(7): 2049-2063.

Hoffmann, S. A., et al. (2012). "Analysis of drug metabolism activities in a miniaturized liver cell bioreactor for use in pharmacological studies." Biotechnology and Bioengineering **109**(12): 3172-3181.

Hollister, S. J. (2005). "Porous scaffold design for tissue engineering." Nature Materials **4**(7): 518-524.

Hong, Z., et al. (2020). "The significance of Runx2 mediating alcohol-induced Brf1 expression and RNA Pol III gene transcription." Chem Biol Interact **323**: 109057.

Hsu, S. H., et al. (2024). "Primary Osteoporosis Induced by Androgen and Estrogen Deficiency: The Molecular and Cellular Perspective on Pathophysiological Mechanisms and Treatments." Int J Mol Sci **25**(22).

Hu, L., et al. (2024). "Wnt/β-catenin signaling components and mechanisms in bone formation, homeostasis, and disease." Bone Research **12**(1): 39.

Hugbart, C., et al. (2020). "Non-oxidative ethanol metabolism in human hepatic cells in vitro: Involvement of uridine diphospho-glucuronosyltransferase 1A9 in ethylglucuronide production." Toxicol In Vitro **66**: 104842.

Hyun, J., et al. (2021). "Pathophysiological Aspects of Alcohol Metabolism in the Liver." Int J Mol Sci **22**(11).

Iacopetta, D., et al. (2023). "Impact of Cytochrome P450 Enzymes on the Phase I Metabolism of Drugs." Applied Sciences **13**(10): 6045.

Iantomasi, T., et al. (2023). "Oxidative Stress and Inflammation in Osteoporosis: Molecular Mechanisms Involved and the Relationship with microRNAs." Int J Mol Sci **24**(4).

Ingólfsson, H. I. and O. S. Andersen (2011). "Alcohol's effects on lipid bilayer properties." Biophys J **101**(4): 847-855.

Iturrospe, E., et al. (2023). "Metabolic signature of HepaRG cells exposed to ethanol and tumor necrosis factor alpha to study alcoholic steatohepatitis by LC-MS-based untargeted metabolomics." Arch Toxicol **97**(5): 1335-1353.

Jadzic, J. and D. Djonic (2023). "Bone loss in chronic liver diseases: Could healthy liver be a requirement for good bone health?" World J Gastroenterol **29**(5): 825-833.

Jaiswal, R. K., et al. (2000). "Adult human mesenchymal stem cell differentiation to the osteogenic or adipogenic lineage is regulated by mitogen-activated protein kinase." J Biol Chem **275**(13): 9645-9652.

Jang, W. G., et al. (2012). "BMP2 protein regulates osteocalcin expression via Runx2-mediated Atf6 gene transcription." J Biol Chem **287**(2): 905-915.

Jeon, S. and R. Carr (2020). "Alcohol effects on hepatic lipid metabolism." J Lipid Res **61**(4): 470-479.

Jeong, H. M. and D. J. Kim (2019). "Bone Diseases in Patients with Chronic Liver Disease." Int J Mol Sci **20**(17).

Jia, Y., et al. (2019). "Disulfiram suppressed ethanol promoted RANKL-induced osteoclastogenesis in vitro and ethanol-induced osteoporosis in vivo via ALDH1A1-NFATc1 axis." Aging (Albany NY) **11**(19): 8103-8119.

Jiang, N., et al. (2019). "Cytokines and inflammation in adipogenesis: an updated review." Frontiers of Medicine **13**(3): 314-329.

Johnson, J. T., et al. (2022). "Chronic Alcohol Consumption and its Impact on Bone and Metabolic Health - A Narrative Review." Indian J Endocrinol Metab **26**(3): 206-212.

Kamm, D. R. and K. S. McCommis (2022). "Hepatic stellate cells in physiology and pathology." J Physiol **600**(8): 1825-1837.

Kapałczyńska, M., et al. (2018). "2D and 3D cell cultures - a comparison of different types of cancer cell cultures." Arch Med Sci **14**(4): 910-919.

Karageorgiou, V. and D. Kaplan (2005). "Porosity of 3D biomaterial scaffolds and osteogenesis." Biomaterials **26**(27): 5474-5491.

Kawaratani, H., et al. (2013). "The effect of inflammatory cytokines in alcoholic liver disease." Mediators Inflamm **2013**: 495156.

Kersten, V., et al. (2023). "Bone Morphogenetic Protein 13 Has Protumorigenic Effects on Hepatocellular Carcinoma Cells In Vitro." Int J Mol Sci **24**(13).

Khan, M. Z., et al. (2025). "The signaling landscape of insulin-like growth factor 1." Journal of Biological Chemistry **301**(1): 108047.

Khundmiri, S. J., et al. (2016). "PTH and Vitamin D." Compr Physiol **6**(2): 561-601.

Kim, J. M., et al. (2020). "Osteoblast-Osteoclast Communication and Bone Homeostasis." Cells **9**(9).

Kimball, J. S., et al. (2021). "Oxidative Stress and Osteoporosis." J Bone Joint Surg Am

103(15): 1451-1461.

Kitto, L. J. and N. C. Henderson (2021). "Hepatic Stellate Cell Regulation of Liver Regeneration and Repair." Hepatol Commun **5**(3): 358-370.

Kizilgul, M., et al. (2016). "Bone health and vitamin D status in alcoholic liver disease." Indian J Gastroenterol **35**(4): 253-259.

Kleckner, M. S. (1957). "Liver: Structure and Function." Yale Journal of Biology & Medicine **29**(6): 630-631.

Klem, J. R., et al. (2025). "Mutations in the bone morphogenetic protein signaling pathway sensitize zebrafish and humans to ethanol-induced jaw malformations." Dis Model Mech **18**(4).

Kode, J. A., et al. (2009). "Mesenchymal stem cells: immunobiology and role in immunomodulation and tissue regeneration." Cytotherapy **11**(4): 377-391.

Kokabu, S., et al. (2012). "Role of Smad phosphatases in BMP-Smad signaling axis-induced osteoblast differentiation." Journal of Oral Biosciences **54**(2): 73-78.

Kong, E. Q. Z., et al. (2024). "Uncovering the impact of alcohol on internal organs and reproductive health: Exploring TLR4/NF-kB and CYP2E1/ROS/Nrf2 pathways." Animal Model Exp Med **7**(4): 444-459.

Koop, D. R. (2006). "Alcohol metabolism's damaging effects on the cell: a focus on reactive oxygen generation by the enzyme cytochrome P450 2E1." Alcohol Res Health **29**(4): 274-280.

Lai, W., et al. (2024). "Oxidative stress in alcoholic liver disease, focusing on proteins, nucleic acids, and lipids: A review." International Journal of Biological Macromolecules **278**: 134809.

Lam, J., et al. (2000). "TNF-alpha induces osteoclastogenesis by direct stimulation of macrophages exposed to permissive levels of RANK ligand." J Clin Invest **106**(12): 1481-1488.

Lamplot, J. D., et al. (2013). "BMP9 signaling in stem cell differentiation and osteogenesis." Am J Stem Cells **2**(1): 1-21.

Le, G., et al. (2025). "Exosomal miR-122 derived from M2 macrophages induces

osteogenic differentiation of bone marrow mesenchymal stem cells in the treatment of alcoholic osteonecrosis of the femoral head." J Orthop Surg Res **20**(1): 107.

LeBoff, M. S., et al. (2022). "The clinician's guide to prevention and treatment of osteoporosis." Osteoporosis International **33**(10): 2049-2102.

Lee, S.-Y., et al. (2023). "In Vitro three-dimensional (3D) cell culture tools for spheroid and organoid models." SLAS Discovery **28**(4): 119-137.

Lee, S. Y., et al. (2022). "Alternative experimental approaches to reduce animal use in biomedical studies." Journal of Drug Delivery Science and Technology **68**: 103131.

Li, H., et al. (2016). "Bone morphogenetic protein-9 promotes the differentiation of mouse spleen macrophages into osteoclasts via the ALK1 receptor and ERK 1/2 pathways in vitro." Mol Med Rep **14**(5): 4545-4550.

Li, H., et al. (2021). "Role of Exosomal Non-Coding RNAs in Bone-Related Diseases." Front Cell Dev Biol **9**: 811666.

Li, Q., et al. (2017). "The role of mitochondria in osteogenic, adipogenic and chondrogenic differentiation of mesenchymal stem cells." Protein Cell **8**(6): 439-445.

Li, Y., et al. (2022). "Non-alcoholic Fatty Liver Disease and Liver Fibrosis during Aging." Aging Dis **13**(4): 1239-1251.

Li, Z., et al. (2019). "Dual Targeting of Bile Acid Receptor-1 (TGR5) and Farnesoid X Receptor (FXR) Prevents Estrogen-Dependent Bone Loss in Mice." J Bone Miner Res **34**(4): 765-776.

Li, Z., et al. (2023). "The roles of hepatokine and osteokine in liver-bone crosstalk: Advance in basic and clinical aspects." Front Endocrinol (Lausanne) **14**: 1149233.

Li, Z. H., et al. (2017). "High-dose PMA with RANKL and MCSF induces THP-1 cell differentiation into human functional osteoclasts in vitro." Mol Med Rep **16**(6): 8380-8384.

Lima, L. C. D., et al. (2019). "Hepatic encephalopathy: Lessons from preclinical studies." World J Hepatol **11**(2): 173-185.

Lin, J., et al. (2012). "Comparative analysis of phase I and II enzyme activities in 5 hepatic cell lines identifies Huh-7 and HCC-T cells with the highest potential to study

drug metabolism." Arch Toxicol **86**(1): 87-95.

Lin, S., et al. (2016). "The biological function of type I receptors of bone morphogenetic protein in bone." Bone Research **4**(1): 16005.

Liu, J. (2014). "Ethanol and liver: recent insights into the mechanisms of ethanol-induced fatty liver." World J Gastroenterol **20**(40): 14672-14685.

Lovely, C. B. (2025). "Bone morphogenetic protein signaling pathway– Ethanol interactions disrupt palate formation independent of gata3." Reproductive Toxicology **131**: 108754.

Lu, K., et al. (2022). "Defects in a liver-bone axis contribute to hepatic osteodystrophy disease progression." Cell Metabolism **34**(3): 441-457.e447.

Luo, Z., et al. (2017). "Cellular and molecular mechanisms of alcohol-induced osteopenia." Cell Mol Life Sci **74**(24): 4443-4453.

Ma, N., et al. (2019). "The regulatory mechanism of p38/MAPK in the chondrogenic differentiation from bone marrow mesenchymal stem cells." J Orthop Surg Res **14**(1): 434.

Mackowiak, B., et al. (2024). "Alcohol-associated liver disease." J Clin Invest **134**(3).

Marie, P. J. (2015). "Osteoblast dysfunctions in bone diseases: from cellular and molecular mechanisms to therapeutic strategies." Cell Mol Life Sci **72**(7): 1347-1361.

Martín González, C., et al. (2022). "Sclerostin in Excessive Drinkers: Relationships with Liver Function and Body Composition." Nutrients **14**(13): 2574.

Marupanthorn, K., et al. (2017). "Bone morphogenetic protein-2 enhances the osteogenic differentiation capacity of mesenchymal stromal cells derived from human bone marrow and umbilical cord." Int J Mol Med **39**(3): 654-662.

Medina-Leyte, D. J., et al. (2020). "Use of Human Umbilical Vein Endothelial Cells (HUVEC) as a Model to Study Cardiovascular Disease: A Review." Applied Sciences **10**(3): 938.

Memic, A., et al. (2019). "Latest Advances in Cryogel Technology for Biomedical Applications." Advanced Therapeutics **2**(4): 1800114.

Monti, F., et al. (2024). "RANK–RANKL–OPG Axis in MASLD: Current Evidence

Linking Bone and Liver Diseases and Future Perspectives." International Journal of Molecular Sciences **25**(17): 9193.

Moon, A. M., et al. (2020). "Contemporary Epidemiology of Chronic Liver Disease and Cirrhosis." Clin Gastroenterol Hepatol **18**(12): 2650-2666.

Nelson, L. J., et al. (2017). "Human Hepatic HepaRG Cells Maintain an Organotypic Phenotype with High Intrinsic CYP450 Activity/Metabolism and Significantly Outperform Standard HepG2/C3A Cells for Pharmaceutical and Therapeutic Applications." Basic Clin Pharmacol Toxicol **120**(1): 30-37.

Neuman, M. G., et al. (2015). "Alcoholic Liver Disease: Role of Cytokines." Biomolecules **5**(3): 2023-2034.

Nguyen-Lefebvre, A. T. and A. Horuzsko (2015). "Kupffer Cell Metabolism and Function." J Enzymol Metab **1**(1).

Nochi, H., et al. (2004). "Adenovirus mediated BMP-13 gene transfer induces chondrogenic differentiation of murine mesenchymal progenitor cells." J Bone Miner Res **19**(1): 111-122.

Nussler, A. K., et al. (2014). "Chronic CCl4 intoxication causes liver and bone damage similar to the human pathology of hepatic osteodystrophy: a mouse model to analyse the liver-bone axis." Arch Toxicol **88**(4): 997-1006.

Nussler, A. K., et al. (2014). "Chronic CCl4 intoxication causes liver and bone damage similar to the human pathology of hepatic osteodystrophy: a mouse model to analyse the liver–bone axis." Archives of Toxicology **88**(4): 997-1006.

O'Brien, F. J. (2011). "Biomaterials & scaffolds for tissue engineering." Materials Today **14**(3): 88-95.

Oliver, J. C., et al. (1993). "Cytokine kinetics in an in vitro whole blood model following an endotoxin challenge." Lymphokine Cytokine Res **12**(2): 115-120.

Ono, T., et al. (2020). "RANKL biology: bone metabolism, the immune system, and beyond." Inflammation and Regeneration **40**(1): 2.

Ono, T., et al. (2020). "RANKL biology: bone metabolism, the immune system, and beyond." Inflamm Regen **40**: 2.

Osna, N. A., et al. (2017). "Alcoholic Liver Disease: Pathogenesis and Current Management." Alcohol Res **38**(2): 147-161.

Owen, R. and G. C. Reilly (2018). "In vitro Models of Bone Remodelling and Associated Disorders." Front Bioeng Biotechnol **6**: 134.

Panganiban, J., et al. (2025). "Metabolic dysfunction-associated steatotic liver disease (MASLD) in children with obesity: An Obesity Medicine Association (OMA) and expert joint perspective 2025." Obesity Pillars **14**: 100164.

Parent, R., et al. (2004). "Origin and characterization of a human bipotent liver progenitor cell line." Gastroenterology **126**(4): 1147-1156.

Park, G., et al. (2024). "Replacing Animal Testing with Stem Cell-Organoids : Advantages and Limitations." Stem Cell Reviews and Reports **20**(6): 1375-1386.

Park, J. H., et al. (2023). "BMP-9 Improves the Osteogenic Differentiation Ability over BMP-2 through p53 Signaling In Vitro in Human Periosteum-Derived Cells." Int J Mol Sci **24**(20).

Pastorino, P., et al. (2024). "Ethical principles and scientific advancements: In vitro, in silico, and non-vertebrate animal approaches for a green ecotoxicology." Green Analytical Chemistry **8**: 100096.

Paton, A. (2005). "Alcohol in the body." Bmj **330**(7482): 85-87.

Pautke, C., et al. (2004). "Characterization of osteosarcoma cell lines MG-63, Saos-2 and U-2 OS in comparison to human osteoblasts." Anticancer Res **24**(6): 3743-3748.

Pereira, V. B. S., et al. (2023). "Biological and Cellular Properties of Advanced Platelet-Rich Fibrin (A-PRF) Compared to Other Platelet Concentrates: Systematic Review and Meta-Analysis." Int J Mol Sci **25**(1).

Peschl, V., et al. (2022). "Bone morphogenetic protein 13 in hepatic stellate cells and hepatic fibrosis." J Cell Biochem **123**(10): 1544-1552.

Pflaum, T., et al. (2016). "Carcinogenic compounds in alcoholic beverages: an update." Arch Toxicol **90**(10): 2349-2367.

Pina, S., et al. (2015). "Natural-based nanocomposites for bone tissue engineering and regenerative medicine: a review." Adv Mater **27**(7): 1143-1169.

Place, E. S., et al. (2009). "Synthetic polymer scaffolds for tissue engineering." Chem Soc Rev **38**(4): 1139-1151.

Polidoro, M. A., et al. (2021). "Experimental liver models: From cell culture techniques to microfluidic organs-on-chip." Liver Int **41**(8): 1744-1761.

Puche, J. E., et al. (2013). "Hepatic Stellate Cells and Liver Fibrosis." Comprehensive Physiology **3**(4): 1473-1492.

Qu, X. and R. Donnelly (2020). "Sex Hormone-Binding Globulin (SHBG) as an Early Biomarker and Therapeutic Target in Polycystic Ovary Syndrome." Int J Mol Sci **21**(21).

Ramachandran, A. and H. Jaeschke (2019). "Acetaminophen Hepatotoxicity." Semin Liver Dis **39**(2): 221-234.

Rezwan, K., et al. (2006). "Biodegradable and bioactive porous polymer/inorganic composite scaffolds for bone tissue engineering." Biomaterials **27**(18): 3413-3431.

Rhyu, J. and R. Yu (2021). "Newly discovered endocrine functions of the liver." World J Hepatol **13**(11): 1611-1628.

Rowland, A., et al. (2013). "The UDP-glucuronosyltransferases: their role in drug metabolism and detoxification." Int J Biochem Cell Biol **45**(6): 1121-1132.

Rumgay, H., et al. (2021). "Global burden of cancer in 2020 attributable to alcohol consumption: a population-based study." The Lancet Oncology **22**(8): 1071-1080.

Ruoß, M., et al. (2020). "Towards improved hepatocyte cultures: Progress and limitations." Food Chem Toxicol **138**: 111188.

Sahu, N., et al. (2020). "Preconditioning of mesenchymal stromal cells with low-intensity ultrasound: influence on chondrogenesis and directed SOX9 signaling pathways." Stem Cell Research & Therapy **11**(1): 6.

Salomao, M. A. (2021). "Pathology of Hepatic Iron Overload." Clin Liver Dis (Hoboken) **17**(4): 232-237.

Sampson, H. W. (1998). "Alcohol's harmful effects on bone." Alcohol Health Res World **22**(3): 190-194.

Sanchez-Duffhues, G., et al. (2020). "Bone morphogenetic protein receptors: Structure, function and targeting by selective small molecule kinase inhibitors." Bone **138**: 115472.

Sarcognato, S., et al. (2021). "Autoimmune biliary diseases: primary biliary cholangitis and primary sclerosing cholangitis." Pathologica **113**(3): 170-184.

Sato, K., et al. (2019). "Ductular Reaction in Liver Diseases: Pathological Mechanisms and Translational Significances." Hepatology **69**(1): 420-430.

Schulze, R. J., et al. (2019). "The cell biology of the hepatocyte: A membrane trafficking machine." J Cell Biol **218**(7): 2096-2112.

Schyschka, L., et al. (2013). "Hepatic 3D cultures but not 2D cultures preserve specific transporter activity for acetaminophen-induced hepatotoxicity." Arch Toxicol **87**(8): 1581-1593.

Seemann, L. L., et al. (2024). "Metabolic Bone Disease." Prim Care **51**(3): 445-454.

Seitz, H. K., et al. (2023). "Pathogenesis of Alcoholic Fatty Liver a Narrative Review." Life **13**(8): 1662.

Sellin, M. L., et al. (2023). "IL-6-induced response of human osteoblasts from patients with rheumatoid arthritis after inhibition of the signaling pathway." Clin Exp Med **23**(7): 3479-3499.

Serras, A. S., et al. (2021). "A Critical Perspective on 3D Liver Models for Drug Metabolism and Toxicology Studies." Front Cell Dev Biol **9**: 626805.

Sharma A, N. S. (2023 Jul 3). Chronic Liver Disease.

Shen, B., et al. (2009). "BMP-13 emerges as a potential inhibitor of bone formation." Int J Biol Sci **5**(2): 192-200.

Shen, B., et al. (2009). "BMP-13 Emerges as a Potential Inhibitor of Bone Formation." International Journal of Biological Sciences **5**(2): 192-200.

Singh, V. P., et al. (2016). "Critical evaluation of challenges and future use of animals in experimentation for biomedical research." International Journal of Immunopathology and Pharmacology **29**(4): 551-561.

Song, H., et al. (2019). "Reversal of Osteoporotic Activity by Endothelial Cell-Secreted Bone Targeting and Biocompatible Exosomes." Nano Lett **19**(5): 3040-3048.

Song, T. H., et al. (2018). "Increased Bone Mineral Density after Abstinence in Male Patients with Alcohol Dependence." Clin Psychopharmacol Neurosci **16**(3): 282-289.

Song, Y., et al. (2021). "Identification of hepatic fibrosis inhibitors through morphometry analysis of a hepatic multicellular spheroids model." Scientific Reports **11**(1): 10931.

Sözen, T., et al. (2017). "An overview and management of osteoporosis." Eur J Rheumatol **4**(1): 46-56.

Sreekumar, V., et al. (2018). "Resveratrol protects primary cilia integrity of human mesenchymal stem cells from cigarette smoke to improve osteogenic differentiation in vitro." Arch Toxicol **92**(4): 1525-1538.

Šromová, V., et al. (2023). "A Brief Review of Bone Cell Function and Importance." Cells **12**(21).

Stremmel, W. and R. Weiskirchen (2022). "Wilson disease: more complex than just simply a copper overload condition?—a narrative review." AME Medical Journal **7**.

Sun, Y., et al. (2021). "Recent Advances in Osteoclast Biological Behavior." Front Cell Dev Biol **9**: 788680.

Swaminathan, S., et al. (2019). "Need for alternatives to animals in experimentation: An Indian perspective." Indian J Med Res **149**(5): 584-592.

Takahashi, Y., et al. (2015). "3D spheroid cultures improve the metabolic gene expression profiles of HepaRG cells." Biosci Rep **35**(3).

Takegahara, N., et al. (2022). "RANKL biology." Bone **159**: 116353.

Talwani, R., et al. (2011). "Infectious diseases and the liver." Clin Liver Dis **15**(1): 111-130.

Tan, H. K., et al. (2020). "Oxidative stress in alcohol-related liver disease." World J Hepatol **12**(7): 332-349.

Thakur, S., et al. (2024). "Biomarkers of Hepatic Toxicity: An Overview." Curr Ther Res Clin Exp **100**: 100737.

Thayer, T. E., et al. (2020). "The Role of Bone Morphogenetic Protein Signaling in Non-Alcoholic Fatty Liver Disease." Sci Rep **10**(1): 9831.

Thayer, T. E., et al. (2020). "The Role of Bone Morphogenetic Protein Signaling in Non-Alcoholic Fatty Liver Disease." Scientific Reports **10**(1): 9831.

Thomes, P. G., et al. (2021). "Natural Recovery by the Liver and Other Organs after Chronic Alcohol Use." Alcohol Res **41**(1): 05.

Thoudam, T., et al. (2024). "Mitochondrial quality control in alcohol-associated liver disease." Hepatology Communications **8**(11).

Thoudam, T., et al. (2024). "Mitochondrial quality control in alcohol-associated liver disease." Hepatol Commun **8**(11).

Tokunaga, T., et al. (2020). "TGFβ1 Regulates Human RANKL-Induced Osteoclastogenesis via Suppression of NFATc1 Expression." Int J Mol Sci **21**(3).

Trefts, E., et al. (2017). "The liver." Curr Biol **27**(21): R1147-r1151.

Turner, R. T. (2000). "Skeletal response to alcohol." Alcohol Clin Exp Res **24**(11): 1693-1701.

Tutty, M. A., et al. (2022). "Three-dimensional (3D) liver cell models - a tool for bridging the gap between animal studies and clinical trials when screening liver accumulation and toxicity of nanobiomaterials." Drug Deliv Transl Res **12**(9): 2048-2074.

Umur, E., et al. (2024). "Exploring the Role of Hormones and Cytokines in Osteoporosis Development." Biomedicines **12**(8): 1830.

Urzì, O., et al. (2023). "Three-Dimensional Cell Cultures: The Bridge between In Vitro and In Vivo Models." International Journal of Molecular Sciences **24**(15): 12046.

van der Merwe, S. W., et al. (2003). "Hepatic osteodystrophy in rats results mainly from portasystemic shunting." Gut **52**(4): 580-585.

Vandrovcova, M., et al. (2014). "Interaction of human osteoblast-like Saos-2 and MG-63 cells with thermally oxidized surfaces of a titanium-niobium alloy." PLoS One **9**(6): e100475.

Veidal, S. S., et al. (2010). "Procollagen type I N-terminal propeptide (PINP) is a marker for fibrogenesis in bile duct ligation-induced fibrosis in rats." Fibrogenesis Tissue Repair **3**(1): 5.

Wang, W., et al. (2020). "Aldehyde Dehydrogenase, Liver Disease and Cancer." Int J Biol Sci **16**(6): 921-934.

Wang, Y., et al. (2024). "The role of matrix metalloproteinase 9 in fibrosis diseases and its molecular mechanisms." Biomedicine & Pharmacotherapy **171**: 116116.

Wang, Y. W. and C. W. Luo (2025). "Unveiling the signal valve specifically tuning the TGF-β1 suppression of osteogenesis: mediation through a SMAD1-SMAD2 complex." Cell Commun Signal **23**(1): 38.

Wawrzyniak, A. and K. Balawender (2022). "Structural and Metabolic Changes in Bone." Animals (Basel) **12**(15).

Wawrzyniak, A. and K. Balawender (2022). "Structural and Metabolic Changes in Bone." Animals **12**(15): 1946.

Weitzmann, M. N. (2013). "The Role of Inflammatory Cytokines, the RANKL/OPG Axis, and the Immunoskeletal Interface in Physiological Bone Turnover and Osteoporosis." Scientifica (Cairo) **2013**: 125705.

Wen, Y., et al. (2021). "Hepatic macrophages in liver homeostasis and diseases-diversity, plasticity and therapeutic opportunities." Cellular & Molecular Immunology **18**(1): 45-56.

Weng, W., et al. (2023). "Tobacco heating system has less impact on bone metabolism than cigarette smoke." Food and Chemical Toxicology **173**: 113637.

Weng, W., et al. (2020). "Material-Dependent Formation and Degradation of Bone Matrix-Comparison of Two Cryogels." Bioengineering (Basel) **7**(2).

World Health, O. (2018). Global status report on alcohol and health 2018. Geneva, World Health Organization.

World Health, O. (2024). Global status report on alcohol and health and treatment of substance use disorders. Geneva, World Health Organization.

Wu, D. and A. I. Cederbaum (2003). "Alcohol, oxidative stress, and free radical damage." Alcohol Res Health **27**(4): 277-284.

Wu, M., et al. (2016). "TGF-β and BMP signaling in osteoblast, skeletal development, and bone formation, homeostasis and disease." Bone Research **4**(1): 16009.

Wu, M., et al. (2016). "TGF-β and BMP signaling in osteoblast, skeletal development, and bone formation, homeostasis and disease." Bone Res **4**: 16009.

Wu, Q.-J., et al. (2022). "The sirtuin family in health and disease." Signal Transduction and Targeted Therapy **7**(1): 402.

Wu, Z., et al. (2024). "Regulation of bone homeostasis: signaling pathways and therapeutic targets." MedComm (2020) **5**(8): e657.

Xie, X., et al. (2014). "Biology of platelet-rich plasma and its clinical application in cartilage repair." Arthritis Res Ther **16**(1): 204.

Xu, L., et al. (2005). "Human hepatic stellate cell lines, LX-1 and LX-2: new tools for analysis of hepatic fibrosis." Gut **54**(1): 142-151.

Xu, Q., et al. (2024). "Mesenchymal stem cells lineage and their role in disease development." Molecular Medicine **30**(1): 207.

Yi, J., et al. (2024). "The crosstalk between cholangiocytes and hepatic stellate cells promotes the progression of epithelial-mesenchymal transition and periductal fibrosis during Clonorchis sinensis infection." Parasit Vectors **17**(1): 151.

You, M. and G. E. Arteel (2019). "Effect of ethanol on lipid metabolism." J Hepatol **70**(2): 237-248.

Young, K., et al. (2022). "Regulation of 1 and 24 hydroxylation of vitamin D metabolites in the proximal tubule." Exp Biol Med (Maywood) **247**(13): 1103-1111.

Yu, C., et al. (2023). "The Role of the NLRP3 Inflammasome and Programmed Cell Death in Acute Liver Injury." Int J Mol Sci **24**(4).

Yuan, Y., et al. (2019). "Gene expression profiles and bioinformatics analysis of insulin-like growth factor-1 promotion of osteogenic differentiation." Mol Genet Genomic Med **7**(10): e00921.

Yue, J. and J. M. López (2020). "Understanding MAPK Signaling Pathways in Apoptosis." International Journal of Molecular Sciences **21**(7): 2346.

Zahmatkesh, E., et al. (2022). "In vitro modeling of liver fibrosis in 3D microtissues using scalable micropatterning system." Arch Toxicol **96**(6): 1799-1813.

Zakhari, S. (2013). "Alcohol metabolism and epigenetics changes." Alcohol Res **35**(1): 6-16.

Zeng, G., et al. (2023). "Systematic review and meta-analysis: Comparing

hepatocellular and cholestatic patterns of drug-induced liver injury." iLIVER **2**(2): 122-129.

Zhang, L., et al. (2023). "Consequences of Aging on Bone." Aging Dis **15**(6): 2417-2452.

Zhao, C., et al. (2006). "Bidirectional ephrinB2-EphB4 signaling controls bone homeostasis." Cell Metab **4**(2): 111-121.

Zhao, W., et al. (2014). "Effects of substrate stiffness on adipogenic and osteogenic differentiation of human mesenchymal stem cells." Mater Sci Eng C Mater Biol Appl **40**: 316-323.

Zhao, Y., et al. (2025). "Beyond Bone Loss: A Biology Perspective on Osteoporosis Pathogenesis, Multi-Omics Approaches, and Interconnected Mechanisms." Biomedicines **13**(6): 1443.

Zhivodernikov, I. V., et al. (2023). "Molecular and Cellular Mechanisms of Osteoporosis." Int J Mol Sci **24**(21).

Zhou, R., et al. (2021). "Endocrine role of bone in the regulation of energy metabolism." Bone Research **9**(1): 25.

Zhu, S., et al. (2021). "Maqui berry extract prevents cigarette smoke induced oxidative stress in human osteoblasts in vitro." EXCLI J **20**: 281-296.

Zhu, S., et al. (2020). "Bisphosphonates Reduce Smoking-Induced Osteoporotic-Like Alterations by Regulating RANKL/OPG in an Osteoblast and Osteoclast Co-Culture Model." Int J Mol Sci **22**(1).

Zorov, D. B., et al. (2014). "Mitochondrial reactive oxygen species (ROS) and ROS-induced ROS release." Physiol Rev **94**(3): 909-950.

Chapter 8

8. Declaration

The research was entirely conducted in Siegfried Weller Institute for Trauma Research, Eberhard Karls Universität Tübingen, Tübingen.

Prof. Dr. rer. nat. Andreas K. Nüssler, Dr. sc. hum. Romina H. Aspera-Werz and I conceptualized the study. Dr. sc. hum. Romina H. Aspera-Werz and I designed the experiments. All experiments were carried out and analyzed by myself.

I declare that all relevant data are our original work, except for the quoted references and figures.

I hereby declare that the submitted thesis entitled: "Alcohol-Induced Liver Fibrosis Alters Bone *via* BMP Signaling: Modeling Hepatic Osteodystrophy *in vitro*" has been written by myself. This work has not been submitted for any other degree. This thesis was linguistically edited by a commercial Professional English Proofreading Service (Proof-Reading-Service.com; Proof reading for language errors in spelling, grammar and word choice).

_____

Place/date/signature of doctoral candidate

Chapter 9

9. Own academic achievements

Results of this thesis were partially used for publication and congress:

Publication：

Guanqiao Chen, **Yuxuan Xin**, Mohammad Majd Hammour, Sabrina Ehnert, Andreas K. Nüssler and Romina H. Aspera-Werz, et al. Establishment of a human 3D in vitro liver-bone model as a potential system for drug toxicity screening. *Archives of Toxicology*, 2025, 99(1):333-356 IF 6.9

Mohammad Majd Hammour , Yelda Anuk , Regina Breinbauer , Romina H Aspera-Werz , **Yuxuan Xin** , Guanqiao Chen , Tina Histing , Sabrina Ehnert , Andreas K Nüssler , Stefan Döbele, et al. Impact of alcohol consumption on outcomes and potential of immune biomarkers for postoperative complications in trauma patients. *Frontiers in Immunology*, 2025, 14:16:1492288 IF 5.9

Presentation in international or national congress:

- Poster in Symposium: The Liver´s Influence on Immune Cell Function and its Consequence for Liver Disease, GASL, Munich, 2025
- Oral presentation in 27. Chirurgische Forschungstage, Tübingen, 2024.
- Oral presentation in 26. Chirurgische Forschungstage, Mannheim, 2023.

Chapter 10

10. Acknowledgements

First and foremost, I would like to express my sincerest gratitude to my advisor, Prof. Dr. rer. nat. Andreas K. Nüssler. Throughout my doctoral studies, Professor Nüssler has been a constant source of guidance, encouragement, and inspiration. From the initial stages of defining my research direction to the final steps of writing this dissertation, his insightful feedback, constructive criticism, and his mentorship have been invaluable. It has been a true privilege to learn from and work alongside such an outstanding mentor.

I would also like to sincerely thank Dr. sc. hum. Romina H. Aspera-Werz for her valuable input and support during my doctoral degree studies. Her expertise and constructive feedback at key stages of my research helped me refine my approach and strengthen the overall direction of my work. I truly appreciate her availability to discuss ideas, her thoughtful suggestions, and her kind assistance throughout this journey.

I am also deeply grateful to my colleagues at SWI — Sabrina, Svetlana, Majd, Engin, Filiz, Maximilian, Melike, Kevin, Leonie, and Elisabeth — whose collaboration and friendship made the challenges of research more manageable and the journey more rewarding. I would also like to thank my Chinese colleagues — Guanqiao Chen, Xiang Gao, Ruizhuo Zhang, Sanhuan Yuan, Pengcheng Zhou, and Yangfan Li — for the many insightful discussions, shared experiments, and long hours we spent working together.

Finally, I would like to express my deepest gratitude to my family. To my parents, thank you for your unconditional love, patience, and unwavering belief in. To my girlfriend, Yanchen Li, thank you for always being by my side. Your understanding during difficult times, your quiet strength, and your constant encouragement have meant more to me than words can express. I am truly grateful for your presence throughout this journey.

Completing this dissertation is both an end and a beginning. I leave this chapter of my life filled with gratitude. To everyone who has accompanied me on this journey—thank you from the bottom of my heart.